Monitoring Underground Mine Displacement Using Photogrammetry and Laser Scanning

Brent Allan Slaker

Dissertation submitted to the faculty of the Virginia Polytechnic Institute and State University in partial fulfillment of the requirements for the degree of

Doctor of Philosophy

In

Mining Engineering

Erik C. Westman, Chair

Mario G. Karfakis Gabriel S. Esterhuizen

Nino S. Ripepi Michael M. Murphy

24 February 2015

Blacksburg, VA

Keywords: photogrammetry, laser scanning, underground mines, longwall mining, monitoring

MONITORING UNDERGROUND MINE DISPLACEMENT USING PHOTOGRAMMETRY AND LASER SCANNING

Brent Slaker

ABSTRACT

Photogrammetry and laser scanning are remote sensing technologies with the potential to monitor movements of rock masses and their support systems in underground mine environments. Displacements underground are traditionally measured through point measurement devices, such as extensometers. These are generally restricted to measuring one dimension, may change behavior with installation, may obstruct mining operations, and are restricted to monitoring the behavior of a small area. Photogrammetry and laser scanning offer the ability to monitor rock mass movements at millions of points in a local area, both accurately and quickly. An improved, or augmented, method for measuring displacements underground in a practical, cost-effective manner will lead to an improved understanding of rock mass behavior.

Several experiments were performed that demonstrate the applicability of these remote sensing techniques to monitoring rock mass changes. An underground mining environment presents unique challenges to using these tools for monitoring rock movements, such as: poor lighting, dust, fog, and unfavorable geometries. It is important, therefore, to demonstrate that these tools which have applications in other industries, can also be adapted to the conditions of an underground mine. The study sites chosen include two different underground limestone mines, two different underground coal mines, and the Mine Roof Simulator (MRS) at the Pittsburgh Office of Mine Safety and Health Research.

Both photogrammetry and laser scanning were tested at different limestone mines to detect scaling and spalling on ribs that occurred over several weeks. Both methods were successfully used to reconstruct three-dimensional models of the limestone ribs and detect areas of rock change between visits. By comparing the reconstructed point clouds, and the triangulated meshes created from them, volumes of rock change could be quantified. The laser scanned limestone mine showed a volume of 2.3 m^3 and 2.6 m^3 being displaced across two ribs between visits. The

photogrammetry study involved seven different pillars and at least one rib face modeled on each, with volume changes of 0.29 to 4.03 m^3 detected between visits. The rock displaced from the ribs could not be measured independently of the remote sensing, but a uniform absence of rock movement across large areas of the mine validates the accuracy of the point clouds. A similar test was performed using laser scanning in an underground coal mine, where the displacement was induced by removing material by hand from the ribs. Volume changes as small as 57 cm^3, or slightly larger than a golf ball, and as large as 57,549 cm^3, were detectable in this environment, despite the change in rib surface reflectance and mine geometry.

In addition to the rib displacement, photogrammetry was selected as a tool for monitoring standing supports in underground coal mines. The additional regulatory restrictions of underground coal may preclude the use of laser scanning in these mines where deformation is most likely to occur. The camera used for photogrammetry is ATEX certified as explosion proof and is indicative of the specifications that could be expected in an MSHA approved camera. Three different experiments were performed with this camera, including a laboratory controlled standing support deformation at the MRS and an in-mine time-lapse experiment measuring the response of a wooden crib and steel support to abutment loading. The experiment reconstructing a standing support in the MRS showed a cumulative convergence of 30.93 cm through photogrammetry and 30.48 cm as measured by the system. The standing support monitoring in the underground coal mine environment showed a steel support cumulative convergence of 1.10 cm, a wooden crib cumulative convergence of 0.62 cm, and a measured cumulative convergence on the wooden crib of 0.62 cm.

These techniques explored in this report are not intended to supplant, but rather supplement, existing measurement technologies. Both laser scanning and photogrammetry have physical and regulatory limitations in their application to measuring underground mine deformations, however, their ability to provide time-lapse three-dimensional measurements of entire mine sections is a strength difficult to emulate with traditional point measurement techniques. A fast, cost-effective, and practical application of remote sensing to monitoring mine displacements will improve awareness and understanding of rock mass behavior.

Acknowledgements

The Department of Mining and Minerals Engineering at Virginia Tech has been the quality, supportive, and enjoyable atmosphere that they promised me 9 years ago. I want the faculty and staff to know that I appreciate your help, the fact that your doors are always open, and that you value my growth as an engineer. I would also like to thank my fellow graduate students of 115A, who over the past few years have encouraged me, acted as sounding boards, and made my time at Virginia Tech more enjoyable than I could have ever hoped. In a particular order, but an irrelevant one, thank you Andy, Benjamin, Billy, Kyle, Michael, Sarah, Will, and Xu.

I want to thank my advisor, Dr. Westman, for not only giving me the opportunity to pursue my Master's and Doctorate, but also for his guidance, encouragement, and the respect he showed me. I could not have asked for a better graduate experience. I would also like to thank my other committee members: Nino Ripepi, Gabriel Esterhuizen, Michael Murphy, and Mario Karfakis for their assistance with my research and for being both available and invaluable resources, with a special mention to Mario for regularly sneaking into the office make sure we were "advancing the science."

Thank you to the good people at NIOSH, who are not only funding my project, but have always been friendly, welcoming, and open to me picking their brain. Many people have been involved in opening their facilities and lending their expertise to my work, from NIOSH and elsewhere, whether they realized they were helping or not. I would like to thank Tim Batchler, David Gearhart, John Ellenberger, Wes Johnson, Stephen Iverson, Mark Luxbacher, and Cheston Weese for their help along the way.

A special thanks to all my friends and family, including the extra family I picked up along the way. Thank you all for being supportive of what I do and understanding when I became unavailable through some of the busier times in my graduate career. Also, a thank you to my wonderful wife Katie, who has stood behind me as my biggest supporter through my entire PhD career.

Finally, I would like to thank God for the blessings He has put in my life, and for the wisdom and strength to make it this far.

Table of Contents

List of Figures

List of Tables

Chapter 1 Introduction

Underground mining presents many unique and challenging obstacles to engineering design, stemming from a harsh, dark, mechanically complex environment. Ensuring a safe working environment and operational continuity are of paramount concern to mine planning. One method of improving mine safety and efficiency is a proper understanding of rock masses and their behavior. The heterogeneity and anisotropy of many rock masses make predicting rock mass behavior difficult, and gathering as much site-specific information as is feasible a top priority.

The underground coal mining sector will be the focus, although not the extent, of this research, due to a need for better understanding of the ground response surrounding longwall coal mines and gate road behavior. Underground coal mining remains one of the largest sectors of the mining industry in the United States [1][2]. Due to the prevalence of underground coal mining, a considerable amount of research has been performed with the intention of furthering the understanding of underground rock masses in an attempt to improve mine safety. In the United States, falls of ground in underground coal mines have been responsible for 2300 operator and contractor injuries and 35 fatalities from January 2007, the year of the Crandall Canyon mine disaster, through July 2013 [3]. The injury and fatality rate has been on the decline for the past 50 years, in no small part due to advances in ground control research [4].

Longwall mining presents unique structural challenges due to the large stress redistributions that occur as panels are mined. The abutment stresses that form necessitate the use of secondary supports to maintain gate road stability. The ground response curve, a method of determining required secondary support pressures, can be inferred by monitoring standing support displacements underground. Determining support response in laboratory settings is well documented but monitoring their behavior underground is more difficult. The installation of instrumentation in an underground environment can be difficult for a variety of reasons. The uncontrolled mine environment may load the support in an inconsistent and unpredictable manner, it may be difficult to install extensometers in the most appropriate locations, and mine conditions or regulations may prevent personnel access or certain equipment installation.

Convergence measurements are some of the most frequently made measurements underground. These are simply measurements of the change in position of two points relative to

each other, however, the information they provide is critical to understanding rock masses and designing engineering systems that most safely and efficiently address the mechanical uncertainty of geologic structures. Underground mining instrumentation, in which displacement monitoring instrumentation plays a large role, is performed to [5]:

1. Observe the behavior of mining-influenced rock masses
2. Evaluate current support systems and their usefulness
3. Provide early detection of hazards
4. Determine remedial actions for hazards
5. Evaluate the effectiveness of hazard-remediating measures

The tools used to monitor ground movements in underground mining and tunneling environments are typically point measurement devices such as extensometers, although laser scanning has seen increased use in monitoring tunneling excavations and mine mapping. The most common extensometers found underground are either surface or borehole extensometers. Surface extensometers measure the movement of two anchor points on a rock surface. These can be as simple as a tape measure, dial gage, or may be vibrating wire transducers or Linear Variable Differential Transformers (LVDTs) [6]. Borehole extensometers operate similarly to surface extensometers, by measuring the change position of points on the surface of a rock, but are installed inside boreholes. These are particularly useful in mining operations for showing the separation of roof strata or the magnitude of roof sag.

These measurement devices are fundamentally limited by the points on which they are anchored. While some extensometers do allow anchoring at multiple points, each instrument is severely restricted in measurement breadth. In the case of a continuous rock mass response, extensometers may be perfectly capable of recording accurate and precise convergence measurements, but in the case of a discontinuous rock mass response, these point measurements may not report, or may misreport ground movements [7]. In addition to missing areas of displacement, mechanical sources of error in extensometers may occur for a variety of reasons. These reasons include the accumulation of dust or dirt, damage to the instrument head, dial indicator, signal cable, or cable connectors, and moisture or dirt in the cable connectors [8]. Large temperature changes and ice accumulation can also interfere with extensometer readings [8], although these are uncommon in most U.S. underground mines.

As a solution to the need for collecting time-lapse spatial data in underground coal mines, laser scanning and close range digital photogrammetry (CRDP), henceforth referred to simply as "photogrammetry," are being explored. Both laser scanning and photogrammetry provide a three-dimensional point cloud as an output, which allows for a time-lapse geometric comparison. Photogrammetry, however, will form the bulk of this study as the regulatory environment may prevent the adoption of laser scanners for coal mine displacement monitoring.

Photogrammetry is a form of image measurement that derives the geometric properties of an object or scene from one or more photographs. The primary purpose of this process is to recreate a three-dimensional object in a digital format [9]. The results from photogrammetry or laser scanning are not distances or voltages as might be expected in other displacement monitoring technologies, but are rather three-dimensional point clouds which, in a time-lapse manner, can reveal the deformational behavior of objects underground. Photogrammetry is not a new science, but the application of it to the hostile environment of underground mining has received little attention.

Using photogrammetry and laser scanning as monitoring tools, instead of point measurement devices, offers the added ability to obtain time-lapse three-dimensional measurements of mine workings quickly. The goal of this study is to show the potential use of photogrammetry and laser scanning in monitoring underground displacements. Overcoming the environmental obstacles present in underground mining, and implementing remote sensing monitoring tools in a practical manner will lead to an increased understanding of how rock masses behave and how best to design mines tailored to their individual geologic conditions. Implementing these technologies in a way that allows for fast, precise, cost-effective, and practical data collection is necessary to ensure that they can be applied in as many different mining environments and to monitoring as many mine behaviors as possible.

Chapter 2 Literature Review

If photogrammetry or laser scanning are to be used to monitor gate road deformational characteristics and standing support response, it is important to first investigate the principles that govern this behavior. Nearly every subsection could comprise a literature review in its own right. As a result, the review will be limited in scope to the topics considered to be most applicable to the research of applying photogrammetry to underground coal monitoring are discussed.

2.1 Longwall Mining

Longwall mining is a mining method commonly applied to ore deposits characterized by large lateral extents and a thin, constant ore thickness, such as coal, potash, or South African gold reefs [10]. Longwall mining differs from room and pillar mining in that the primary coal extraction is performed by retreat mining large panels of coal, as shown in Figure 2.1. The longwall panels vary in length and width, but their length dimension generally greatly exceeds their width. The panels are blocked out by development entries along either side, and then connected by bleeder entries once they have been developed to their final length. Coal is extracted by means of a shearer loader or plow cutting across the face, parallel to the short axis of the panel. The coal then falls onto an armored face conveyor (AFC), to be conveyed to the belt line, which acts as a track for the shearer to move across the face. This system is protected by powered roof supports, called shields, which protect the AFC and personnel at the face, and are capable of advancing along the face in the direction of mining. As the system advances in the direction of mining, the roof above the mined out area begins to collapse behind the shields. This region will be referred to as the *gob* [11].

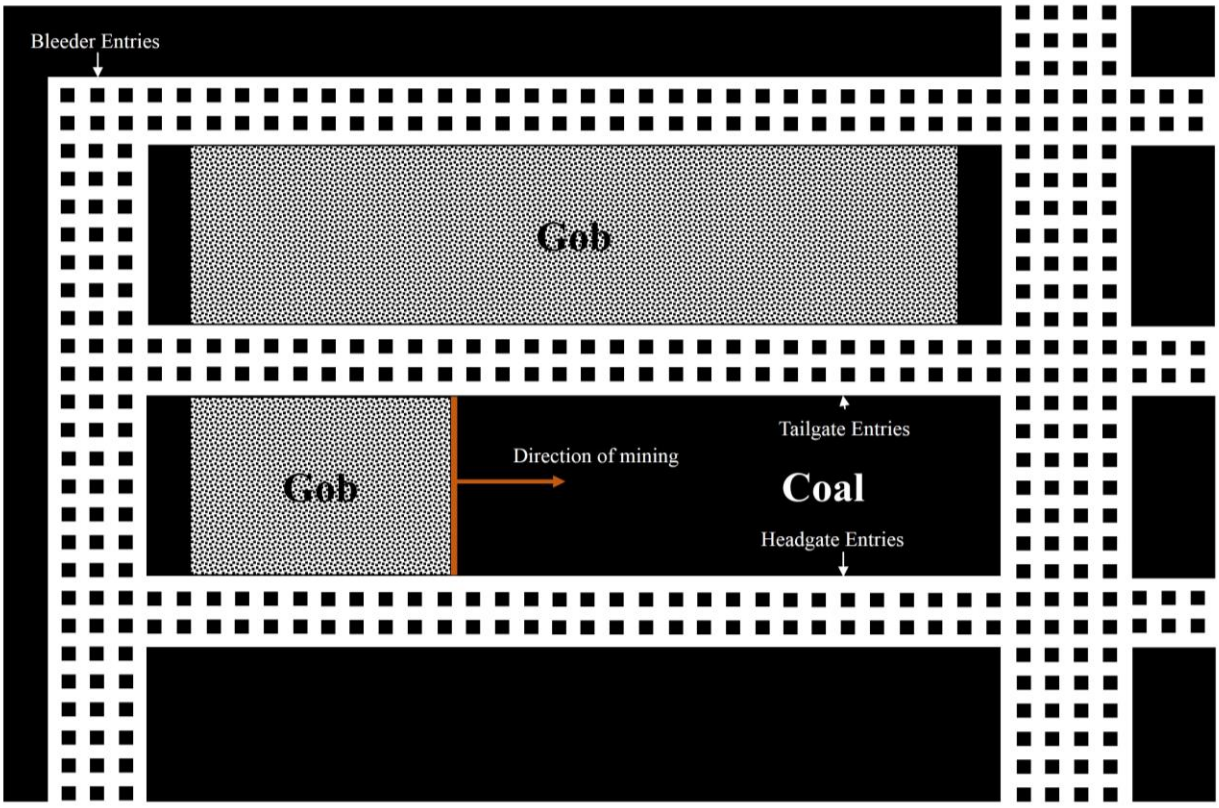

Figure 2.1: Example longwall section layouts

As material is removed, it creates a support deficit, which is then transferred to pillars around the opening. This occurs when creating development entries, and then more load is transferred as adjacent longwall panels are mined. An idealized representation of an abutment stress is shown in Figure 2.2. The stresses transferred to the chain pillars in the gate roads are called side abutment stresses, while the stresses transferred ahead of the face and behind the face are called the front and rear abutment stresses respectively. These abutment stresses are discussed further in Section 2.2.2.

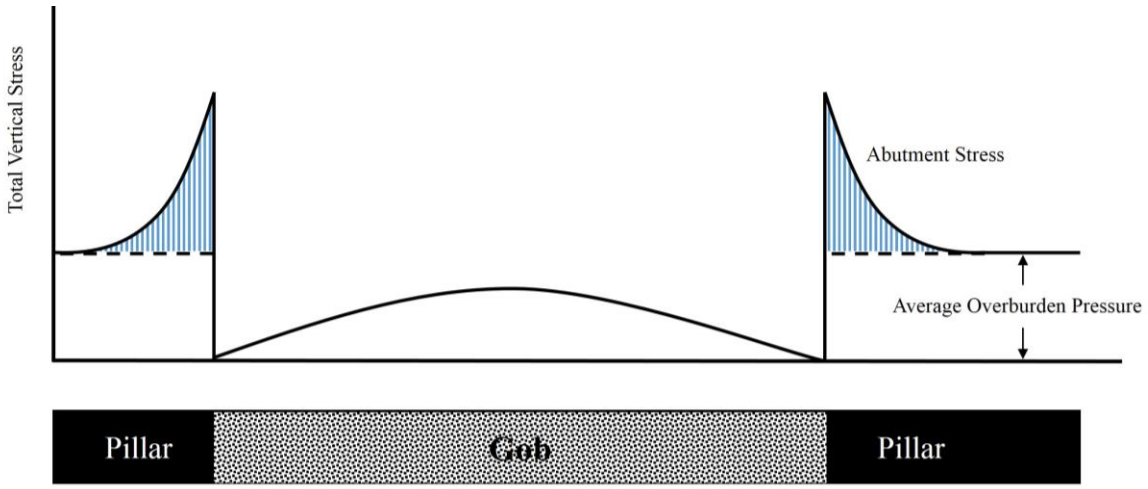

Figure 2.2: Idealized representation of side abutment pressures around the gob

It is important to maintain favorable conditions in the tailgate for several reasons. In gassy mines, it may be necessary to provide adequate ventilation to the bleeder entries, which requires the tailgate remains open [12]. The inability to access the development entries can lead to long production delays and may even affect the longwall face conditions [13]. The tailgate is also used as a secondary escapeway, and in the event that it must be used, it must be traversable according to 30 CFR § 75.222 (2014)[14]. The importance of maintaining open tailgate entries has been illustrated by the tragic events of the 1984 Wilberg Mine Fire, in which 27 people died while the tailgate was blocked as an escapeway [15], spurring legislation requiring that the tailgate be kept open.

2.2 Mechanical Behavior of Rock Masses and Support Systems

Before assessing the response of a secondary support system to the movement of a rock mass, it is important to understand what mechanical principles are causing the rock mass to move. Rock mechanics is the application of engineering mechanics to understanding rock mass response to applied disturbances. The topic is a part of the broader subject of geomechanics, which encompasses the response of other geologic materials, such as soils [16]. Understanding how rock masses will behave is important to many civil and mining engineering projects, as both can change the in-situ state of stress in rock, and both are significantly affected by the mechanical response of the rock mass to excavation.

The behavior of rock masses can be difficult to predict due to the heterogeneous and discontinuous nature of many rock structures. Unlike many other engineering materials, rock is distinguished by the presence of inherent discontinuities, such as joints, bedding planes, or faults, which influence its engineering behavior [17]. The uncertainty inherent in quantifying rock mass responses creates a complex system of necessary assumptions, but the risk of making them can be mitigated by understanding the stress and strain fields, strengths, and the elastic behavior of materials in that system.

2.2.1 Stress and Strain

Evaluation of how rock masses will respond to excavation relies on an understanding of the in-situ stress field and how it will change after losing confinement. The state of stress at an element can be represented by six independent stress components, as shown in Figure 2.3.

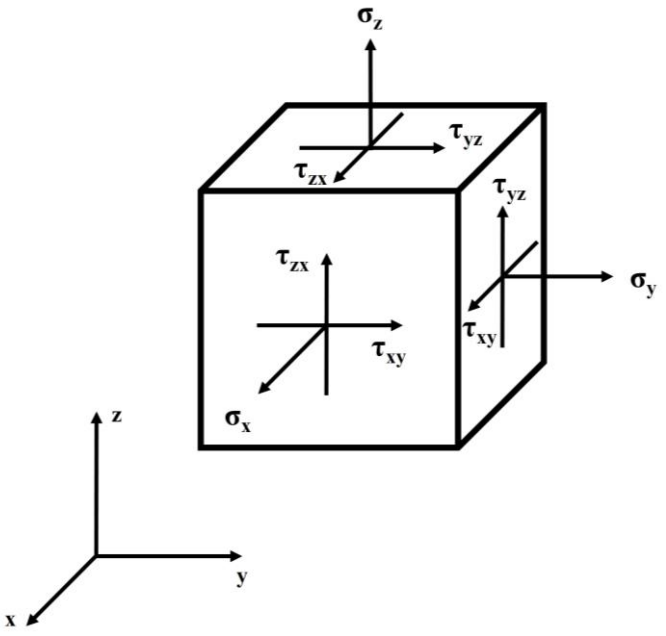

Figure 2.3: Three-dimensional stress components

In an isotropic rock mass, the choice of reference axes are arbitrary, but a non-arbitrary way of determining the state of stress at a point is achieved through determining the principal stresses and invariant quantities under any reference axis rotation. It is possible to orient a plane

such that it only experiences normal stresses, allowing the state of stress to be defined by three principle stresses acting on mutually orthogonal planes [16]. These stress components will be defined as positive in compression with σ_1 as the major principle stress, σ_2 as the intermediate principle stress, and σ_3 as the minor principle stress. Uniaxial stress ($\sigma_1 \neq 0$, $\sigma_2 = \sigma_3 = 0$) is the state of stress commonly assumed in pillars, although the core of the pillar is provided some confinement. Polyaxial stress ($\sigma_1 \neq \sigma_2 \neq \sigma_3$) is found in-situ and on supported excavation boundaries, and biaxial stress ($\sigma_1 \geq \sigma_2$, $\sigma_3 = 0$) is found on unsupported excavation boundaries. A special case of polyaxial stress ($\sigma_2 = \sigma_3$) is commonplace in laboratory testing [16].

Strain (ε) in rock masses represents its change in length divided by its original length. The ratio of transverse strain to vertical strain is known as the Poisson's ratio (ν). As pressure is applied along one axis of a material, inducing strain, a strain tends to occur along the other two orthogonal axes. This can affect the stresses experienced underground as increasing vertical stress could induce horizontal expansion, increasing the horizontal stress. Due to the complicated nature of geologic conditions and stress transfer, it is important to follow the stress pathway when applying the Poisson's effect to infer horizontal stresses. Seedsman (2001) found a horizontal stress change in the roadway roof of 3% of the vertical stress change, due to most of the horizontal stress change occurring in the same location as the largest vertical stress change, above the pillar [18].

Horizontal stresses can be more important to roof stability than vertical stresses in underground coal mines. Most of the vertical stresses are transferred to the abutting pillars through an arching effect, described more in Section 2.5.1, while the horizontal stresses are felt fully in the roof strata [19]. These horizontal stresses are largely caused by global plate tectonic forces [20], and in the Eastern United States form in a biaxial manner where the maximum stress is about 40% greater than the minimum [21]. Horizontal stresses, like vertical stresses, can also form abutments due to these stresses not being transmitted through the gob. These horizontal stress abutments are highest where the direction of the maximum horizontal stress intersects a corner of a longwall panel, without passing through a gob [20]. If the horizontal stress does have to pass through a gob, then the corner of that longwall panel is said to be in a "stress shadow" [20].

2.2.2 Abutment Stresses

There are four primary loading conditions that gate roads are subjected to, each shown in Figure 2.4, and listed below [22]:

1. Development loading: neither adjacent panel has been mined sufficiently to create abutment stresses
2. Side abutment: one side of the gate road has been completely mined, but the advancing long wall face is not nearby
3. Side and face abutment: the longwall face has approached the monitoring location
4. Two side abutments: the face has passed and the monitoring point is surrounded by gob on both sides

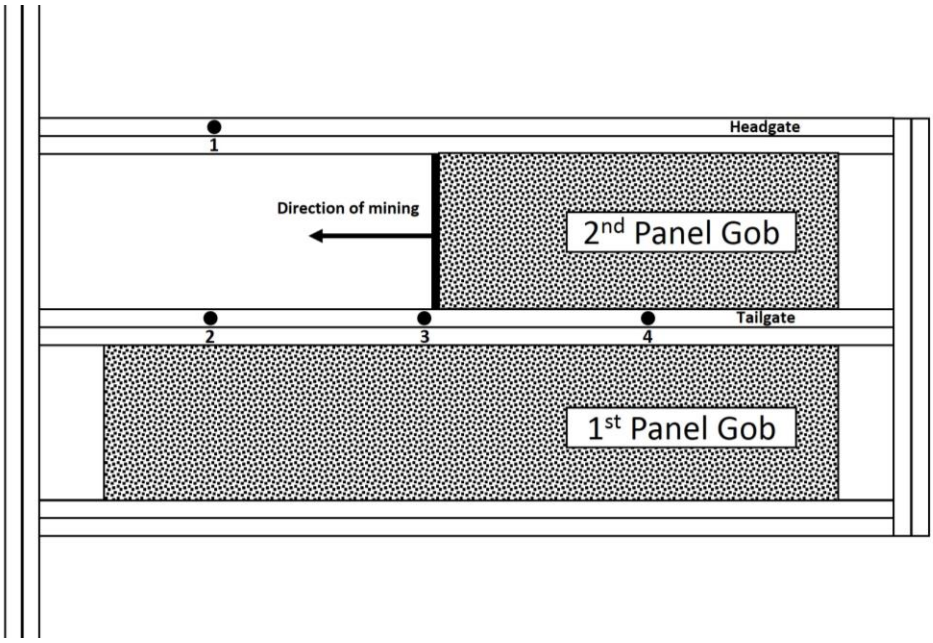

Figure 2.4: Four stages of tailgate loading (after [22])

As mentioned previously, abutment stresses develop around openings underground as the overburden stresses that were being supported by in-situ rock must now be supported by rock adjacent to the opening. The side abutment stresses are of the greatest concern to this study, as they are the largest contributor to increased headgate and tailgate loading. Peng and Chiang (1984)

found that the side abutment pressure reaches its maximum before the face arrives and that the side abutment influences an area described by Equation 1:

$$W_S = 9.3\sqrt{h} \qquad \textit{Equation 1}$$

where W_S is the distance the side abutment reaches and h is the thickness of overburden. It was determined that neither the panel width, nor thickness of the seam, influenced the area of influence from the side abutment [11]. As the longwall face approaches, the gate roads begin to experience the side abutment pressures and converge in a manner similar to Figure 2.5 [11], a behavior confirmed by other authors including Cox [23] and Cassie et. al. [24].

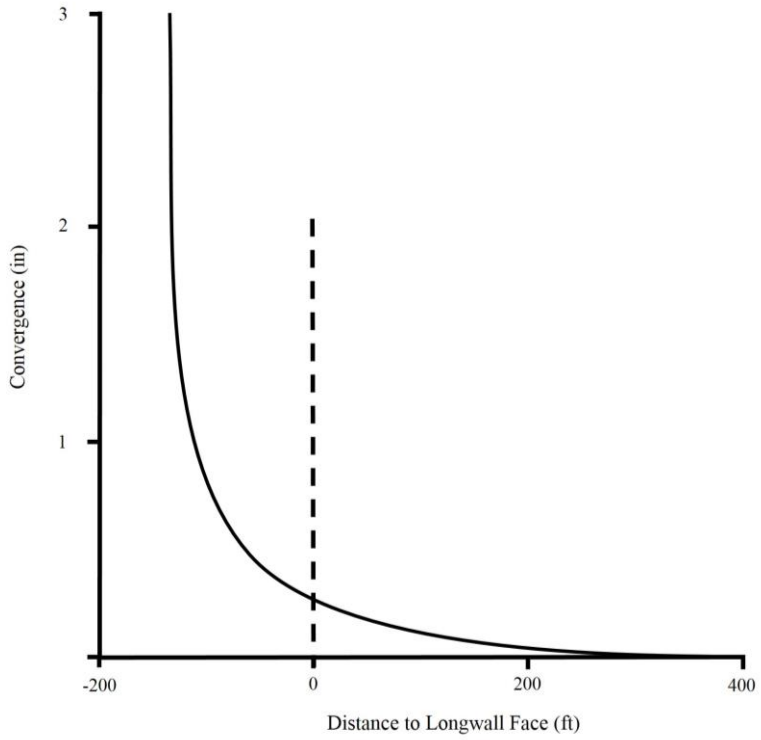

Figure 2.5: Entry convergence as the longwall face approaches (after [11])

2.2.3 Strength

The strength of an engineering material is usually dependent on the distribution and nature of discontinuities within it, and this distribution of structural features throughout a rock mass is known as its rock structure [16]. When considering rock as an engineering material, rock possesses extraordinary qualities. Scaling down areas of interest to cubic decimeters, rock may behave as

an elastic, isotropic medium with strong mechanical properties. However, as scale is increased, separation planes are introduced to the rock structure, compromising the structural integrity of the rock mass [25], as shown in Figure 2.6. This scale effect led to the development of failure the Hoek-Brown Failure Criterion [26] for handling heavily jointed rock masses. Bieniawski (1968) helped to highlight this scale phenomenon by testing large blocks of coal to determine their deformational characteristics [27]. Large-scale in-situ tests on coal specimens showed decreased modulus of elasticity with increasing specimen size, along with increasing Poisson's ratio with increasing specimen size [27]. The range of values obtained in these tests also helps to highlight the variability of coal deformational properties within a single seam.

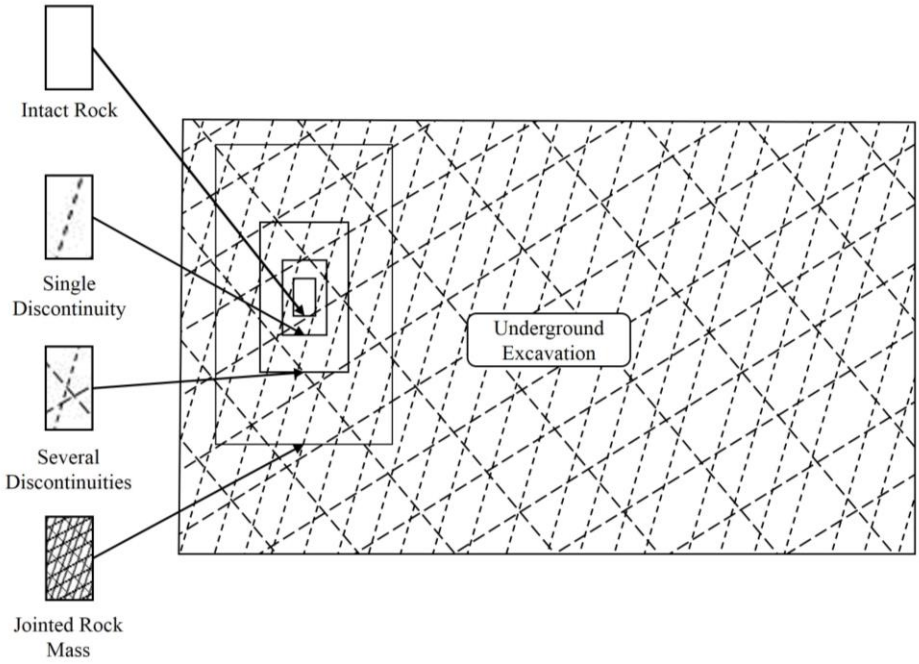

Figure 2.6: The effect of scale on jointing in a rock sample (after [26])

It is unlikely that a rock mass will be isotropic, so an analysis of the effect of anisotropy on rock strength is necessary to determine the rock mass behavior. Many rock masses found in mining environments are sedimentary, resulting in a transverse anisotropy due to bedding planes. It is found that rocks show a higher compressive strength when loaded perpendicular to the stratification, while the lowest rock compressive strengths are generally found where angles β = 30°-45° between the weakness plane and direction of maximum principle stress [28]. Confining

stress usually reduces the impact of weakness planes on the strength of the material; however, several experiments have shown confining stress to not reduce the impact of anisotropy, but to potentially increase the impact [28]. Mark et al. (2004) show an instance in underground coal mining where failure occurred in a shale where the shear strength of the laminations was unable to withstand even the minimum horizontal stress [29].

2.2.4 Constitutive Behaviors

The way in which stresses are related to strains in materials under load is referred to as a material's constitutive behavior. A number of constitutive behaviors are used to describe engineering materials, including elasticity, plasticity, viscosity, and creep. The constitutive behaviors may be time-dependent or time-independent. For any constitutive model, the state of stress and strain may be related through sets of constitutive equations [16].

Elasticity, the most common of the constitutive behaviors in engineering materials, serves as a useful base for describing more complex behaviors [16]. Elastic deformation is deformation that is recovered immediately upon unloading [30]. Considering axial loading, the ratio of stress to strain along the elastic portion of deformation is known as the Young's Modulus, E, as shown in Figure 2.7a for the case of a linear-elastic material.

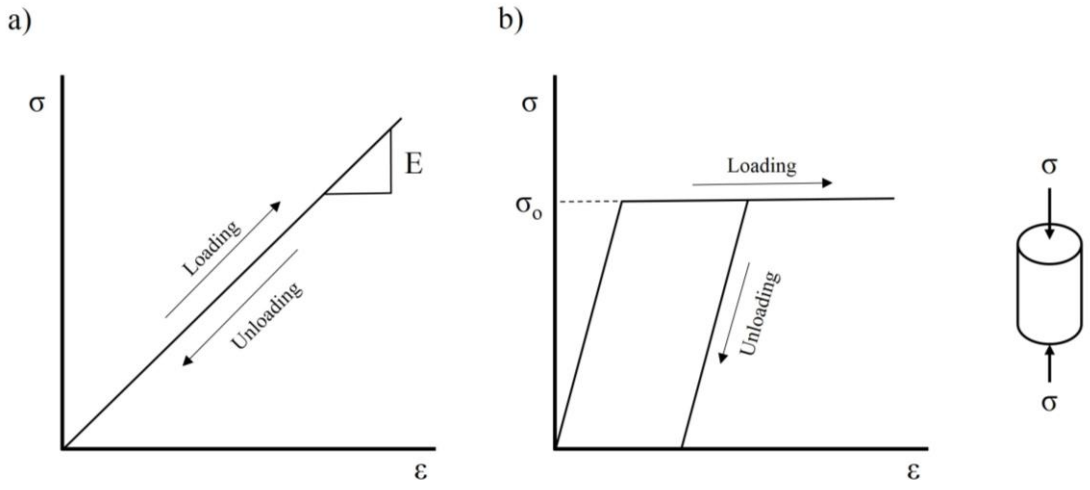

Figure 2.7: a) Elastic and b) Plastic deformation

Plastic deformation is not recovered upon unloading, resulting in permanent deformation, as shown in Figure 2.7b. The stress at which the material begins to experience plastic deformation is known as the yield strength, σ_o. Materials can respond in either a brittle or a ductile manner once the yield strength has been reached. Brittle behavior is characterized by fracture after very little plastic deformation, whereas ductile behavior is characterized by a material being able to sustain large plastic deformations [30]. If the material increases its resistance with increasing strain it is referred to as strain hardening, while decreasing resistance with increasing strain is referred to as strain softening. In hard, brittle rocks the softening behavior is often the result of microfractures occurring as the sample is loaded near its peak strength, which compromise the continuity of the sample being tested [31]. These responses, as well as brittle fracture are shown in Figure 2.8.

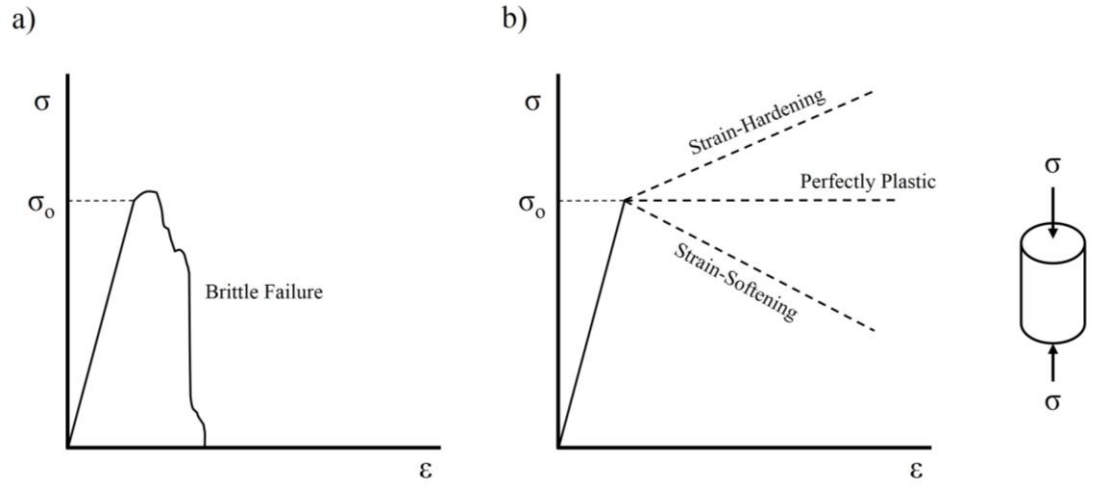

Figure 2.8: a) Brittle and b) ductile behavior

Elastic and plastic deformation are inherently time-independent. Time-dependent strain is called creep. At room temperature, plastics and low-melting-temperature metals may creep, while nearly any material will creep as it approaches its melting temperature [30].

The elastic properties of materials include, in addition to the Young's modulus, E, the bulk modulus, K, shear modulus, G, and Poisson's ratio, ν. The bulk modulus characterizes the change in material volume under hydrostatic stress. The shear modulus relates shear stress and shear strain. The Poisson's ratio relates axial and lateral strain. These values are, in the generalized form of Hooke's Law for isotropic materials, related by Equation 2 and Equation 3 [32]:

$$K = \frac{E}{3(1-2v)} \qquad \textit{Equation 2}$$

$$G = \frac{E}{2(1+v)} \qquad \textit{Equation 3}$$

In the case of anisotropy, each direction of stress will have its own Poisson's ratio and Young's modulus. The challenge in dealing with anisotropic elastic properties is not in the computational requirements, but rather in the ability to obtain or measure the required elastic constants [33].

2.3 Standing Support

A gate road can be thought of as having three components to its support system: natural, primary, and secondary. The natural support system is comprised of the pillars, which provide the most support in response to overburden loading and transferred abutment stresses. The primary support system, consisting of roof bolts, pins the stratified layers of the roof together to prevent them from separating from one another and falling into the opening. The secondary support system is meant to prevent closure of the opening when the abutment stresses develop as the adjacent longwall panels are mined [34].

As mentioned previously, large abutment stresses will develop in the headgate and especially in the tailgate entries. It is necessary to keep the tailgate from collapsing, so that it may be used as a secondary escapeway, or for ventilation purposes. In order to prevent the collapse or undesirable convergence of these entries, standing support is installed to provide additional support pressures. The types of supports most commonly used in U.S. longwall mines today fall into four categories: non-yielding (brittle), constant yielding, load increasing (strain hardening), and load-shedding (strain softening) [34].

Several factors influence the selection of a secondary support system, including the ease of installation, cost, support stiffness, and support load density. The support stiffness is the rate at which a support increases its support pressure with increasing convergence. A support that requires a large amount of deformation before it reaches its ultimate strength could be considered low-stiffness, whereas a support that reaches its ultimate strength after very little convergence

would be considered very stiff. The support load density is the pressure applied by the support at a corresponding magnitude of deformation [12].

A design methodology for secondary support systems was developed by NIOSH that incorporates ground reaction data into the selection of the different, available standing support systems, called the Support Technology Optimization Program (STOP). Without this, a mine is typically required to create a trial section where the new support system is monitored for its response to abutment loading [35]. The support systems considered in this paper belong to the constant yielding and strain hardening categories, as they will be the only ones available for testing.

2.3.1 Strain-Hardening Support

Conventional timber supports, prior to the mid-1980s, were the only available option for tailgate support, however, their low stiffness lead to the development of higher capacity and stiffer supports, such as the concrete supports mentioned in Section 2.3.2. Wooden cribs, shown in Figure 2.9, are easier for personnel to handle due to the relative lightness of wooden crib components compared to other standing supports. Wood also has the advantage of providing visible and audible signals during deformation, which can be useful to miners present during the loading [36]. Engineered timber supports, such as Strata's Link-N-Locks ™ [37], which consists of a series of interlocking wooden beams, seek to remedy the stiffness issues found in their predecessors. Installing these supports is more labor intensive, limiting their use, but they can be installed without the use of specialized machinery [34]. However, installation of wooden cribs using manpower instead of specialized machinery increases the injury risk associated with installing standing support [34].

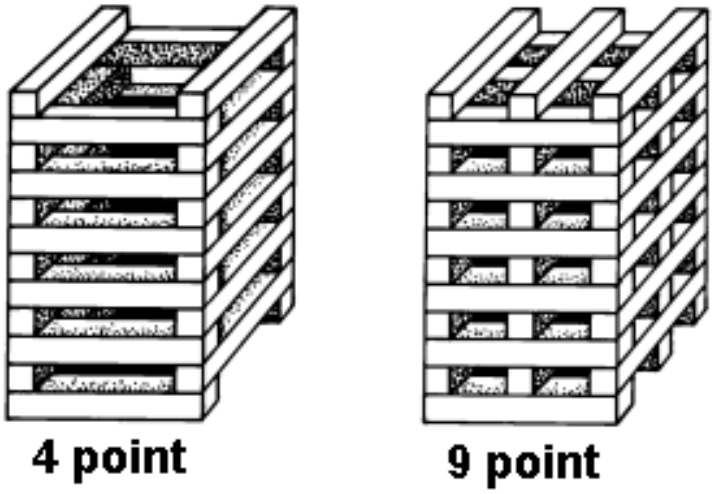

Figure 2.9: 4-point and 9-point wooden crib supports (STOP software [35])

Wooden cribs are typically constructed with hardwoods due to their high compressive strengths. The Eastern United States has over 40 different species of hardwood trees suitable for crib material, each with unique material properties, leading to mechanical variability even before considering the support-strata interaction and crib design. Some softwoods are capable of having higher compressive strengths but due to their value in other industries, it is generally more economical to use hardwoods [38] .

Using wood as an engineering material introduces several design considerations that may be overlooked. It has been found that wooden supports exhibit a time-dependent load-bearing capacity. Their load-bearing capacity is reduced when exposed to the slower strain rates in a gate entry compared to the faster strain rates in laboratory tests [38]. Wood cribbing is also dependent on the performance of any layer of its structure, making mixing of wood species dangerous [39].

2.3.2 Continuously Yielding Support

In the mid-1980s, high-capacity concrete supports began to be introduced. At this time, a thinking prevailed that compressive strengths and moduli an order of magnitude higher than the traditional timber cribs would prove to be more capable at controlling gate road convergence. This thinking, however, neglected the fact that a period of uncontrollable convergence occurs in the

initial stages of rock mass stress relief which the brittle concrete supports were both unable to prevent and unable to sustain [40].

The CAN support, shown in Figure 2.10, is a commonly used constant yielding support, which provided excellent load bearing capacity and deformability. The CAN is the most widely used tailgate standing support in the United States, especially where timber is scarcer, such as in Western longwall mines [41]. It contains a yieldable cement core confined by a cylindrical steel canister, which resembles a can [42]. The Can has the ability to withstand large deformations, up to several feet, without significant loss of strength. In addition, it is installed by machine, reducing the injuries due to manual installation of supports such as timbered cribs. One significant drawback to CAN supports is the need for a contact to be established with the roof, which if improperly installed or poorly selected, can affect the stiffness of the support as a whole [34]. This contact area must be carefully engineered. Timber contacts are often used, and it is important to allow the CAN to remain the softer member, controlling the deformation. Too few timbers can cause the wood to become the softer member, deforming before the CAN reaches its yield strength [39]. Case studies have shown the CAN to have a high Ground Reaction Curve Safety Factor (GRCSF) while maintaining a high support safety factor. The larger CAN-roof contact area has also been attributed to maintaining favorable entry conditions [12].

Figure 2.10: CAN support (STOP software [35])

2.4 Ground Response Curve

The ground response curve was originally developed for tunneling, relating the convergence of an underground opening with the support required to arrest it. The measurement points along the curve are determined from support monitoring [43]. The stages of stress redistribution experienced in tunneling will differ from those experienced in mining. In the case of longwall mining, for example, a point will experience loading differently during development, one-sided abutment loading, and two-sided abutment loading. These different loading stages, discussed in Section 2.2.2, result in multiple ground response curves [22]. For design purposes, the ground response curve should be established for the worst-case scenario, which is in the tailgate immediately behind the shields at the longwall face [12].

When pre-existing rock support is excavated, displacements occur in the surrounding rock as stresses are redistributed. Both artificial supports and the adjacent rock mass are capable of providing the necessary support required to prevent further displacements. The amount of support required as mining progresses, from the artificial supports, can be visually represented by the ground reaction curve, shown in Figure 2.11. The ground response curve is a well-established visual aid for understanding tunnel support mechanics [43].

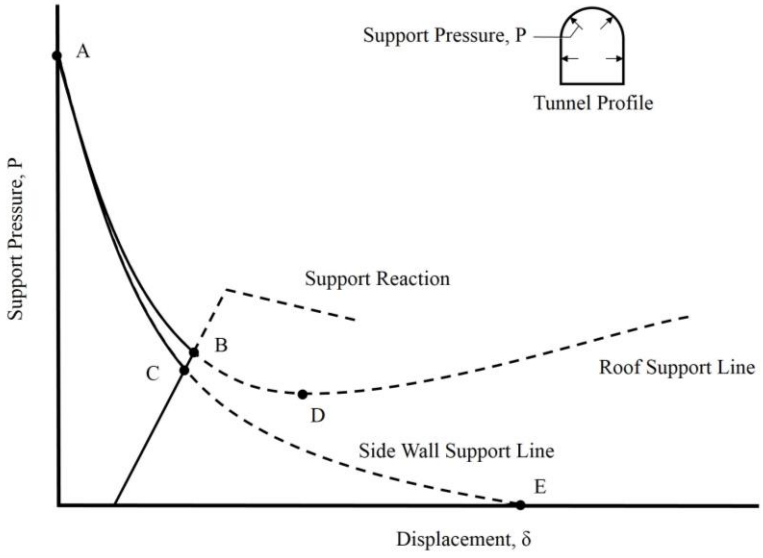

Figure 2.11: Ground Response Curve (after [16])

The ground response curve shows many different stages of ground reaction. Point A represents the in-situ support provided. It is impractical to expect to be able to provide this support before deformation occurs, as the rock will experience relaxation ahead of the excavated surface. Points B and C are the pressures at which the support provided is sufficient to prevent further displacement. Point D is the point along the roof support line where the roof begins to lose its self-supporting capabilities and will require more support pressure as displacement is allowed to continue, until failure. Point E is the point along the side wall support line where no support pressure is required to prevent further displacement. Competent rocks may be capable of supporting themselves without failure after sufficient displacement has taken place, however, if displacement of the rock is undesirable, support can be installed, as at point C, to prevent that displacement.

The support reaction curve is a property of the support, rather than the supported rock, and can be determined prior to installation. The ground response curve is a property of the rock mass and may be difficult to obtain as the support pressure required to prevent further displacement can only be determined by applying sufficient pressure to the rock. The problem that exists with obtaining the curve is that the support pressure must be varied to obtain different points along the curve, yet most mines do not significantly vary the standing supports they use [40].

As a means of addressing the difficulty of obtaining stress and displacement data, the National Institute for Occupational Safety and Health (NIOSH) has performed extensive research into numerical modeling of ground response curves for underground coal mining. Barczak et al. (2005) showed that there is an uncontrollable convergence which cannot be prevented by standing support, and that supports must be able to survive this loading [44]. Esterhuizen and Barczak (2006) showed the impact of the mechanical properties of strata and their interfaces on the ground response has been demonstrated through FLAC modeling [22]. Barczak et al. (2008) studied the effect of changing depths of cover, mining heights, and abutment stresses on the ground response curve [45]. Building on this, is the concept of a support design threshold, representing the point on the ground response curve where the nonlinearity begins and support above that point has little benefit and support below increases the risk of roof instability [45].

Mucho et al. (1999) presented a Ground Reaction Curve Safety Factor (GRCSF) which compares the support load density of the standing support to the minimum allowable support load density, known the critical point where the roof strata begins to fail [12]. This is different from

the support safety factor in that it represents an allowable increase in roof deformation before the onset of failure in the roof, rather than the allowable increase in support deformation before support yield [12]. Considering research into the importance of surviving uncontrollable convergence, it would stand to reason that there exists a support limit past which higher safety factors would not necessarily translate into more stable support systems.

2.4.1 Monitoring

Measuring stresses and displacements associated with underground openings is important to the safety of miners. Many mines do not use roof monitors, instead relying on the sound of cracking rocks or visual inspection to indicate unstable ground conditions [46]. When they are monitored, the current methods of monitoring ground displacements in underground environments are commonly in the form of point measurements, such as from extensometers[47] [45][48] or telltales [24]. Monitoring is especially important for the development of secondary support systems because of a need to develop them on a site-specific basis [49], as the geologic conditions will change from mine to mine. Barczak et al. (2003) found local variations in support response, likely a result of changing geologic conditions [47].

Convergence is one of the most common underground measurements performed [16]. Numerous displacement-monitoring technologies exist, although an underground mining environment prevents the use of most of them. Perhaps the most common of these technologies are extensometers. These are often divided into surface extensometers and borehole extensometers. Surface extensometers refer to an extensometer that measures the movement between two points that lie on an excavation surface or object [50]. Surface extensometers are further divided into crack gages and convergence gages. Crack gages measure the width of discontinuities, or cracks, in a surface, whereas convergence gages are used to monitor convergence that occurs within a tunnel or mine [50].

Dunnicliff (1993) provides an excellent overview of the different types of extensometers and their applications, although convergence gages specifically will form the remainder of this discussion, as they most closely resemble the deliverable created with photogrammetry and laser scanning. Convergence gages, or convergence extensometers, are typically composed of a displacement indicator connected to a wire, rod, tube, or tape connected [50].

Tape extensometers consist of a portable [5] tape measure, tensioned with a compression string that is anchored at two points. A dial indicator on the extensometer displays a reading that must be added to the tape reading to establish a convergence. These extensometers generally have a precision of ± 0.13 mm at a 10 m span, with decreasing precision per additional unit span [50].

Wire extensometers operate fundamentally similar to tape extensometers. The extensometer is anchored at two points, with a tensioned wire running between them. An electric motor tensions the wire, which is geared to a counter. The precision of steel wire extensometers is similar to that of tape extensometers, but the precision can be improved by using an invar wire, which is resistant to thermal expansion. Precision, with an invar wire, is reported to be ±0.03 mm over a 6 m span [5].

Rod and tube extensometers are rigid rods or telescoping tubes that form a physical brace between the two anchor points. A micrometer or dial indicator is often used to display convergence and the rod or tubes are spring loaded to provide a contact with the anchors. These extensometers typically range between 0.15 to 8 m and are often more convenient than wire or tape extensometers when the upper anchor is inaccessible. Precision using rod and tube extensometers at vertical spans is generally ±0.13 mm with reduced precision if horizontally installed, due to sag [5].

Ultrasonic extensometers eschew the traditional physical contact and take a remote sensing approach to measuring convergence. An ultrasonic transducer produces a frequency every several seconds that is projected through the air and is reflected back at the source. The time this audio signal takes to travel is converted into a convergence value. The range for these extensometers is 0.3-11m and convergence values of less than 1.3 mm cannot be detected [5].

2.5 Entry Deformations

Stratified rock presents different rock mechanics challenges than would be expected in massive elastic or massive jointed rock masses. Stratified mining environments are usually associated with sedimentary deposition, such as that found in coal deposits. In these environments, the geologic geometry can be assumed to be persistent through an extent greater than that of the excavations created during mining. Excavations often result in the excavated boundary existing along a bedding plane, to coincide with the ore constituting an entire bedding plane, resulting in the following factors to be considered in the design of such excavations [16]:

1. The state of stress at both the excavation boundary and surrounding rock mass, compared to the strength of the anisotropic rock mass
2. The stability of the roof
3. Floor heave experienced after excavation

The causes of roof, rib, and floor deformations are as numerous as the ways in which they are capable of deforming. This section will provide an overview of the modes of failure and the geologic conditions stress states that can cause them.

2.5.1 Roof Behavior

An arching effect occurs in the overburden which distributes stresses around the opening and toward the pillars, known as the pressure arch [51], shown in Figure 2.12. The first arching effect is a distribution of the above loading towards the pillar support on either side of the opening. This arching effect is more pronounced in stronger overburden rocks, and distributes a larger percentage of the load to the abutments [52]. The second arching effect occurs in the strata layer comprising the immediate roof, where it can be considered to be decoupled from the overlying roof. This arch can begin deflecting under its own weight, distributing the load to the abutments as an analogue to the voussoir beam [53].

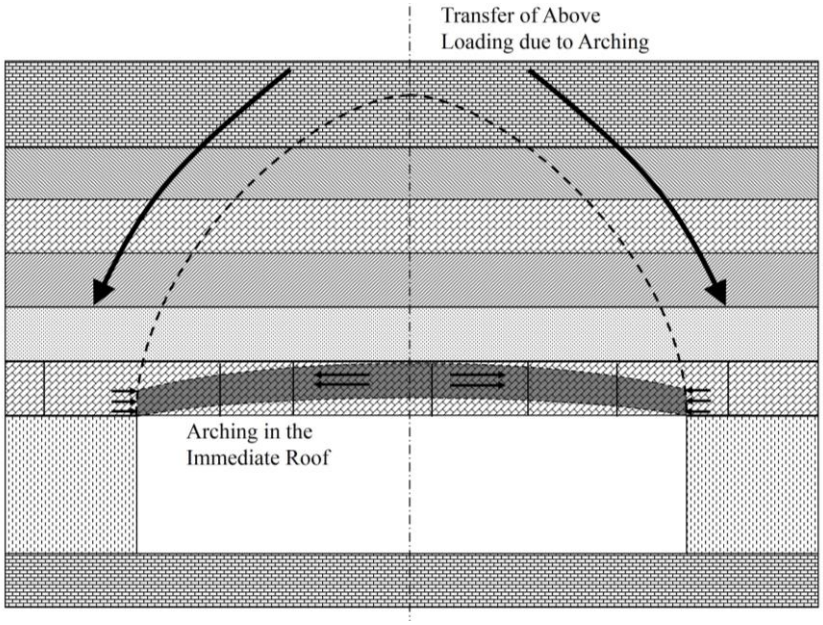

Figure 2.12: Arching effect

In stratified rock masses, the roof spanning an entry can be thought of as a series of stacked beams, which are loaded vertically by their own weight. In bedded rock, the roof may fail in tension, heavily influenced by the length of roof span, sagging in the middle and eventually pulling apart. It may also fail by shearing at the rib-roof interface if the frictional resistance cannot support the weight of the beams [54].

Due to this arching, much of the vertical stress is transferred to the abutting pillars. The horizontal stress, however, receives no such dilution when it reaches the roof strata and can be particularly troublesome [19]. High horizontal stresses in the roof can cause compressive failure of thinly laminated strata. This becomes increasingly more likely if the opening is oriented perpendicular to the maximum horizontal stress rather than parallel to it [19] because horizontal stresses tend to be biaxial, with a much larger maximum horizontal stress than minimum [20]. This compressive failure is often called "cutter roof" and begins in the entry corner, near the abutments, and cuts upward, or begins in the roof and cuts downward until the cantilever beam shears on the entry side opposite the compressional buckling [55].

There are many rock mass classification schemes, but perhaps the most prevalent in coal mining is the Coal Mine Roof Rating (CMRR) [56], which was developed to meet the needs of mine planners in the underground coal mining industry in characterizing roof structures while maintaining the familiarity of Bieniawski's Rock Mass Rating (RMR) [57]. Some of the most important geologic factors related to ground control that were incorporated into the CMRR are bedding interfaces, bed properties, moisture sensitivity, and discontinuities [58].

2.5.2 Floor Behavior

Much like the mine roof, the subcoal strata, or mine floor, is composed of bedded rock layers, and the behavior of the floor unit is dependent on the mechanical properties of these layers. There are four types of floor failure that result from the interaction between the floor and pillars: floor heaving, floor punching, floor displacement, and floor bending [54], each shown in Figure 2.13.

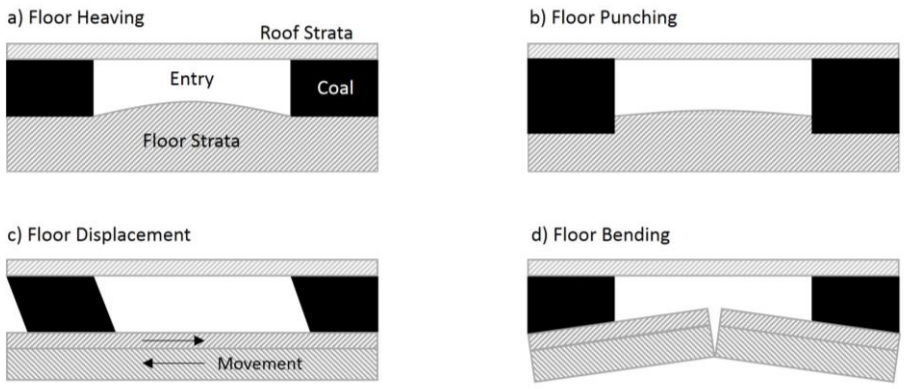

Figure 2.13: Floor behavior

Floor heave may occur where the floor rock has a low strength, high deformability, often in the presence of moisture. While both occur in thick, weak, moist floor strata, observations suggest that floor punching, unlike floor heave, is not due to creep deformations but additional incremental loading. Floor displacement can occur if high horizontal stresses in the subcoal strata exceed the shear resistance of the interface between those strata. This, like the previous floor behaviors, is also compounded by the presence of moisture in the interface. The last floor behavior, bending, can be found with alternating strong and weak floor strata. High horizontal stresses will confine the strong strata while the weak strata is unable to accumulate the stress, and pushes the overlying strata upwards [53].

The stability of the mine floor is dependent on the thickness of the subcoal strata, the competency of the subcoal strata, and any movement that may be occurring. A weak floor rock overlying a strong rock will decrease stability with increasing thickness. A strong floor rock overlying a weak rock will become more stable with increasing thickness. Wear on the mine floor may also decrease its stability as fractures are created. These fractures could expose an incompetent subcoal strata layer, which decreases mine stability, especially if moisture is allowed to collect there, exacerbating the problem [54]. It should be noted that for the design of standing support systems, floor heave is considered uncontrollable movement, and the support must be able to survive these movements rather than prevent them. Floor heave can even transfer enough stresses, through the standing support, to damage the roof and cause additional roof instability [39].

2.5.3 Pillar Behavior

Pillars act as the natural, and most significant, support mechanism in underground mining, and as such their performance is a widely studied, and behavior highly variable. The most common types of pillar behavior are displayed in Figure 2.14, although not all are commonly found in coal measure rocks.

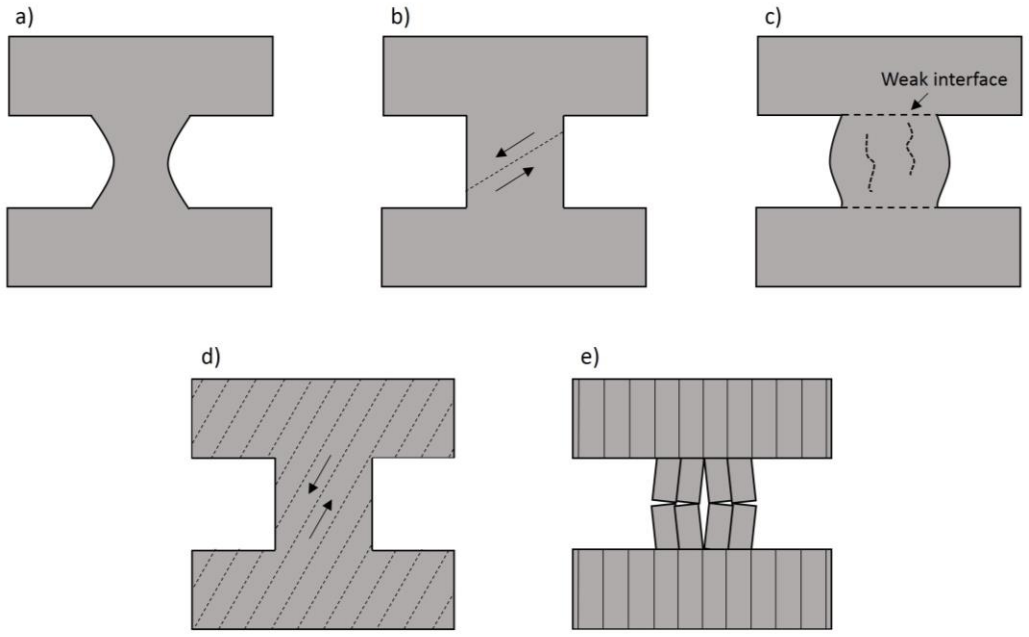

Figure 2.14: Deformational behavior of pillars (after [16])

Figure 2.14a shows pillar spalling, a common pillar behavior in high width/height ratio pillar. This is often an indication that a pillar may be overstressed. Figure 2.14b shows the formation of a dominant shear zone through the pillar, which daylights on both sides providing the possibility of failure along this plane. Figure 2.14c highlights a pillar behavior that may occur when the interface between a pillar and the overlying or underlying strata is weak and does not provide confinement at the top or bottom of the pillar. This allows the pillar to "bulge" or "barrel" which promotes internal fracturing. Figure 2.14d, much like Figure 2.14b, shows a pillar susceptible to failure along discontinuities, although this failure is more related to the geologic structure of the surrounding rock mass and its fracture network rather than one predominant shear

zone feature. Lastly, Figure 2.14e shows a pillar buckling due to a prevalent vertical schistosity or foliation [16].

2.6 Laser Scanning

Three-dimensional laser scanning, known as LIDAR, is a method of remote imaging which collects a high-resolution three-dimensional coordinates of a scanned scene, called a point cloud. Laser scanning has been employed in many different environments, including aerial, terrestrial, and underwater environments [59]. In recent years laser scanning has seen increased use in underground excavation applications, including the measurement of overbreak or underbreak, mine mapping, and geotechnical characterization. Several studies highlighting these laser-scanning applications are presented.

Fekete et al. (2010) apply laser scanning to characterizing geotechnical properties of a rock mass, such as the location of discontinuities, their orientation, frequency, and roughness. In addition, they also identify locations of underbreak and overbreak in tunneling, which is very similar in concept to the practice of monitoring rib and roof movement. These data were be collected quickly, without interfering with operations, and detailed the rock mass in both the small and large scale. Several issues were encountered during scanning, such as active mine workings constraining the visible scene in addition to occlusions caused by the rock mass itself due to the roughness of the rock face. This could be particularly troublesome if the number of scans are operationally limited, however the range of viewing angles available in the tunnel profile may be sufficient to overcome the occlusions in certain area, especially when discontinuity sets repeat [59].

Huber and Vandapel (2006) used a cart-mounted laser scanning system to model the MSHA research mine in Bruceton, PA. The work was a proof of concept, but through 23 scans, a large section of the research mine was successfully modeled with approximately 1 cm geometric errors. A high degree of overlap was found to be necessary to correctly register laser scans with one another [60]. Similarly, Ferguson (2003) showed the application of three-dimensional mine modeling with an automated robotic transport system. Three mines were modeled, including two that were not accessible by people, and the robot was able to successfully render the mine workings

in three-dimensions, while avoiding hazards. Also included in this research were new lazy techniques for data association and a fast technique for improving navigation of rough terrain [61].

Mah et al. (2013) applied laser scanning to measurement of joint orientation, surface roughness, and roughness anisotropy. They were able to do this successfully and significantly less laboriously than when these measurements are performed by hand. The authors suggest that the limited number of measurements taken when hand-characterizing these values can lead to biases which are not present in the laser scanned data set [62].

Fekete and Diederichs (2012) described a workflow and application of laser scanning to modeling tunnels for both rock mass characterization and stability analyses. They were able to reconstruct the tunnel geometries and use the high-precision point clouds to improve discontinuum modeling of the openings. An ability to highlight the impact of individual parameters is suggested as an advantage of the large amounts of data collected through laser scanning, as well as a reduced data collection time [63].

Using laser scanning for monitoring underground mine deformation requires two conditions to be satisfied: the ability to generate accurate and precise three-dimensional underground mine models, and the ability to quantify ground movements. Both have been satisfied, with the aforementioned mine mapping, and the surface mining application of terrestrial laser scanning to slope or rock face monitoring [64][65]. It is likely the cost associated with laser scanning, and a technical barrier to MSHA approval, that has thus far precluded its use in displacement monitoring. The focus of this research will remain on photogrammetry for this reason, however, many of the point cloud manipulation methods for determining ground movements are shared between these remote sensing technologies, and the advancement of one technique can often mean the advancement of the other.

2.7 Photogrammetry

The increasing adoption of remote sensing techniques such as laser scanning and photogrammetry removes the restriction of point measurements by allowing entire entry profiles to be measured through time-lapse analyses. Photogrammetry is a form of image measurement that derives the geometric properties of an object or scene from one or more photographs. The dimensions of an object are reconstructed using bundles of rays comprised of an image point and

a perspective center for each camera, as shown in Figure 2.15. If the geometry within the camera as well as the geometry of the position of the camera in three-dimensional space are known, the ray bundles can be defined as well. A large number of rays will create a dense network, from which images can be oriented along with their associated points through a bundle triangulation with high geometric strength [9].

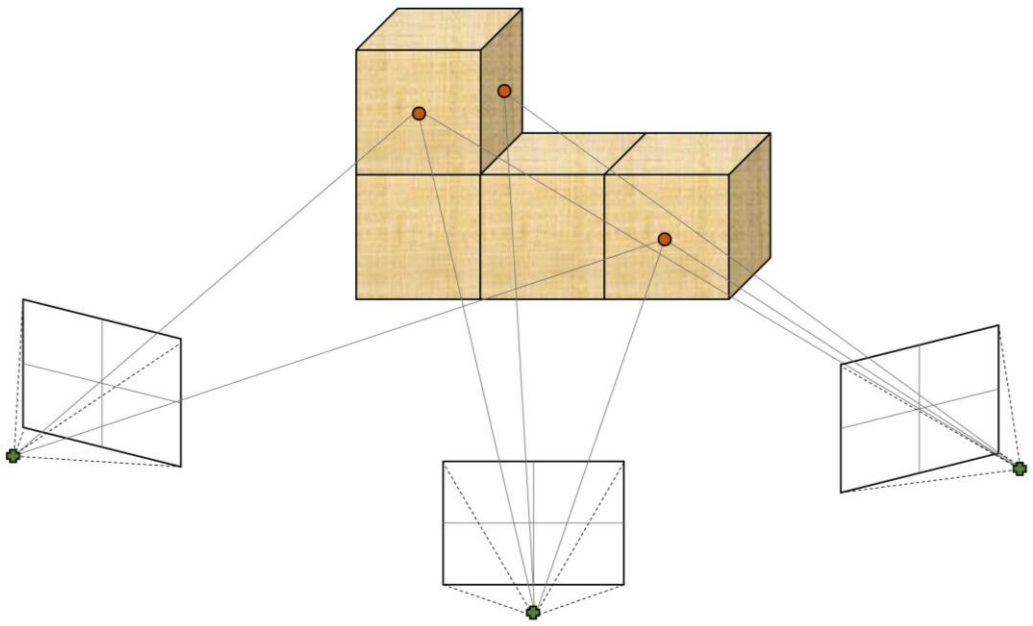

Figure 2.15: Photogrammetric measurement

The primary purpose of this process is to recreate a three-dimensional object in a digital format [9]. This study will focus on close range digital photogrammetry (CRDP), which is defined as the technique of measuring objects closer than 100 meters with digital camera positions that surround the object or are contained within it [66]. The science of photogrammetry is nearly as old as the camera, originating in 1851 with Aime Laussedat [67].

Modern photogrammetry applications are too numerous to list, but the applications are as varied as generating 3D city models, reconstruction of damaged buildings, evidence documentation, measurement of large civil engineering sites, tooth measurement, accident recording, and measuring wave topography [9]. Several free, user-friendly options exist for casual photogrammetry such as Microsoft's Photosynth [68] [69], or Autodesk's 123D Catch [70] [71] where users can generate three-dimensional objects or scenes without photogrammetric expertise.

Photogrammetry has a variety of interdisciplinary applications, but the challenges faced in underground mine environments are unique, such as dark, dusty conditions with minimal features and, depending on the location, consideration of normal mine operations or intrinsic safety of the photography equipment. Despite these challenges, photogrammetry has been converted to use for a variety of underground mine applications.

Styles et al. (2010) used photogrammetry to reconstruct a pillar in three-dimensions. They stated a need for surveyed locations on the pillar to connect the multiple pillar faces. Brittle fracture characterization, geotechnical mapping, and observation of pillar geometry post-spalling were successfully performed using the 3DM Analyst and Polyworks software packages [72].

Kim et al. (2005) performed photogrammetry using image pairs at a tunnel construction site with a new algorithm for interpreting joint orientations. Major joint sets were obtained using the photogrammetric reconstruction, with maximum errors in the direction of the tunnel advance less than 2 mm. The approximate time that was required to survey a single rock face in this experiment was 14 minutes, which is not only faster than manual joint mapping, but higher quality data was produced [73].

Somervuori and Lamberg (2010) performed a number of experiments with photogrammetry, among them modeling several tunnels in Finland and Sweden. Using the 3DM Analyst Mine Mapping Suite, auxiliary lighting, and a tripod mounted DSLR camera, and known control points, they successfully reconstructed a variety of tunnels. Reported accuracies are 1 mm with between 10 and 20 photos and an image capture time of between 15 and 20 minutes depending on the tunnel environment. The photogrammetric accuracy was high enough to also be able to generate a stereonet of joint features and determine shotcrete thickness [74].

Heal et al. (2004) mapped a simulated rock burst in a time-lapse manner using CSIRO photogrammetry system, specifically designed for structural mapping of rock faces, and a DSLR camera. The system was designed to identify areas of rock bulking and ejection, deformation of surface support, and rockbolt displacement. While clear volumes of material were not presented, the experiment highlights another application of photogrammetry to underground mining [75].

These underground photogrammetry experiments are summarized in Table 2.1. Applications of photogrammetry in underground excavations is largely limited to discontinuity characterization. Several authors have briefly mentioned the ability to quantify rock movements with photogrammetry, but this research is still in its infancy. In addition to this, the processes

presented would suggest photogrammetry could only be performed using high cost equipment and software, expensive stationary lighting, and intrusive collection techniques, albeit for only a short period.

Table 2.1: Summary of underground photogrammetry studies

Authors	Environment	Camera	Software	Lighting	Application
Styles, Zhang, Stead, Elmo, Roberts, and Yanske (2010)	Underground lead mine	Canon EOS 5D Mark II (20 mm lens)	3DM Analyst, Polyworks	Three separate panels of LEDs 5 m from the face	Characterization of the fracture network and pillar damage
Kim, Kim, and Won (2005)	Tunnel	Q-cam MicroPublisher	Non-commercial	Two 500 W mercury lamps	Discontinuity mapping
Somervuori and Lamberg (2010)	Tunnel	Canon Mark D (varying lens sizes)	3DM Analyst	Portable 2000 lumen LED	Discontinuity mapping and shotcrete thickness assessment
Heal, Hudyma, and Potvin (2004)	Underground nickel mine	Sirovision camera	Sirovision software	Not stated	Rock bulking and ejection quantification
Hagan (1980)	Hanging wall	Two Nikon (35 mm lens)	Non-commercial	On-board flash	Discontinuity mapping
Singh, Chapman, Atkinson (1997)	Simulated sandstone roof	CCD Camera	Non-commercial	Laboratory	Measurement of a textureless, and featureless object with laser dots projected on the surface

Monitoring underground deformations requires both the ability to record movements with respect to time and record those movements accurately and precisely. Seven criteria are proposed by Maerz et al. (1996) which need to be satisfied when measuring tunnel profiles: speed, accuracy and precision, simplicity, low cost, reliability, versatility, and clarity of results [76]. These criteria will be used as a baseline for evaluating the potential of photogrammetry as a monitoring and measurement tool in underground mining environments.

2.7.1 Speed

Mine geometries are in a constant state of change, due to ore extraction increasing the extent of the excavation and altering stress fields. In addition to this, equipment frequently travels

in the underground workings, inhibiting monitoring of the roadways and limiting the number of feasible monitoring technologies, especially near active faces where monitoring may be most important. Underground measurements must be performed without interfering with mining operations, and these measurements must be completed, analyzed, and addressed before their use is no longer relevant.

Industrial photogrammetric systems can be broadly separated into *online* and *offline* systems. Online systems provide nearly real time measurements, while offline systems separate the data acquisition from the data processing, forcing a staged process [77]. Offline systems are likely to be the instrument of choice until communications networks underground are sophisticated enough to allow the real time streaming of large quantities of data. However, offline systems are still capable of significant speed increases over traditional methods. In the case of fracture mapping, Hagan (1980) noted a reduction in mapping times of 90% [78], while Tonon and Kottenstette (2006) claim a five times faster data acquisition through photogrammetry [79].

2.7.2 Accuracy and Precision

The accuracy and precision of photogrammetric measurements is scalable to meet the needs of different engineering projects. In typical industrial applications where the subject's largest dimension is about 1 m to 100 m, precisions have been achieved less than 0.1 mm on the smaller end and 1 cm on the larger end [9]. For more qualitative estimates of accuracy and precision, Hagan (1980) found negligible errors in dip and dip directions during fracture mapping using photogrammetry [78]. Rezaei and Rahnama (2013) applied photogrammetry to monitoring slope movement with both a camera and total station and found reasonable correlation between the two methods [80]. Modern industrial CRDP accuracy is independent of the operator's expertise, assuming correctly adopted operational procedures [77].

2.7.3 Simplicity

As of July 2013, 65% of Americans own a standalone digital camera, and 80% own a mobile phone, most of which contain a digital camera [81]. The data acquisition side of CRDP is, at its core, taking pictures with a digital camera. Taking pictures is a process that has proliferated

contemporary culture, and should not be difficult to apply to underground monitoring from an operational data acquisition standpoint. The complicated nature of CRDP is computational (although proper data acquisition techniques can decrease the computational complexity) but still variable. As mentioned previously in Section 2.7, several free, user-friendly software packages do exist [69][71], and with increasing proliferation of the technology and increasing commercial availability of computational power, there is no reason to assume a trend towards the technology becoming less accessible.

2.7.4 Low Cost

It is impractical to adopt a monitoring tool with costs greater than the benefits. There are three primary costs associated with CRDP: operational, hardware, and software. The operational costs will depend on the scale of the project, but if similar trends are to be expected in underground dimensioning as were seen in fracture mapping [78][79], the speed of data collection should improve over installing and collecting data from extensometers or other point measurement devices.

The costs for camera systems and software packages used in the operation will vary significantly depending on the desired level of precision and ease of use. Both components, software and hardware, are developing at a rate that would make cost estimating in this format irresponsible, however, the scholarly consensus suggests that photogrammetry offers a low-cost alternative to laser scanning, the most similar 3D data acquisition method [82].

2.7.5 Reliability

Conditions in underground mining present unique challenges for monitoring equipment. A CRDP system would need to be able to withstand a wide range of temperatures, humidity, and dust levels. The presence of dust could, depending on its prevalence and the lighting method, create a significant number of features that are unique to each photograph. In addition to ruggedness, in underground U.S. coal mines, the system may need to be either intrinsically safe or explosion-proof according to 30 CFR § 18 (2014) [83] depending on the subject area.

2.7.6 Versatility

A CRDP system used in a mining environment must be capable of measuring different shapes and sizes of excavations. As mentioned in Section 2.7, examples of CRDP applications include generating 3D city models, reconstruction of damaged buildings, evidence documentation, measurement of large civil engineering sites, tooth measurement, accident recording, and measuring wave topography [9]. Changing shapes and sizes of tunnels is no more drastic than changing the scale of photogrammetry from measuring the dimensions of civil engineered dams to the dimensions of teeth.

Most current photogrammetry software packages are negatively impacted by occlusions, number of photographs, lighting, subject movement, and gloss [84]. The movements expected underground are not occurring at a rate that should negatively impact the ability to find common surface features, and the number of photographs is controlled by the researcher. The gloss of the subject may be an issue depending on the support being monitored. Wooden cribs, for example, do not possess significant reflective properties, while steel supports can produce significant glare from nearby light sources. The largest issue associated with changing tunnel geometries is likely to be the difficulty providing light. If light sources are changing (cap lamps and a flash at different camera locations), the surface features will show different coloring. Some systems address the problem of lighting by providing high-powered portable lights that travel to the area of interest [74]. In the case of particularly featureless surfaces, CRDP has also been applied to featureless objects, by projecting features onto them, as demonstrated by Singh et al. measuring a sandstone roof [85].

2.7.7 Clarity of Results

While data may not be immediately usable in offline systems, photogrammetry does offer a separation of workloads and flexibility in timing. Data acquisition and processing can be performed at different locations and at different time, by personnel of varying expertise [86]. In addition, the results from photogrammetry provide a permanent record that can be referred to later for both ground control and legal issues [87].

Chapter 3 Determination of Volumetric Changes from Laser Scanning at an Underground Limestone Mine

B. A. Slaker, Graduate Research Associate

E. C. Westman, Associate Professor

B. P. Fahrman, Graduate Research Associate

Geomechanics Observation and Imaging, Mining and Minerals Engineering

Virginia Polytechnic Institute and State University, Blacksburg, VA, 24061

M. Luxbacher, Mine Manager, Lhoist North America

This work is published in *Mining Engineering*, Volume 65, Issue 11

3.1 Abstract

The ability to detect and quantify ground movements in underground mine workings is of the utmost importance to the safety of miners and continuity of operations. Rib sloughage is one of the most common forms of underground deformations. Remote sensing techniques, such as laser scanning, can be used to quantify this rib sloughage, by recording precise, time-lapse point clouds of mine workings. In order to determine sloughage volumes and locations, two sets of laser scans were performed 42 days apart at a working section of an underground limestone mine. During this period, significant sloughing and scaling occurred, allowing for differentiation between the initial and final point clouds. Volumetric changes of 2.3 – 2.6 m^3 were detected on rib faces during the time-lapse study. In addition, displacement in the mine roof was, as expected, not detected, suggesting well surveyed scans and an appropriate scan resolution.

3.2 Introduction

Understanding rock mass stresses and the deformations associated with them is incredibly important in the design of underground mines and ensuring the safety of the miners working in them. Current techniques for monitoring underground stresses and deformations involve collecting point measurements, through methods such as borehole relief methods or extensometers [88]. These instruments can only record data at the installation location. The extent of deformation or magnitude of stress for the surrounding areas must be extrapolated. Using wide-area monitoring techniques, such as terrestrial laser scanning, it may be possible to compliment current monitoring practices by providing non-invasive and large scale measurements.

Three-dimensional laser scanning, also known as LiDAR, is a method of remote imaging which collects a high-resolution three-dimensional point coordinates of a scanned scene, called a point cloud. Laser scanning has been employed in many different environments, including aerial, terrestrial, and underwater environments [59]. In recent years laser scanning has become more popular for underground excavation applications, such as measuring underbreak and overbreak [59], automated mine mapping [60] [61], surface roughness analysis [62], and rock mass characterization [63], [89], [90].

3.2.1 Laser scanner theory

The FARO Focus3D laser scanner [91] used in this experiment measures distances through "phase shift" technology, which involves the projection of constant waves of varying frequencies. Rather than measuring the time required for a reflection to be recorded after a laser pulse is sent out from the scanner, the phase shift in the waves of infrared light is recorded and used to determine the time traveled, as shown in Figure 3.1, where t_m, the phase shift, is directly proportional to the time it takes the wave to travel the unknown distance at the speed of light.

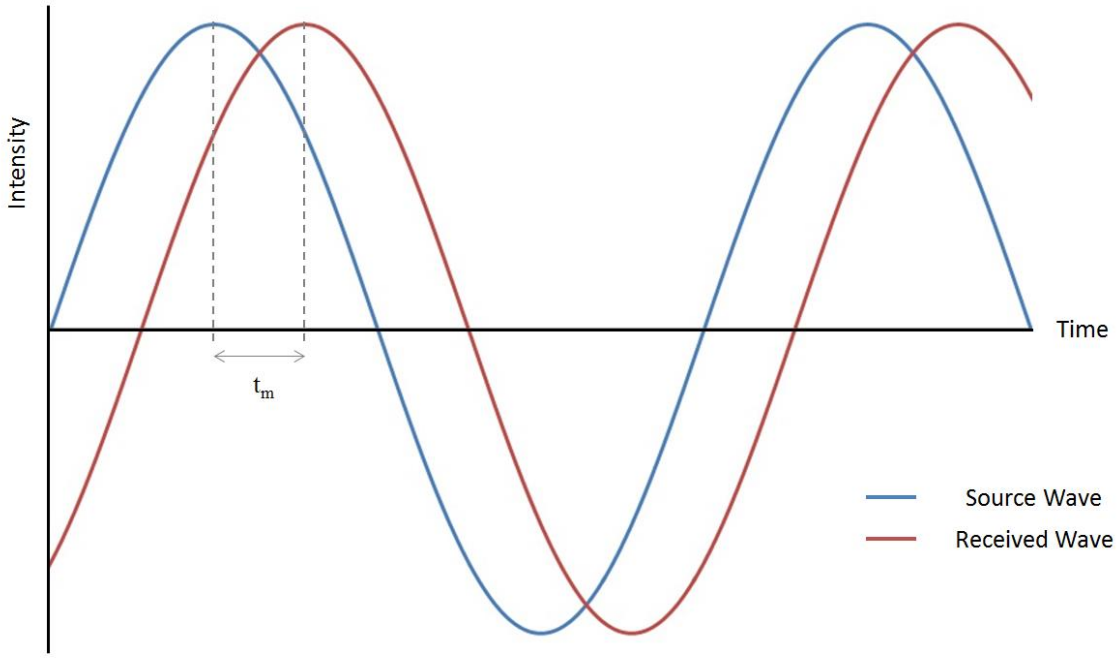

Figure 3.1: Phase Shift distance determination

If the phase shift is exactly 360°, the measured distance will be 0. Any measurements at a phase shift of 360° or beyond will then be ambiguous, requiring that several modulation signals with different frequencies be applied to remove the ambiguity. The highest frequency, and thus the shortest wavelength, will determine the precision to which measurements can be made. The lowest frequency, and thus the longest wavelength, will determine maximum distance that can be scanned without ambiguity [92].

3.3 Methods

Testing the application of laser scanning for roof sag monitoring began at an underground limestone mine. Very little roof and rib deformation was expected from the limestone mine, but differences in roof and rib geometry due to scaling or sloughage would allow for testing of monitoring displacement. Therefore, scanning was performed near the working section, where the most scaling or other displacement was expected to take place. One pillar in this area, Pillar B, was reported by the mine to be experiencing significant sloughage and was scanned for changes.

Pillar A was not reported to be experiencing significant problems, but it was scaled between the two laser scanning trips.

Two separate trips were required to the underground limestone mine to gather data for a time difference analysis. The two trips were separated by 42 days. During the first set of scans, a total of six scans were performed, with all six keeping Pillar B visible, shown in Figure 3.2, and three of the scans performed in an intersection adjacent to a working section. These scans were performed at a resolution of 43.7 million points per scan. The second set of scans contains a total of five scans: two including coverage of Pillar A, two including coverage of Pillar B, and one between the two scans. The locations for each scan are given in Figure 3.2. Scans were not performed in the exact same locations because of uncertainty in original scan location, inaccessibility due to the presence of water, and the presence of known survey points.

Figure 3.2: Mine map showing laser scanner placements in relation to pillars of interest

Each scan places the recorded points on its own local coordinate system. In order to join the multiple scans together, spherical and checkerboard targets were used. These targets provide recognizable common points in each scan, allowing them to be joined together in three-dimensional space. This process is referred to as referencing. The checkerboard targets consisted of four 8.9 by 8.9 cm squares, alternating black and white. These targets required an angle of incidence smaller than 45 degrees to ensure proper referencing. The spheres used for the referencing were 6.6 cm in diameter. The spheres have the advantage of being targetable from any angle, but require a higher resolution scan to detect the curvature of the sphere. This rendered some of the spherical references unusable.

Four checkerboards and two spheres were used at each scan location. An attempt was made to make each checkerboard and sphere viewable from each location. Proper referencing only requires two common targets, when using the laser scanner's inclinometer, but the redundancy was included to account for potential surveying errors or scanning oversights.

At each scan location the position of scanning targets, as well as the laser scanner, were surveyed to allow for integration into mine coordinates. The two scan locations, while near to each other, were discontinuous, so the surveyed coordinates were used to join them.

3.4 Data Processing

In order to create a three-dimensional displacement map of the mine, the raw x, y, z coordinate data were converted into point clouds using FARO's Scene software [93]. These point clouds were then subsampled to manageable resolutions by removing a specified number of rows and columns, subsampled to a manageable size, triangulated, differentiated, and colorized based on the mesh differences. The FARO Scene software was used to reference the scans and export them, uniformly thinning the data set as necessary to meet system specifications. Maptek's iSite software [94] was used to further manipulate the point clouds, including removal of outlying points, mesh generation, and computing distance between two meshes.

3.5 Results

The goal of this study was to determine if roof or rib movement could be detected using time-lapse laser scan data. As no measurable roof or rib convergence was expected at the underground limestone mine, sloughing of material from a pillar or interest was instead used as a proof of concept. The volume of material that had sloughed off during the 42 day period between scans is unknown, however, areas of change can be detected by comparing pictures from the initial scan and the final scan. Figure 3.3 shows the initial state and final state of Pillar A. Figure 3.4 shows the initial and final state of Pillar B.

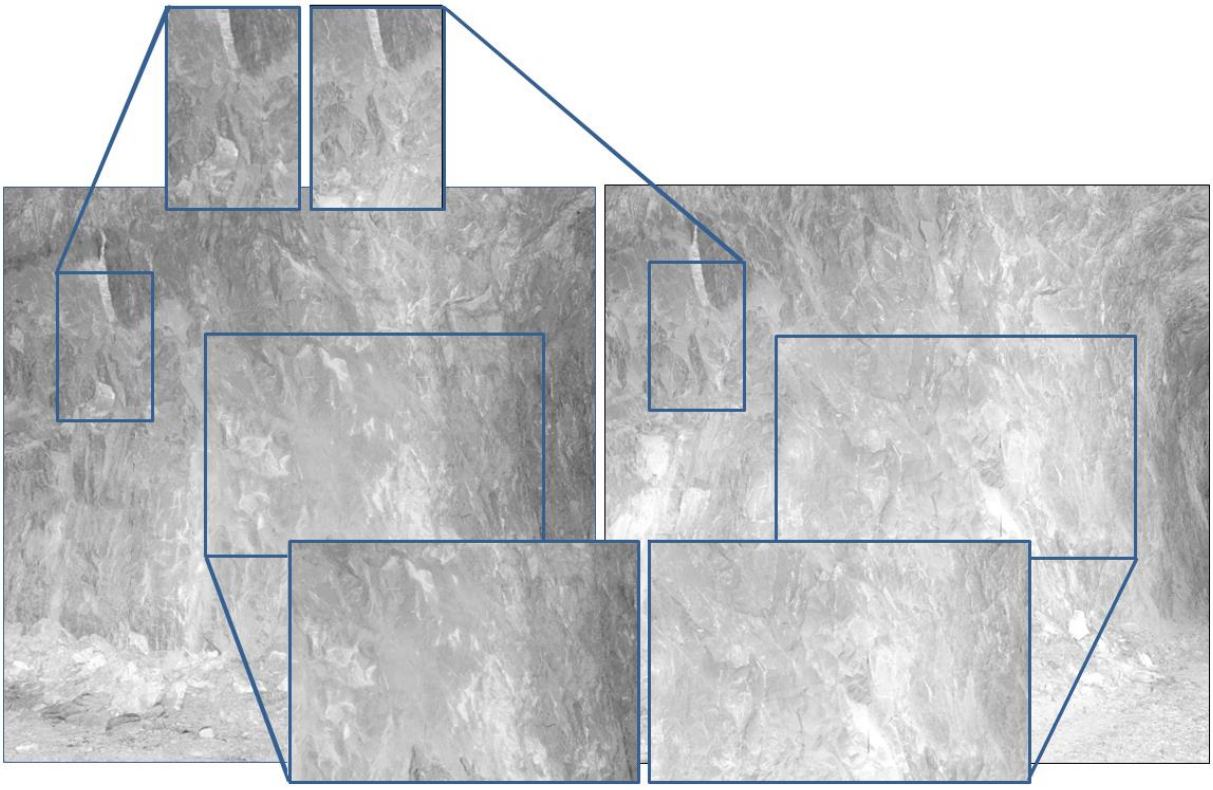

Figure 3.3: Difference between the initial and final scan at Pillar A, with areas of change highlighted

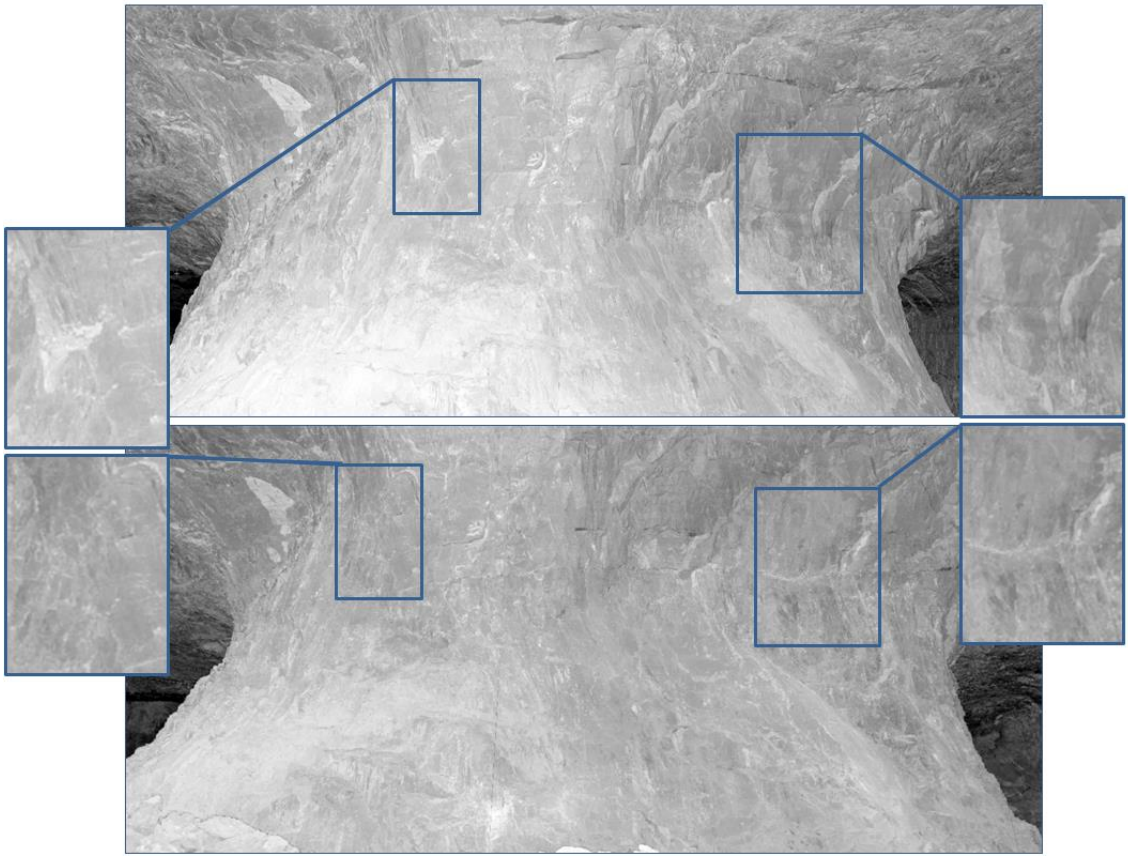

Figure 3.4: Difference between the initial and final scan at Pillar B, with areas of change highlighted

The change in pillar dimensions from the initial to final scan is difficult to recognize visually from features alone. Feature changes, noted from mesh comparisons, were highlighted in Figure 3.3 and Figure 3.4 to illustrate that the change can be verified.

Point clouds were generated for the 11 scans, each taken at a resolution of 43.7 million points. At a distance of 10 m, the distance between adjacent points at this resolution is 7.5 mm. This resolution was reduced to approximately 14.9 mm point spacing to satisfy computational limitations. With rib sloughage in this study affecting areas greater than 1 m2, the resolution is deemed high enough to determine sloughing boundaries accurately.

The magnitude of displacement is visually realized by determining the difference between two surfaces, created by triangulating the initial and final point clouds separately. The change in pillar geometry from the initial to final scan (at the same viewing location shown in Figure 3.3) is shown in Figure 3.5. The change in pillar geometry from the initial to final scan (at the same viewing location shown in Figure 3.4) is shown in Figure 3.6.

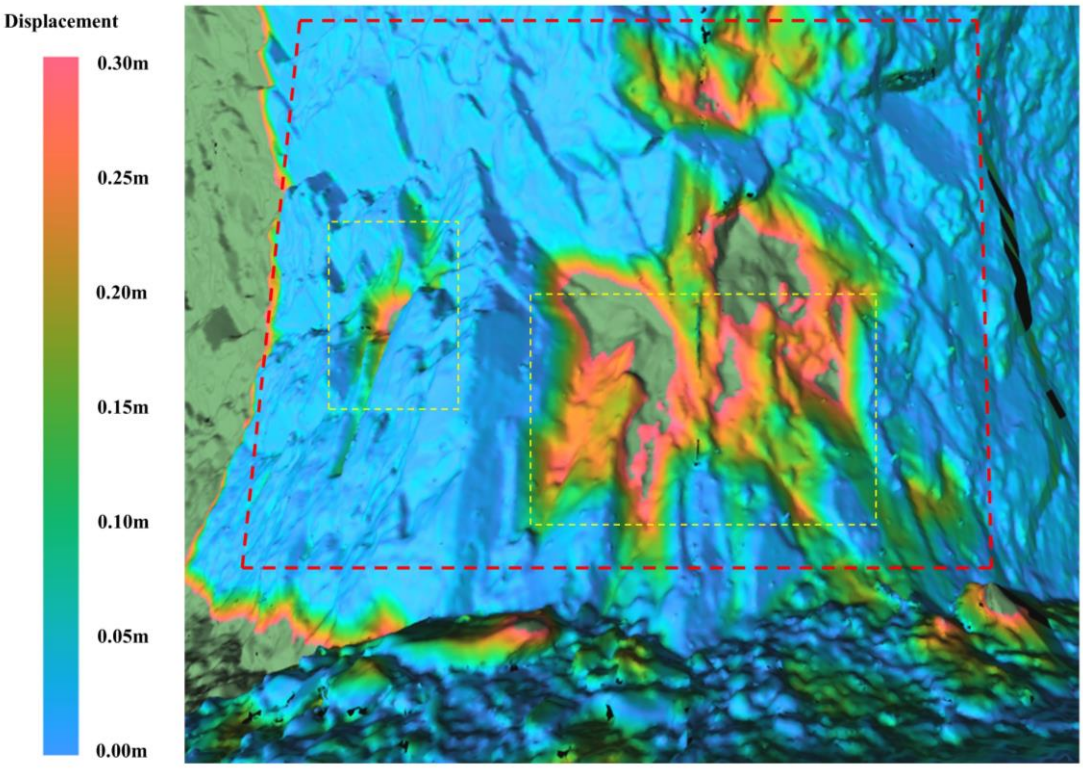

Figure 3.5: Volumetric change on Pillar A with highlighted areas containing noticeable visual change

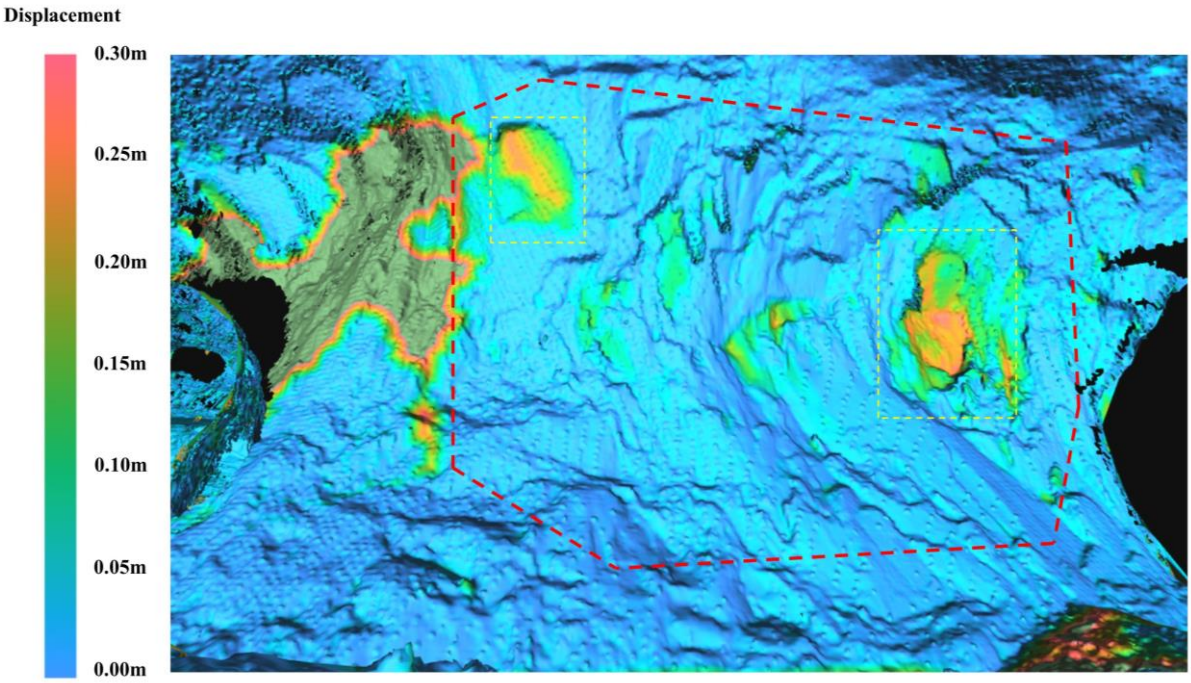

Figure 3.6: Rib deformation on Pillar B with yellow boxes denoting areas containing noticeable visual change from Figure 4, and the red dotted line enclosing the area for deformation calculations

The change shown in Figure 3.5 and Figure 3.6 is an absolute value, meaning the accumulation of material at the base of the pillar and the regions where material has sloughed off, will both show positive displacement. The assumption was made that rib dilation would be negligible compared to sloughing, which may not be applicable to mine environments where both material sloughage and rib dilation are significant. Roof or rib convergence would be represented by a uniform and detectable color change, while scaling or sloughing would likely be represented by pockets of color change. The exception to this would most likely occur in mines with very poor rib conditions where sloughage is expected to be occurring throughout the majority of the scanned area. The rock mass displacement measured in this study is rib sloughing and scaling. The highlighted areas in Figure 3.5 and Figure 3.6 are the same as those in Figure 3.3 and Figure 3.4, allowing for visual confirmation of the displacement.

The displacement observed in Pillar A can be visually confirmed in Figure 3.3. A surface area of 76 m^2 is enclosed by the red dotted line, and this area experienced a net volumetric change of 2.3 m^3 when comparing the first and second triangulation surfaces. This value for this change is not an absolute value, and accounts for both positive and negative changes. The positive volumetric change indicates a net change into the material, suggesting a large amount of material has sloughed off. The displacement observed in Pillar B can be visually confirmed in Figure 3.4. A surface area of 109 m^2 is enclosed by the red dotted line, and this area experienced a volumetric change of 2.6 m^3.

The precision of the results cannot be determined without collecting the volume of material displaced from the rib, which was not logistically feasible in this experiment. The areas of displacement can be visually confirmed from time-lapse images, and the magnitude of displacement is reasonable for the rib being studied, according to operator experience.

No change was detected on the mine roof. If the displacement detected in the ribs was due to artifacts, an indication that the triangulation may be too coarse, those artifacts should also appear on the roof. No displacements are detected in the roof, a result of high scan resolution and surveying accuracy. The ability to rely on laser scanning as a deformation measurement tool is dependent on obtaining precise time-lapse measurements.

3.5.1 Future Work and Sources of Error

The FARO Focus3D reports accuracy to within 1 mm, however, the accuracy depends on more than the ability to record the precise location of a point. There is error associated with referencing targets as well as error associated with surveying. Errors in referencing are due to the center points of checkerboard targets or spherical targets being registered at different locations, due to their angle with respect to the laser scanner or the resolution of the scan. Surveying error is generated initially when locating the first set of checkerboard targets, and placing the scans on mine coordinates. This has little impact on the initial set of scans, but when comparing scans in a time-lapse manner, this error becomes more meaningful. In this study, the targets were not fixed mine surveying points, resulting in a change of location, requiring another set of surveyed coordinates. The expected error due to these practices is small, but if small-scale convergence is a concern, it can mask those movements.

One barrier remaining in the use of laser scanning as a deformation monitoring method, in coal, is the permissibility of the laser scanning equipment. The FARO Focus3D is not permissible in accordance with Title 30 of the Code of Federal Regulations, and as such may not be taken inby the last open crosscut in an underground coal mine. Depending on mine conditions and the scanner used, it may be possible to obtain a waiver, allowing for scanning in these areas. Given the low entry heights and narrow entry widths in underground coal mines, the ability for the laser scanner to generate a detailed point cloud of the roof, ribs, and floor of the working section may also be limited, largely due to the angle of incidence requirement on the checkerboard targets.

3.6 Conclusion

The detection of volumetric changes has been successful and quantifiable through laser scanning in an underground mine environment. The magnitude and location of deformation can be determined through noninvasive time-lapse analyses. Large entry areas can be scanned quickly, and at a distance, allowing operators to assess the amount of displacement occurring without extrapolating the results of point measurements. The lack of deformation detected in the roof is indicative of a high precision in the triangulation generation and comparison. To quantify the precision of displacement monitoring through laser scanning, future tests where the volume of

material removed is known will be required. Additionally, small degrees of surveying error and the chosen triangulation resolution appear to have negligible effect on the ability to detect ground deformations.

The results obtained in this study support the ultimate goal of this project, which is to improve mine safety by developing a more precise, accurate, and comprehensive understanding of ground response to excavation. Laser scanning has proven well suited for measuring rib displacement in a cavernous underground mine setting. The principles that govern displacement measurement through laser scanning do not restrict its use to rib monitoring, but can be applied to monitoring roof and floor behavior as well. Rib displacement was merely chosen as the most convenient application of this monitoring method.

Acknowledgement

This work is supported by NIOSH (contract 200-2011-40313) through the Capacity Building and Ground Control Research for the Mining Industry program.

Chapter 4 Identifying Underground Coal Mine Displacement through Field and Laboratory Laser Scanning

B. A. Slaker, Graduate Research Associate

E. C. Westman, Associate Professor

Geomechanics Observation and Imaging, Mining and Minerals Engineering

Virginia Polytechnic Institute and State University, Blacksburg, VA, 24061

This work is published in the *Journal of Applied Remote Sensing*, Volume 8, Issue 1

4.1 Abstract

The ability to identify ground movements in the unique environment of an underground coal mine is explored through the use of laser scanning. Time-lapse scans were performed in an underground coal mine to detect rib surface change after different volumes of coal were removed from the mine ribs. Surface changes in the rib, as small as 57 cm^3 were detected through analysis of surface differences between triangulated surfaces created from point clouds. Results suggest that the uneven geometry, coal reflectance, and small movements of objects and references in the scene due to ventilation air do not significantly influence monitoring ability. Time-lapse scans were also performed on an artificial coal rib, constructed to allow the researchers to control deformation and error precisely. A test of displacement measurement precision showed relative standard deviations of less than 0.1% are attainable with point cloud densities of greater than 3200 pts/m2. Changing the distance and angle of incidence of the artificial coal rib to the scanner had little impact on the accuracy of results beyond the expected reduction due to a smaller point density of the target area. The results collected in this study suggest that laser scanning can be a useful, comprehensive tool for measuring ground change in an underground coal mining environment.

Keywords: photogrammetry, underground mining, coal, displacement measurement

Address all correspondence to: Brent Slaker, Virginia Polytechnic Institute and State University, 100 Holden Hall, 445 Old Turner Street, Blacksburg, Virginia, 24061; Tel: +1 757-880-3050; E-mail: slaker@vt.edu

4.2 Introduction

Underground coal mining remains one of the largest sectors of the mining industry in the United States, producing 343 million tons of coal in 2012 [1]. Due to the prevalence of underground coal mining, a considerable amount of research has been performed with the intention of furthering the understanding of underground rock masses in an attempt to improve mine safety. Understanding rock masses and their behavior around underground excavations is not a simple task, but it is an important one. In the United States, falls of ground in underground coal mines have been responsible for 2300 operator and contractor injuries and 35 fatalities from January 2007, the year of the Crandall Canyon mine disaster, through July 2013 [3]. The injury and fatality rate has been on the decline for the past 50 years, in no small part due to advances in ground control research [4]. In an effort to further the development of tools available for monitoring ground movements, laser scanning is being assessed as it specifically relates to monitoring in the unique setting of an underground coal mine.

Monitoring underground rock movements is important as increasing rate of movements can be indicative of failure [95] and also provide operators with a better understanding of when to install roof support and how much support is required. Common deformation monitoring equipment, such as extensometers, involve point measurements, but developing technologies such as laser scanning offer the ability to measure large portions of mine entries for movement. This study will use induced rib spalling as a means of determining mine displacement, but the principles that govern laser scanning are not limited to monitoring this behavior. All mine displacements within sight of the laser scanner can be imaged in this way, including roof sag or floor heave.

Laser scanning is a method of remote sensing which involves the collection of many three-dimensional coordinates of a scene, called a point cloud. Laser scanning is a robust measurement method, being employed in aerial, terrestrial, and underwater environments [95]. In recent years, terrestrial laser scanning has gained increased popularity in underground tunneling and mining

applications, such as measuring underbreak and overbreak [95], automated mine mapping [60],[61], surface roughness analysis [62], and rock mass characterization [63],[89],[90].

In addition to being able to scan large areas quickly, remote sensing tools such as laser scanning or photogrammetry, can be used to map these surfaces safely from a distance. This can even be performed in the absence of light, which can be a significant concern in dark, underground environments [96]. Conventional surveying techniques may be superior to laser scanning when measuring individual points, but the strength of laser scanning, and the key to deformation monitoring, is examining the movement of modeled surfaces [97],[98]. Laser scanning does suffer from an ambiguity associated with the target referencing algorithms and triangulated surface generation algorithms, as many of the most popular software packages that perform these tasks are proprietary.

This study is concerned with determining the accuracy and precision of laser scanning measurements for the purposes of measuring underground mine deformation. A FARO Focus 3D laser scanner will be used in these experiments. The laser scanner has a range of up to 120 m, a ranging error of ± 2 mm, can collect up to 976,000 points/sec [91]. It collects data through phase-shift measurement methodology rather than the traditional pulse ranging methods used for data collection at larger distances. Phase shift, also called continuous wave laser ranging, makes use of a modulated wave signal to measure distant objects. Due to the limited power of phase shift scanners, they are restricted to short range terrestrial applications [99].

Measuring underground mine deformation is similar to that of measuring tunnel profiles. Maerz et al. describe seven criteria which need to be satisfied to measure tunnel profiles: speed, accuracy and precision, simplicity, low cost, reliability, versatility, and clarity of results [76]. Each of these criteria is important, but the experiments performed in this study will focus on the accuracy and precision of laser scanning measurements, which is closely related to the speed of data collection. Measuring tunnel deformation with laser scanners has been found to increase the accuracy of identifying displacements over time [96], however these tests were performed in hard rock, rather than coal, which may differ significantly in tunnel geometry.

Concerns with laser scanned subjects include: occlusions or shadows, abrupt texture or shape changes, reflective surfaces, and movement in the scene [82]. All of these problems exist to varying degrees in underground coal mining environments. The targeted area for scanning were the “ribs” which are the non-roof/floor walls lining an entry. These were chosen because they

consist of coal, which can be easily deformed by hand and will not change inadvertently during the experimental time frame, unlike a competent roof rock or a floor disturbed by footprints.

The vitrinite in coal may cause it to exhibit a high degree of reflectance, depending on the rank of the coal [100]. Ranging errors have been associated with laser scanning of different reflective surfaces [101], meaning the reflectance of coal may cause measurement difficulties. Occlusions or shadows can be caused by the roughness of rib face. The roughness of the rib surface may change significantly after entries are excavated due to skin failure. Skin failure is usually described as small pieces of rock that come off the rib due to structural incompetence or the presence of discontinuities in the coal, and does not constitute pillar failure [102]. Unlike mine roof classification, widely accepted or standardized mine rib classifications do not exist, and supporting or controlling rib skin failure is generally performed in a reactive manner [103], and as such it can be difficult to quantify or qualify their spalling behavior. Concerns with movement in the scene are almost entirely limited to dust, as mine entries are usually negligibly dynamic during the period of a scan. The presence of heavy dust can negatively affect laser scanning results, as shown in autonomous vehicle research, where mistaking airborne dust or smoke for objects can create serious complications [104][105]. The level of dust generated will vary by mine and by location within individual mines, but a legal limit for respirable dust in underground coal mines should make the one used in this study typical of other underground coal mines, assuming the study area is away from an active excavation.

While the technology has been applied successfully to similar industrial applications, the unique requirements of taking measurements in the unfavorable conditions of underground coal mines may preclude its use. It is the goal of this study to assess the potential for monitoring ground movements despite the presence of airborne dust and the unique and unfavorable geometry in underground coal mines.

4.3 Field measurements

In the underground coal mine, two scans were performed from the center of an entry for a time-lapse analysis which would allow for differentiation between two point clouds over time. The purpose of the first scan was to establish an initial condition from which volume change could be measured. The second scan was performed in the same approximate location, but after the

removal of coal from the ribs. Coal was removed in six locations, three from a barrier pillar to one side of the entry and three from an interior pillar on the opposite side of the entry as the barrier pillar. Varying amounts of material were removed ranging from tens of cubic centimeters to tens of thousands of cubic centimeters. The locations of the removed material are shown in Figure 4.1, Figure 4.2, and Figure 4.3. The rock dusting of the rib face gives the entry a gray color, and exposing the underlying coal highlights the areas of change in black.

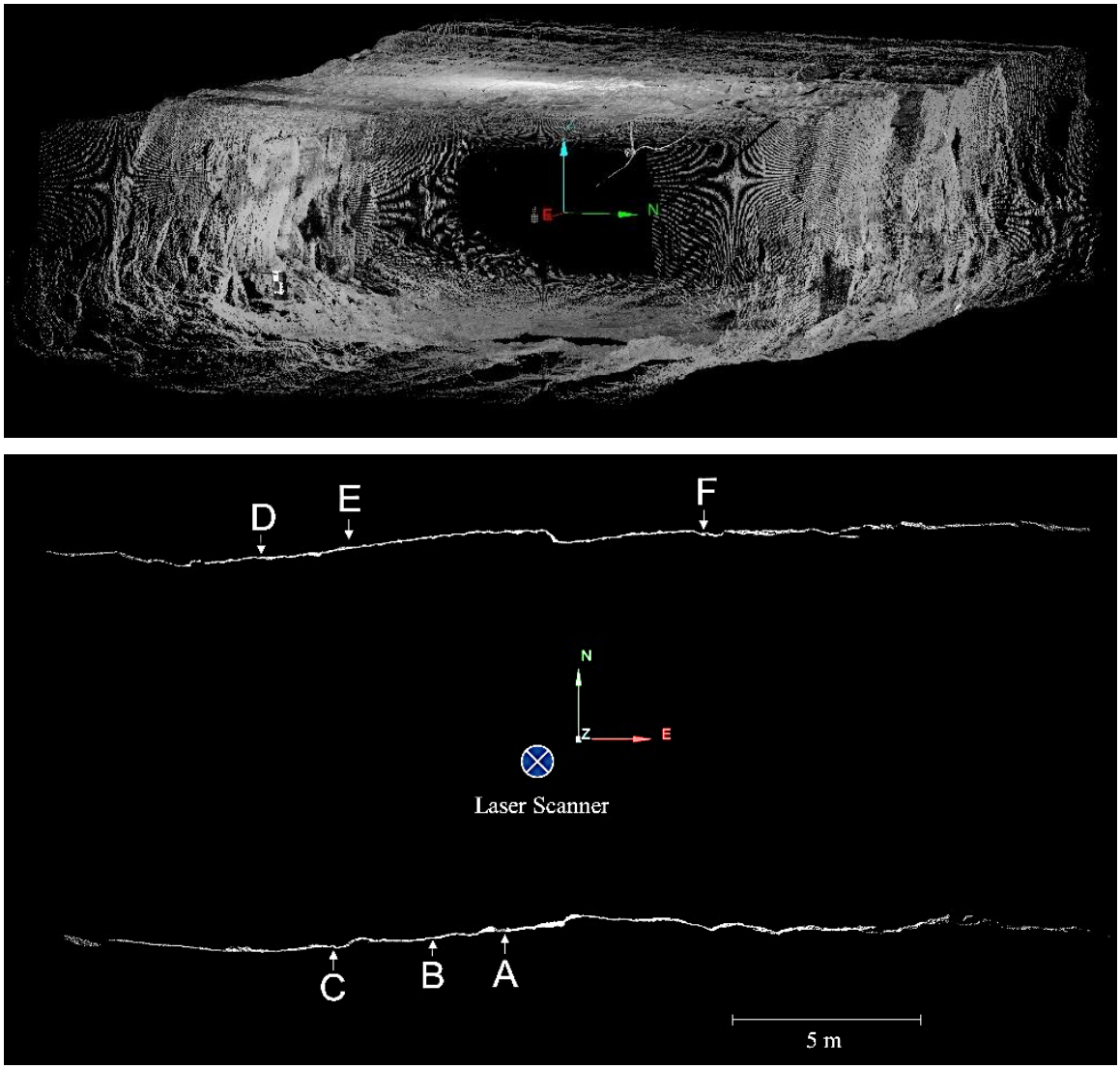

Figure 4.1: Study area and locations of removed coal

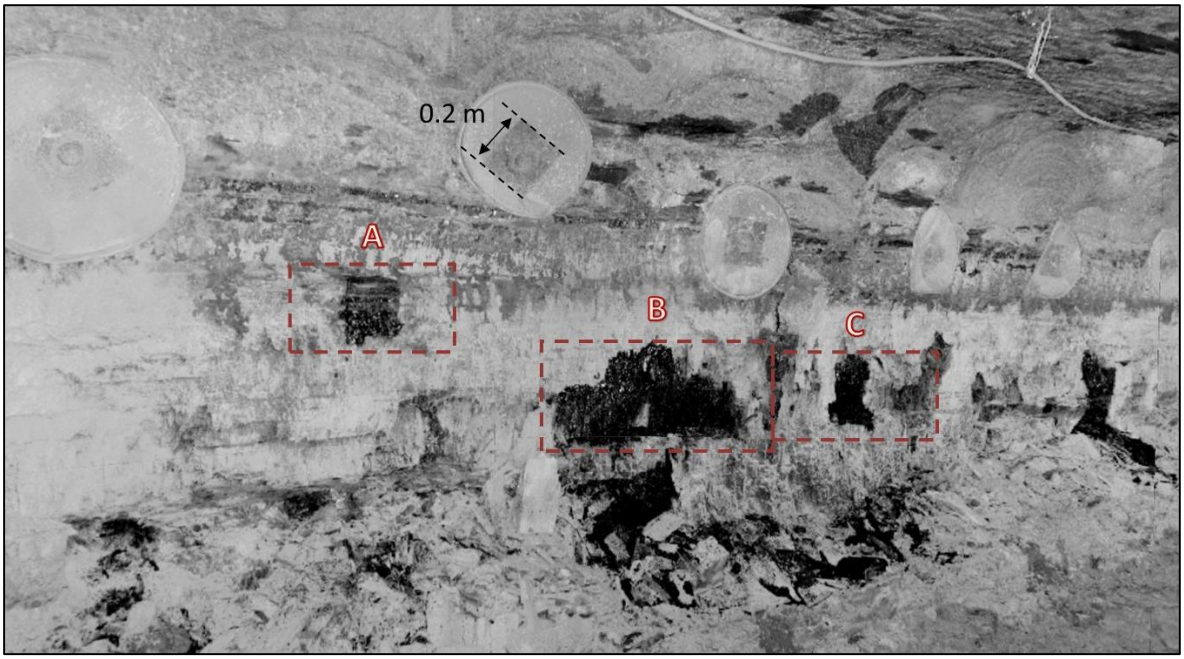

Figure 4.2: Coal removal locations A, B, and C from the barrier pillar

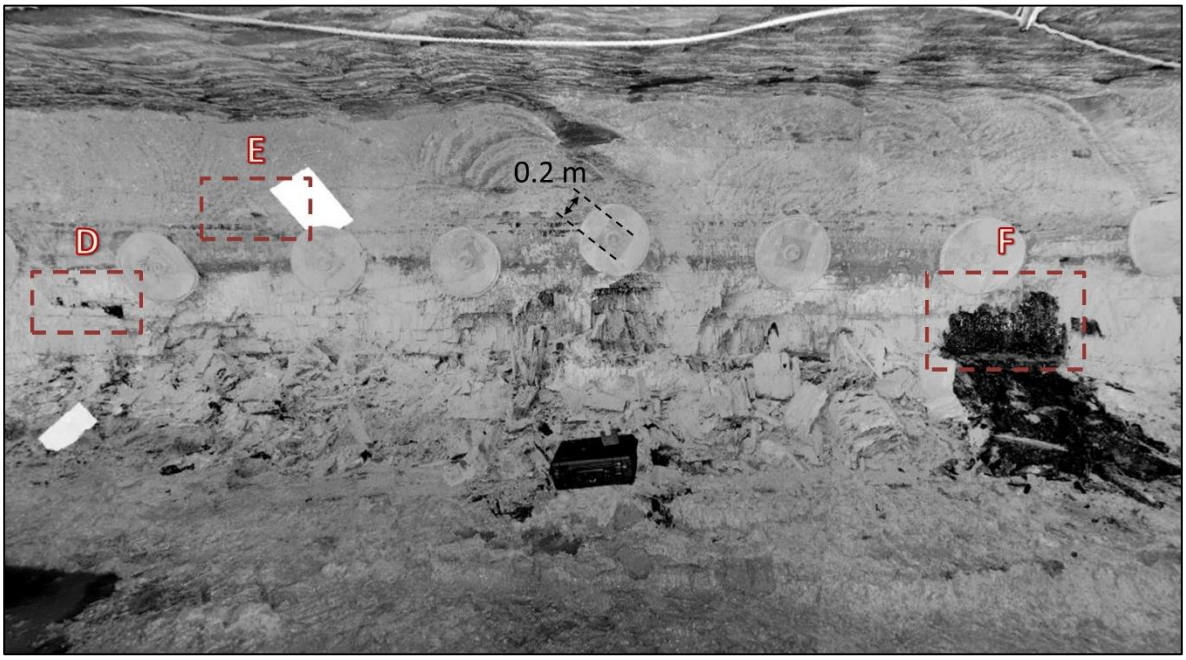

Figure 4.3: Coal removal locations D, E, and F from the interior pillar

Each scan required approximately 7 minutes to perform, not including the time to set up the scanner and references, and approximately 10 minutes elapsed between scans. The scans contained 27.7 million points each and were located roughly 2.3 meters from the barrier pillar, 3.1

meters from the interior pillar, and 1 meter from the roof. At the furthest perpendicular distance, 5.5 meters, the point cloud density on the rib was 76000 pt/m2. A high resolution scan which requires more time than a low resolution scan was performed because it was possible, rather than necessary, merely to ensure enough data was collected. After assessing the computational limitations of processing such large amounts of data, this resolution was reduced in post-processing by 75 percent, through the removal of every even row and column, resulting in a resolution of 18600 pt/m2.

Each scan was initially placed on its own coordinate system by the laser scanner, with accurate distances but an arbitrary location in three-dimensional space. Wooden boards as well as checkerboard targets were used as common reference planes and points respectively. Using the FARO Scene software [93], the checkerboard targets and reference planes in the first scan were identified and aligned to the same references in the second scan. The tension, or difference between reference position between scans, was 5-8 mm for the checkerboard targets.

The point clouds from each scan were then formed into a three-dimensional surface by converting the individual points into triangle vertices. This triangulated surface was created using the Maptek I-Site [94] software's spherical triangulation feature. The spherical triangulation method projects the points in the scene onto a unit sphere with a chosen center point. A triangulated surface is created in a latitude and longitude coordinate system using Delaunay constraints before being returned to its original coordinate system. This method of triangulation is particularly effective when modeling undercut or overhanging surfaces. I-Site was also used to measure the difference in features between the two triangulation surfaces. Figure 4.4 shows the surface changes on the barrier pillar, while Figure 4.5 shows the surface changes on the interior pillar. The surface change, as colored, represents a distance of each vertex to the nearest vertex in the first scan, not necessarily the perpendicular distance into the wall. The color scale reflects an absolute change in position rather than a signed value. This is most evident when rendering the same colored surface change in both Area F and the area immediately below it, where Area F is experiencing negative surface change (into the wall) through losing material while the area below it is experiencing positive surface change (towards the scanner) by accumulating material.

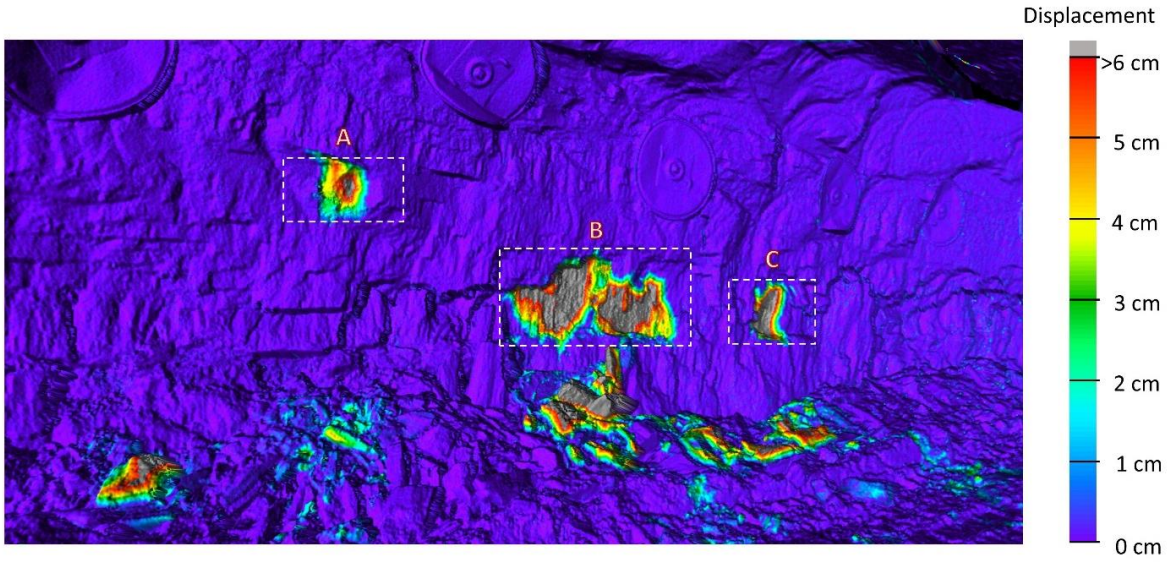

Figure 4.4: Surface change from coal removal on the barrier pillar at locations A, B, and C

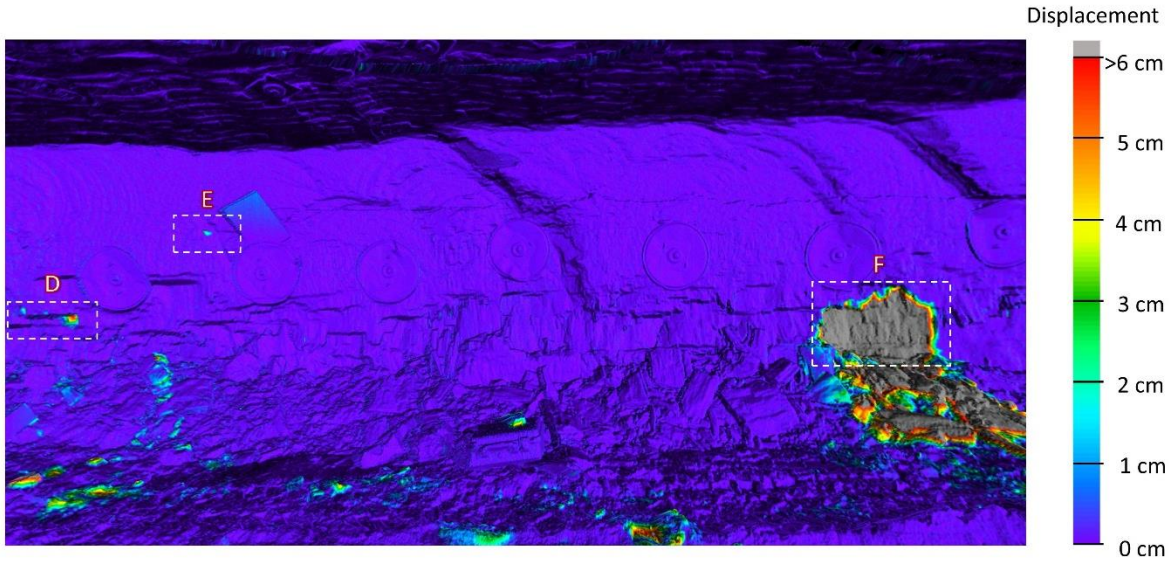

Figure 4.5: Surface change from coal removal on the interior pillar at locations D, E, and F

The six areas where coal has been removed from the rib are clearly visible in each of the colored triangulation surfaces, with the exception of location E, which experienced such a small volume change that it becomes difficult to detect visually, given the color scale and image size. By disturbing the rock dust, it is clear where the movement occurred without comparing the triangulated surfaces, but the same technique could be applied to measuring the movement of an entire rib or roof where there may not necessarily be obvious visual cues that change is occurring.

The volume of material removed at each location, calculated as the volume difference between the two triangulated surfaces at those locations, is shown in Table 4.1. The volume calculations are not determined from the color scale shown in Figure 4.4 and Figure 4.5 but rather by calculating the volume enclosed by the first scanned surface and the second scanned surface at each location.

Table 4.1: Volume change at each coal removal location

Location	Number of Triangles in 2nd Scan	Volume Change (cm3)
A	6533	1246
B	23842	16084
C	2069	5720
D	211	765
E	230	57
F	18026	57549

In addition to the pockets of volume change being readily visible, there are no artifacts appearing in the mesh-difference triangulated surfaces. The changes that appear at the base of the rib and mine floor are due to footprints and material accumulation after removal from the rib. A coarse triangulated surface, or inaccurate point cloud, could lead to differences between the two triangulated surfaces appearing where no change actually occurred. The roof, not being subject to footprints or loose material, was examined as a control case where no surface change should be expected. An examination of an 83 m2 area on the roof showed an average surface change of approximately 0.25 mm between scans.

The presence of dust appears to have had a negligible impact on the ability to recreate an accurate representation of the entry. The scan location was in an area of low-dust concentration, relative to other areas of the mine, due to safety regulations. Ideally the scan location could be in an area of high-dust concentration and a wet coal face, to test extreme conditions. However, it is likely that due to the favorability of these results the amount of dust present at locations, other than in the immediate vicinity of an active excavation, would not be too excessive to preclude the use of laser scanning. Prior to scanning, the effect of environmental factors, such as ventilation air moving the checkerboard references or the reflectance of the coal could was unknown. There were

no issues referencing the checkerboard targets between scans. Any movements of the reference targets between scans were too small to influence scan registration. The reflectance of the coal when exposed in the second time-lapse scan also did not appear to affect the ability of the laser scanner to precisely place points on the exposed coal.

4.4 Synthetic Analysis

A synthetic coal rib (SCR) was constructed to determine the precision of laser scanning on a coal rib in an environment where the deformation and convergence are known. It is experimentally difficult to precisely control deformation underground, but the SCR fulfills the need for controlled deformation and an uneven surface capable of providing occlusions and unfavorable curvatures. The SCR, cross section shown in Figure 4.6, extends 1.8 m horizontally, 1.2 m vertically, and has a depth that varies 0-12 cm from its foundation, simulating irregularity in a rib face. Other statistical measures of the SCR can be found in Table 4.2. The SCR is comprised of a wooden frame with overlain wire mesh and composite material, which was sculpted into an irregular shape with reflectance properties similar to that of bituminous coal.

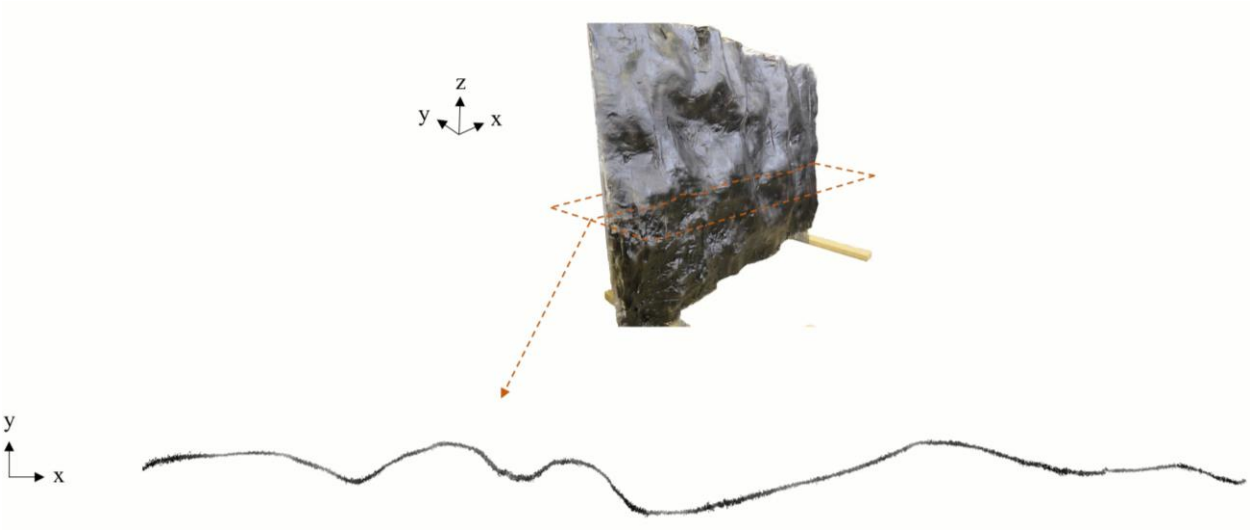

Figure 4.6: Cross-section of the SCR

Table 4.2: Statistical measures for the SCR

Maximum Depth (along y-axis)	Mean	Median	Standard Deviation
12 cm	7.1 cm	7.4 cm	2.3 cm

Two tests were performed to determine volume change monitoring precision and importance of scan location. The first tested the precision of volume change measurements at varying scan resolutions, while the second tested the precision of volume change measurements when the scanner is moved between scans, increasing distance and angle of incidence to the SCR. For both tests the SCR was scanned at a high resolution and then randomly sampled to generate lower resolutions.

4.4.1 Resolution Sensitivity

Determining the necessary point cloud density for accurate and precise deformation monitoring is important because the required resolution governs the speed of data collection and the number of scans that need to be performed. To determine monitoring capabilities at different resolutions, a test was performed in which the volume change was calculated after the SCR was moved approximately 5.0 cm towards the scanner. Moving the SCR creates a volume between the initial and final location. This volume can be calculated by a cut-fill analysis using triangulated surfaces of the point clouds and by calculating a volume using the magnitude of displacement and area displaced. To provide a consistent expected deformation, points lining the perimeter of the SCR were selected, to create a high-density point cloud frame for use in each test. Points outside of the frame were removed and the points contained within the frame change for the individual tests. This perimeter creates a rectangle of 1.191 m2, resulting in an expected volume between scans of 59550 cm3.

A volume between SCR locations was generated for 10 different scan resolutions. The iterations of lower point cloud densities were created by randomly sampling a higher resolution scan. Each resolution was randomly generated ten separate times to create ten unique point distributions at that resolution. The sampling was performed on both the initial and the final scan

to generate similarly sparse point clouds for comparison. The volumes resulting from the difference in these point clouds are provided in Table 4.3.

Table 4.3: Volume calculations at different resolutions

Resolution (points)	Points per square meter	Average volume (cm3)	Volume displacement error (%)	Standard deviation of volume measurement (cm3)
15800	13270	59442	-0.18	13
7600	6383	59447	-0.17	15
3900	3275	59632	0.14	53
2000	1680	59733	0.31	66
970	815	59783	0.39	89
480	403	59911	0.61	251
250	210	59918	0.62	341
120	101	59846	0.50	790
60	50	58672	-1.47	2293
1	1	59071	-0.80	4885

The average volumes displaced for all the different resolutions differ from the true volume of 59550 cm3 by between -1.47 and 0.62 %. However, the average volume displaced would likely approach the true volume, given enough trials, even at the lowest sampling density. The negative values for volume error at 15800 and 7600 points do not necessarily represent an inaccurate set of scans, but may be indicative of a more precise reading of the distance the SCR moved than was originally recorded by line gauge. An indicator of measurement reliability is the standard deviation, which increases significantly as resolution decreases, as illustrated in Figure 4.7. The relative standard deviation of volume change varies from 0.02% at the highest resolution to 8.27% at the lowest resolution.

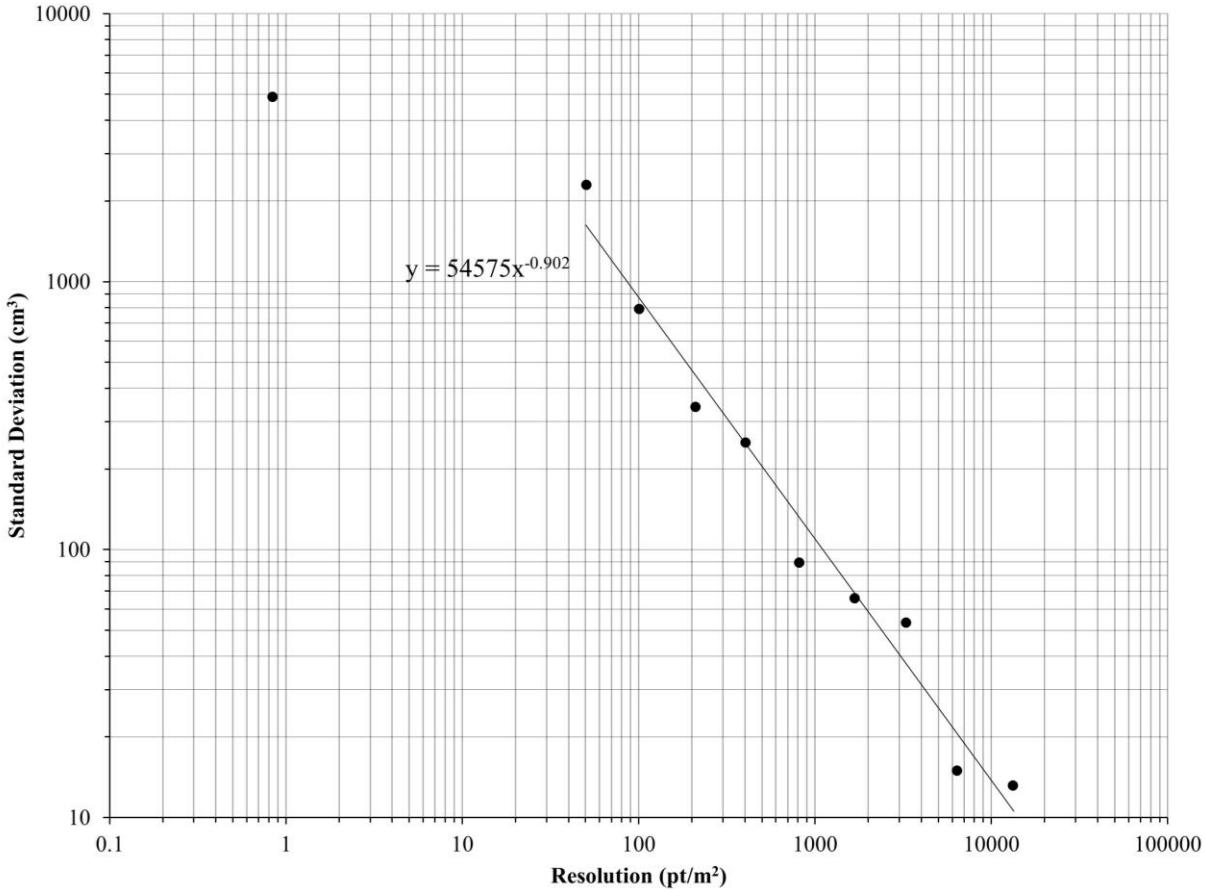

Figure 4.7: Standard deviation of volume calculations for varying scan resolutions

The equation of best fit only includes 50 pt/m^2 tests and above. The standard deviation will approach a finite value as the resolution approaches zero, due to both physical and artificially-imposed constraints. The standard deviation is constrained by the maximum thickness or irregularities on the rib surface as well as the perimeter of dense points included in the analysis to maintain a consistent survey area.

4.4.2 Angle of Incidence Sensitivity

It is unlikely that time-lapse scans will be performed from the same location for each scan unless the scanner is left in place. In addition, the low entry heights and entry widths of underground coal mines may force scans of surfaces with a high angle of incidence to minimize the number of scans along the length of an entry. It is, therefore, important to determine the

precision to which a surface change can be monitored when subsequent scans are performed from different locations and at high angles of incidence. Errors in volume change calculations due to movement of the scanner are likely to be caused by: surveying errors locating subsequent scanner locations, a reduced resolution of the target area, or an increase or decrease in shadows cast on the area of interest, shown in Figure 4.8. The errors associated with locating the scans can be controlled by ensuring care is taken that references are not disturbed between scans, such as movement due to ventilation air.

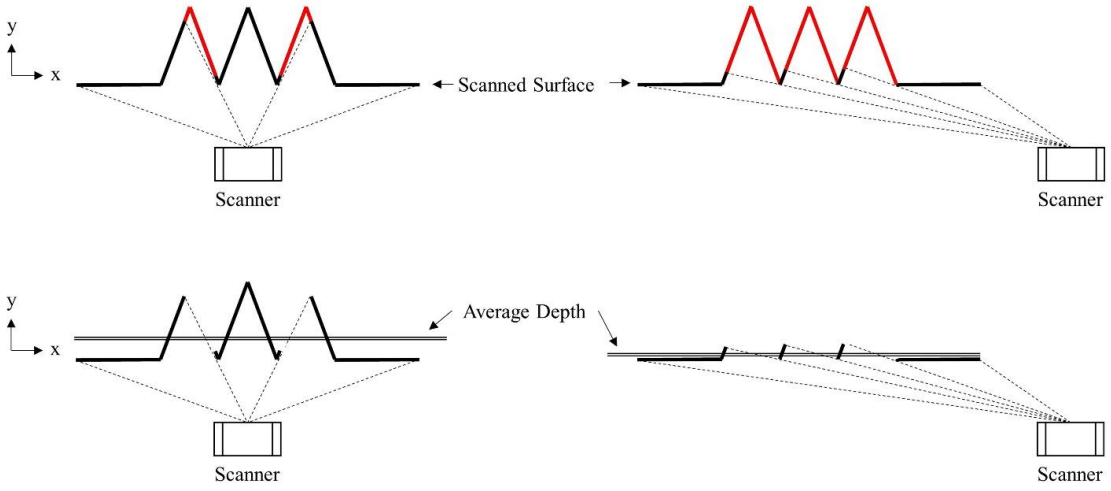

Figure 4.8: Effect of uneven geometry on point cloud coverage

To determine the effect that moving the scanner can have on volume change measurements, the SCR was scanned at a high resolution and then moved 9 cm towards the scan locations. The initial scanner position, after SCR movement, was approximately 1.0 m from the centroid of the SCR (Position 1) with an angle of incidence at the centroid of 6.7°. Subsequent scans were each moved 0.6 m parallel to the SCR after each scan, creating angles of incidence of 32.0° (Position 2), 52.5° (Position 3), and 61.3° (Position 4). These scanner positions are shown in Figure 4.9. In order to maintain similar point densities as the initial test, Position 1, which most resembles the conditions of the first test, was subsampled down to 13000 pts/m2, with the other positions maintaining the same percentage decrease in point density. The standard deviations of the volume calculations from those scans are given in Figure 4.10. If the experiment were to be scaled to actual mine geometries, these distances would be represent approximately 27 cm of rib movement, a perpendicular distance of 3 m from the face, and incremental scanner distances of 2 m.

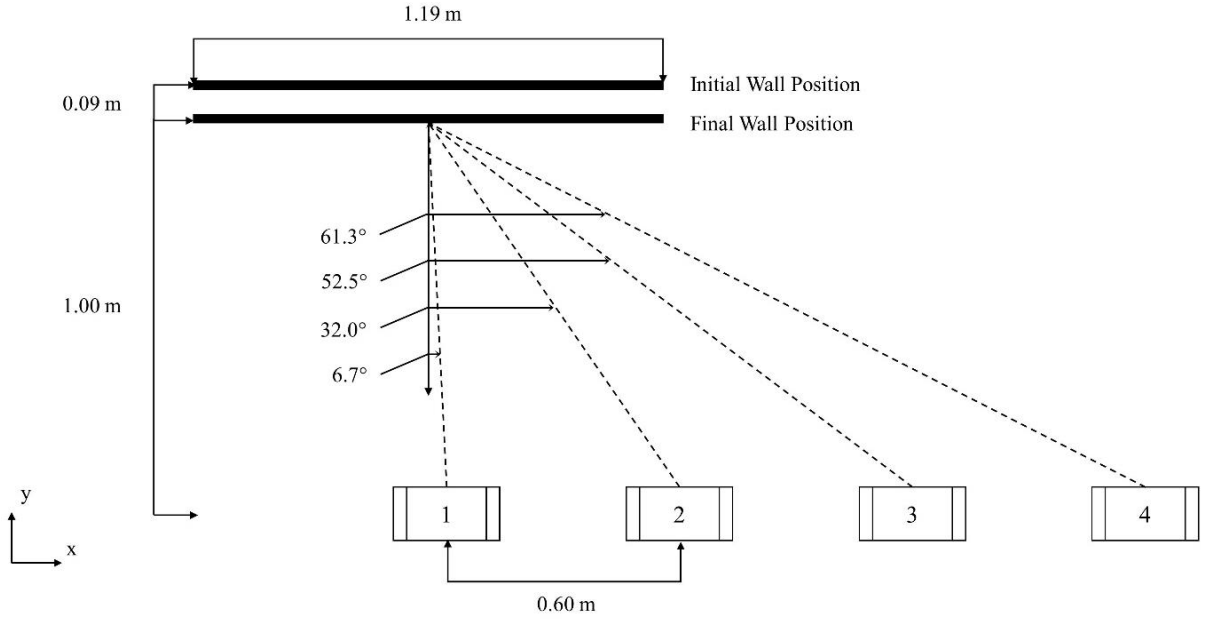

Figure 4.9: Angle of incidence sensitivity test scanner positions

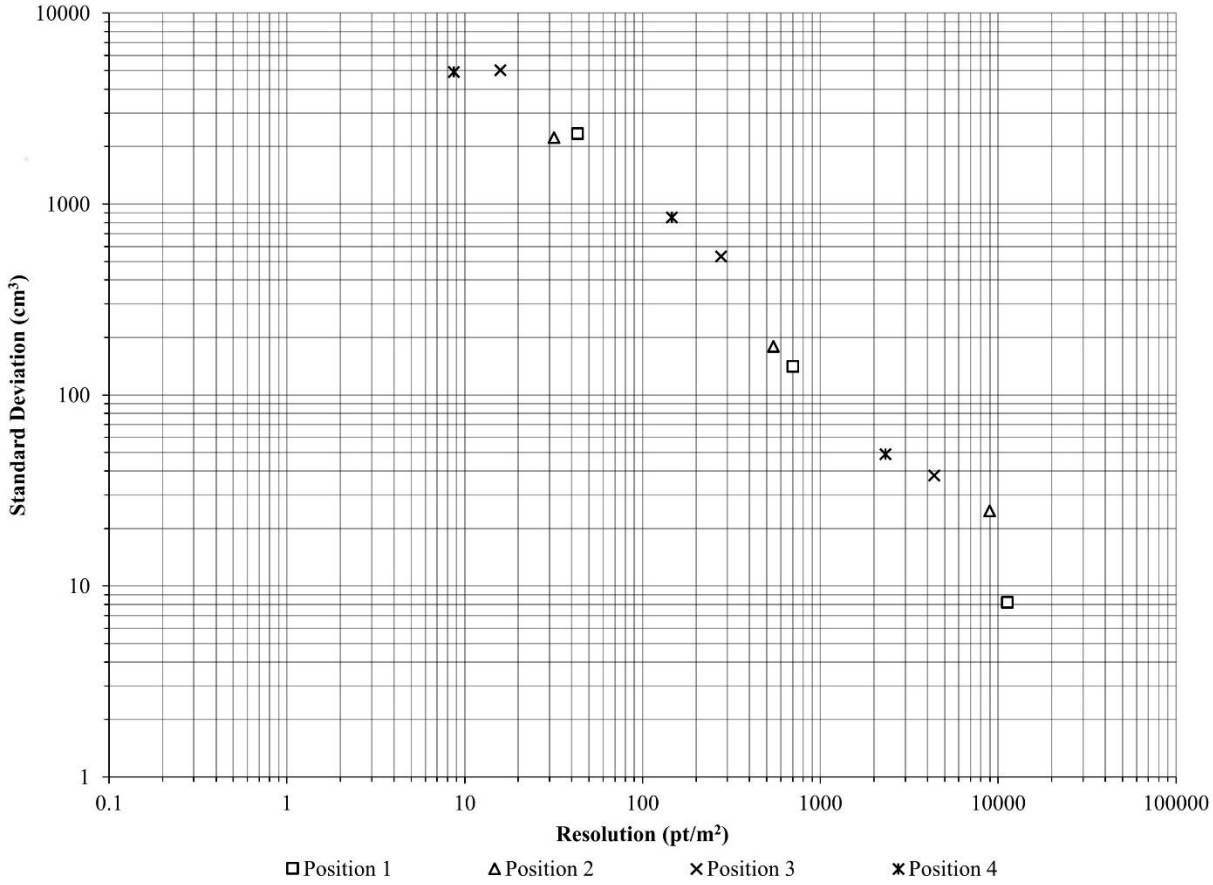

Figure 4.10: Standard deviation of volume calculations for varying scan positions

The standard deviations of the volume calculations appear not to be affected by the movement away from the SCR. The increasing distance from the scanner and the increasing angle of incidence with the scanner do decrease the point cloud density as the position changes, but the shadows cast by the irregular shape of the SCR are not significant enough to affect the volume calculations.

The standard deviations of volume change obtained through these calculations do not perfectly replicate the conditions underground. In an underground scanning application, there will not be a boundary to the entry constraining the surface, and the irregularity of the ribs, roof, and floor may differ from that of the SCR.

4.5 Conclusions

Surface change detection has been shown to be possible in an underground coal mine environment as well as an experiment involving measuring the movement of a synthetic coal rib. Time-lapse triangulated surface comparisons of an underground coal mine entry clearly show areas of surface change where material was removed from the mine ribs. Measurable volume change is only present in the areas where it was expected, suggesting that the measurements were precise enough to be reliable for monitoring underground ground movements.

The reflectance of coal and presence of airborne dust appear to have had negligible impacts on the ability to generate accurate and precise point clouds of the underground coal mining environment. While these conditions were not at their extremes, such as in the highest dust concentration regions of the mine or areas where the coal face may be wet, the absence of problems at the test area may suggest that exacerbating these problems may not cause as many problems as originally expected

The uncertainty associated with the required resolution to maintain an acceptable level of precision, in monitoring surface change, merited a more experimentally controlled study. An artificial coal rib was created, which was moved a controlled amount and scanned in a time-lapse manner. The conditions of the synthetic test would differ from an underground coal rib, but provide an estimate for required point cloud densities for field measurements to reduce oversampling, which is less desirable outside of a research capacity. Underground conditions may

include differing irregularity in the coal rib, resulting in more or fewer shadows in the scans. Underground scans would also not be constrained on the border, resulting in a larger allowable standard deviation in results.

The results of the synthetic tests show that relative standard deviations of volume change less than 0.1% are achievable with point cloud densities greater than 3200 pts/m2. It was also discovered that the irregularity in the coal rib did not have a significant impact on displacement monitoring, even with a large angle of incidence between the laser and SCR. The distribution and magnitude of asperities on a coal rib will be unique for any different scanned area, making the derivation of a "correction factor" from these results unwise. These results, however, may suggest that ensuring a high scan resolution of coal ribs would be more beneficial than maintaining a low angle of incidence.

The results outlined in this study show that laser scanning can be used to detect very small changes in an underground coal mining environment through time-lapse scanning. The geometry of an underground coal mine entry may not be favorable for measuring large surfaces with a single scan, but as shown in Figure 4.10, there is not significant degradation of scanning precision with an increasing angle of incidence considering the rough surfaces found underground. This creates a simpler geometric model where a scanner setup must only consider the number of points that lie on a given area of the entry walls. Monitoring tools typically used underground do not provide the comprehensive tunnel measuring capabilities of laser scanning, and these results suggest that the lack of laser scanning measurements being performed in this environment should not be attributed to a technical limitation of the technology.

Acknowledgement

This work is supported by NIOSH (contract 200-2011-40313) through the Capacity Building and Ground Control Research for the Mining Industry program.

Chapter 5 Determination of Volumetric Changes at an Underground Stone Mine: A Photogrammetry Case Study

Brent Slaker – Virginia Polytechnic Institute and State University, Blacksburg, VA
Erik Westman – Virginia Polytechnic Institute and State University, Blacksburg, VA
John Ellenberger – NIOSH-Office of Mine Safety and Health Research, Pittsburgh, PA
Michael Murphy – NIOSH-Office of Mine Safety and Health Research, Pittsburgh, PA

5.1 Abstract

Photogrammetry, as a tool for monitoring underground mine deformation, is an alternative to traditional point measurement devices, and may be capable of accurate measurements in situations where technologies such as laser scanning are unsuited, undesired, or cost-prohibitive. An underground limestone mine in Ohio is used as a test case for monitoring of structurally unstable pillars. Seven pillars were photographed over a 63-day period, punctuated by four visits. Using photogrammetry, point clouds of the mine geometry were obtained and triangulation surfaces were generated to determine volumes of change over time. Pillar spalling in the range of 0.29 – 4.03 m^3 of rock on individual rib faces was detected. Isolated incidents of rock expansion prior to failure, and the isolated failure of a weak shale band were also observed. Much of the pillars remained unchanged during the monitoring period, which is indicative of proper alignment in the triangulated surfaces. The photographs of some ribs were of either too poor quality or had insufficient overlap, and were not included. However, photogrammetry was successfully applied to multiple ribs in quantifying the pillar geometry change over time.

5.2 Introduction

Adequately measuring underground rock mass movements is integral to understanding how rock masses behave and how to interact with them safely and efficiently. Many modern measurement techniques employed in underground mining environments rely on point

measurements, such as through extensometers or borehole relief methods [88]. These techniques, while commonplace, do not provide a comprehensive view of how the rock mass is behaving. The dynamic changes in stress states underground, coupled with the mechanical uncertainty of rock masses, near active excavations, creates a need for measurement systems which better capture the true behavior of the rock mass. Photogrammetry is a technology capable of producing the wide-area displacement measurements required for a comprehensive understanding of rock mass movements.

Digital photogrammetry is a means of obtaining three-dimensional point clouds from digital photographs. By finding the same point across multiple images, all viewing an object from different angles, the geometric properties of that point in three-dimensional space can be inferred. Close range digital photogrammetry (CRDP) is photogrammetry applied to measuring objects or scenes less than 100 meters away [66], and is used for various functions in underground mining environments. These uses include, but are not limited to mapping fracture networks [73][74], characterizing fractures[72], and measuring volumes of blast rock [75].

One additional application to underground mining environments is monitoring geometric change in support structures, such as pillars. Using time-lapse observations, three-dimensional point clouds or surfaces can be compared to observe temporal change. The ability to measure or observe object displacements in an underground mining setting, using photogrammetry, differs in practice and obstacles from a surface setting. This study demonstrates an example of applying photogrammetry to monitoring temporal geometric change in pillar structures. In an underground mine, especially hard rock, the roof and floor structures are as feature-rich as the rib structures, and an instance of applied photogrammetry to rib movement is a proof-of-concept that it could also be used to quantify roof and floor structures. If photogrammetry can be applied cost-effectively and quickly to monitoring rib movement, it could be a valuable tool for collecting any visible rock mass movement information.

5.2.1 Site Description

The setting for this study is an underground limestone mine in eastern Ohio. The mine follows the Vanport Limestone seam, with a mining depth that ranges from 60 to 75 m, while maintaining a near-horizontal inclination. The mine plan consists of varying pillar sizes and

orientations, with many pillars reduced from their planned size due to overmining and scaling or sloughing. The predominant planned pillar dimension was 7.6 m wide and 18.2 m long, on 30 m crosscut centers and 19.8 m drift centers. This results in the north-south crosscuts being 12 m wide with the east-west crosscuts also being 12 m wide.

The mine has experienced significant structural instabilities. A collapse on May 27th, 2014 encompassed 10 pillars in a 61 m by 107 m region, and an additional collapse, involving 10 pillars, occurred on June 24th, 2014. Spalling and scaling of pillars occurred throughout the mine, and when coupled with overmining, resulted in pillar dimensions likely in the range of 6.4 m by 17.0 m, instead of the planned 7.6 m by 18.2 m.

The instability is believed to be due to the presence of weak 20 to 30 cm shale bands within the pillar and a weak, slickensided, and fine-grained fireclay floor strata that varied in distance from the base of the pillar. The weak floor material caused structural damage to the pillar, reducing its load bearing capacity. Further detail of site characterization and mechanisms of the pillar failures are discussed by Murphy et al. [110]. The collapse of roof structures is beyond the scope of this study, but the sloughing and scaling associated with this instability provides an excellent subject for photogrammetry.

5.3 Methods

Seven pillars were photographed across four different visits: August 26th, September 16th, September 26th, and October 28th 2014. The photographs were taken with a Digital Single-Lens Reflex (DSLR) Nikon D70S camera [111]. Camera settings, shown in Table 5.1, were kept consistent during visits, but slight changes were made between them. The lighting was provided by an external flash, which was moved as needed to provide sufficient light on the subject. The photographs were taken by hand, without the aid of a tripod. Several photographs were of poor quality, but were still used for reconstruction if clearer photographs were unavailable. Fog is believed to be partially responsible for blur in some photographs, as well as a lower f-stop causing spherical aberration in the lens. Thumbnails for the pictures taken at each visit can be found in Appendix A. The photographs were taken by a researcher not associated photogrammetry, but present at the mine for other purposes. The camera equipment used in this study was already

available for use and the instructions for taking photographs in a manner that could be used for photogrammetric reconstruction were given remotely.

Table 5.1: Photograph EXIF data from each visit

Date	Resolution	F Stop	Exposure	Focal Length	Max Aperture
Aug. 26th	3008x2000	f/2.8	1/80s	20 mm	1.6
Sep. 16th	3008x2000	f/2.8	1/80s	20 mm	1.6
Sep. 26th	3008x2000	f/2.8	1/60s	20 mm	1.6
Oct. 28th	3008x2000	f/4.5	1/60s	20 mm	1.6

A map of the pillars that were photographed is shown in Figure 5.1. The pillars are on the boundary of a collapsed area. The number of photographs taken of each pillar is listed in Table 5.2. With the need to move the light sources, the pictures were not taken continuously surrounding the pillar, but rather in distinct segments, fragmenting the pillar into "sides" instead of one contiguous object. Further displacement of material, through spalling, on these pillars was expected, but the magnitude of material being displaced was unknown.

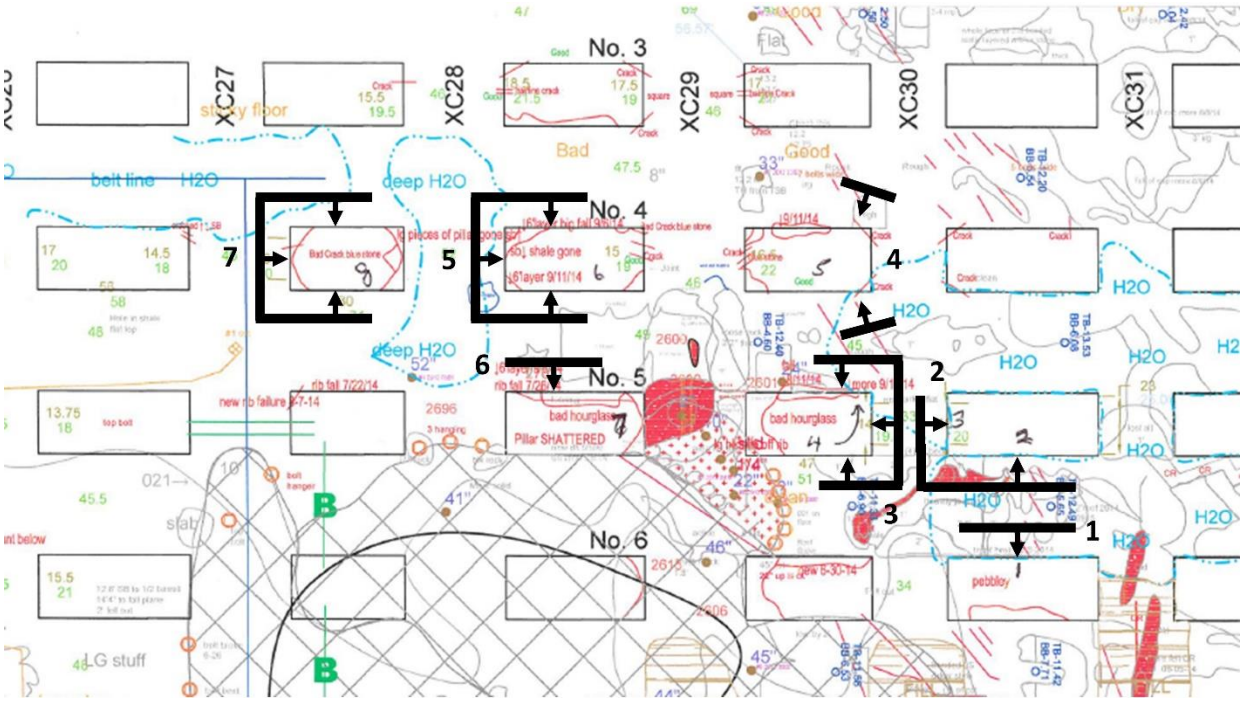

Figure 5.1: Map of the photographed areas of the mine with pillars numbered

Table 5.2: Number of pictures taken at each pillar

Pillar	Aug. 26	Sep. 16	Sep. 26	Oct. 28
1	0	3	5	0
2	0	11	7	2
3	5	9	8	6
4	0	4	11	7
5	2	13	11	5
6	4	5	0	0
7	12	9	0	3

The photographs were processed through a combination of Agisoft Photoscan [108], CloudCompare, and Maptek iSite [94]. Photoscan was used to obtain the point clouds and triangulation surfaces from the photographs. Next, CloudCompare was used to orient and scale the time-lapse photos. Several 30 cm squares were placed in each scene to provide a reference for scaling the resultant triangulation surfaces. The squares were not placed in the same location during subsequent visits, and as a result, would create the appearance of movement on the rib face at the locations they were placed.

Orienting the photos was performed by locating the same points on the rib or roof between visits. Exposed rock faces have a significant number of visual features that can be located across the photographs from different visits and assigned the same three-dimensional coordinate. Four of these features were chosen in each point cloud to align with a point cloud of the same region at the next visit. If reference points moved between scenes, such as in the expansion of a rib, this would cause a systematic error clearly visible when aligning the triangulation surfaces.

Lastly, iSite was used to determine the distances between the triangulation surfaces at different time periods. The volumes reported are the volumes enclosed by two triangulation surfaces. The older surface will always be the reference. Negative volumes correspond to the removal of material from the rib, while positive volumes correspond to an expansion of the rib or accumulation of material that did not previously exist. The same process was applied previously, in an underground limestone mine, using laser scanning as the point cloud collection method [112].

These software packages are not uniquely able to perform these functions, nor are the software packages limited in use to the function presented here. The reason for using each was the preference of the author. Due to the poor quality of some photographs, a significant cascading error may exist in some of the point clouds. Imprecisely constructed point clouds can lead to imprecise scaling and inaccurate referencing, resulting in underestimations or overestimations of

volume change. Point clouds, which appear to be significantly noisier than the rest, are noted in their relevant section.

5.4 Results

The time-lapse analysis of surface change, as calculated by iSite, is shown in Figure 5.2 through Figure 5.9. The colored surface has been overlain on a photograph of the scene at the earlier time in the analysis. The overlain pictures are approximately aligned by hand; however, the volumes of change are calculated by iSite from the two referenced surfaces. Warmer colors, which are positive values, are used to indicate an expansion, or movement of material towards the camera. Cooler colors, which are negative values, are used to indicated a contraction, or spalling of material. A green color, which dominates the majorities of overlays, very little or no change detected between scans.

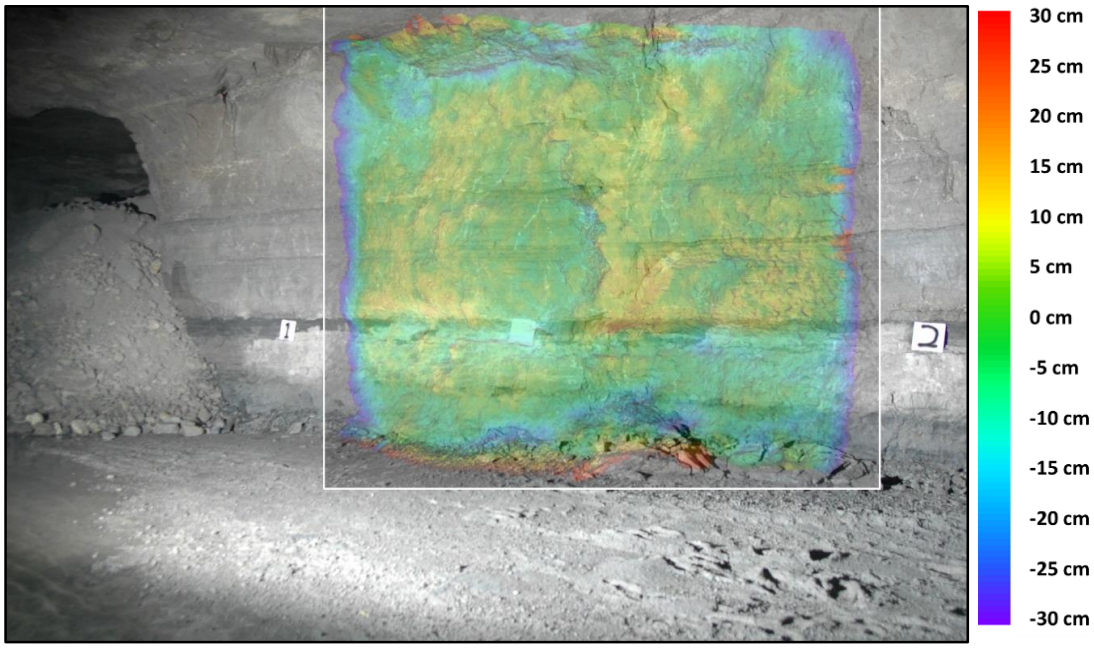

Figure 5.2: Change at Pillar 1 between September 16th and September 26th

The change observed at Pillar 1, in Figure 5.2, is likely to be artifacts of the photogrammetry. The September 16th pictures were both blurry and in very low light, resulting in

a questionable point cloud. The presence of localized expansion of the magnitude being shown should result in visible tension cracks when comparing the photos, but no such cracks exist.

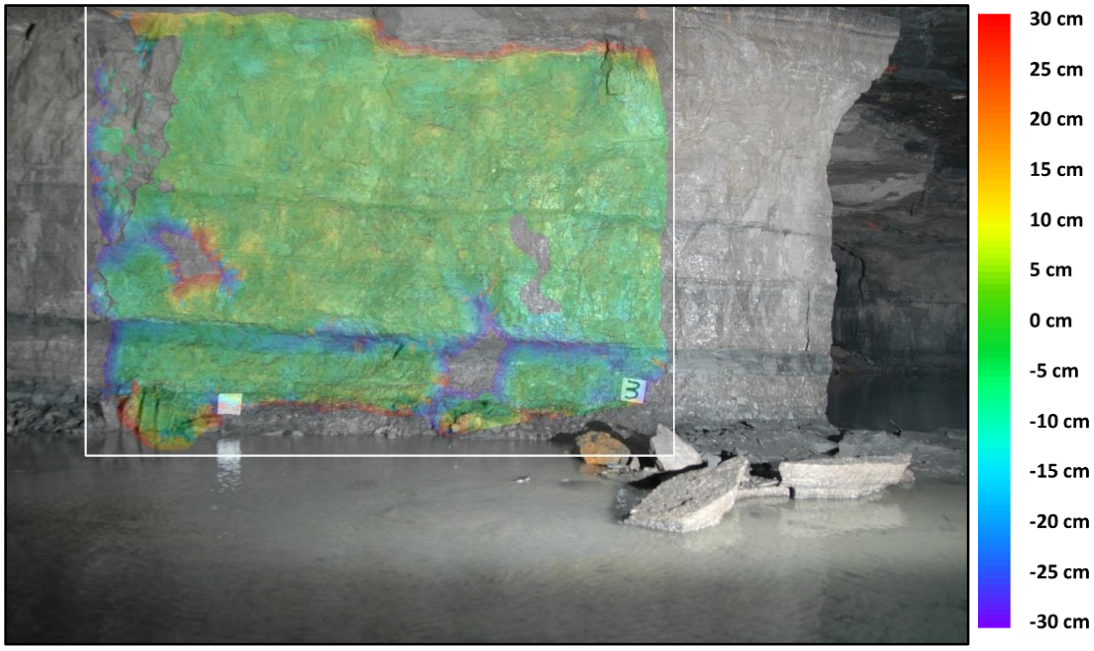

Figure 5.3: Change at Pillar 2 between September 16th and September 26th

The change in Pillar 2, on the side shown in Figure 5.3, is confined to the weak shale band nearest to the base of the pillar. The uniform absence of deformation elsewhere, combined with the spalling of material from this band, follows the behavior suggested by Murphy et al. [110]. The holes in the overlay at the left-center and bottom-center do not indicate that large portions of the rib changed between photographs, but were merely areas that were unable to be reconstructed.

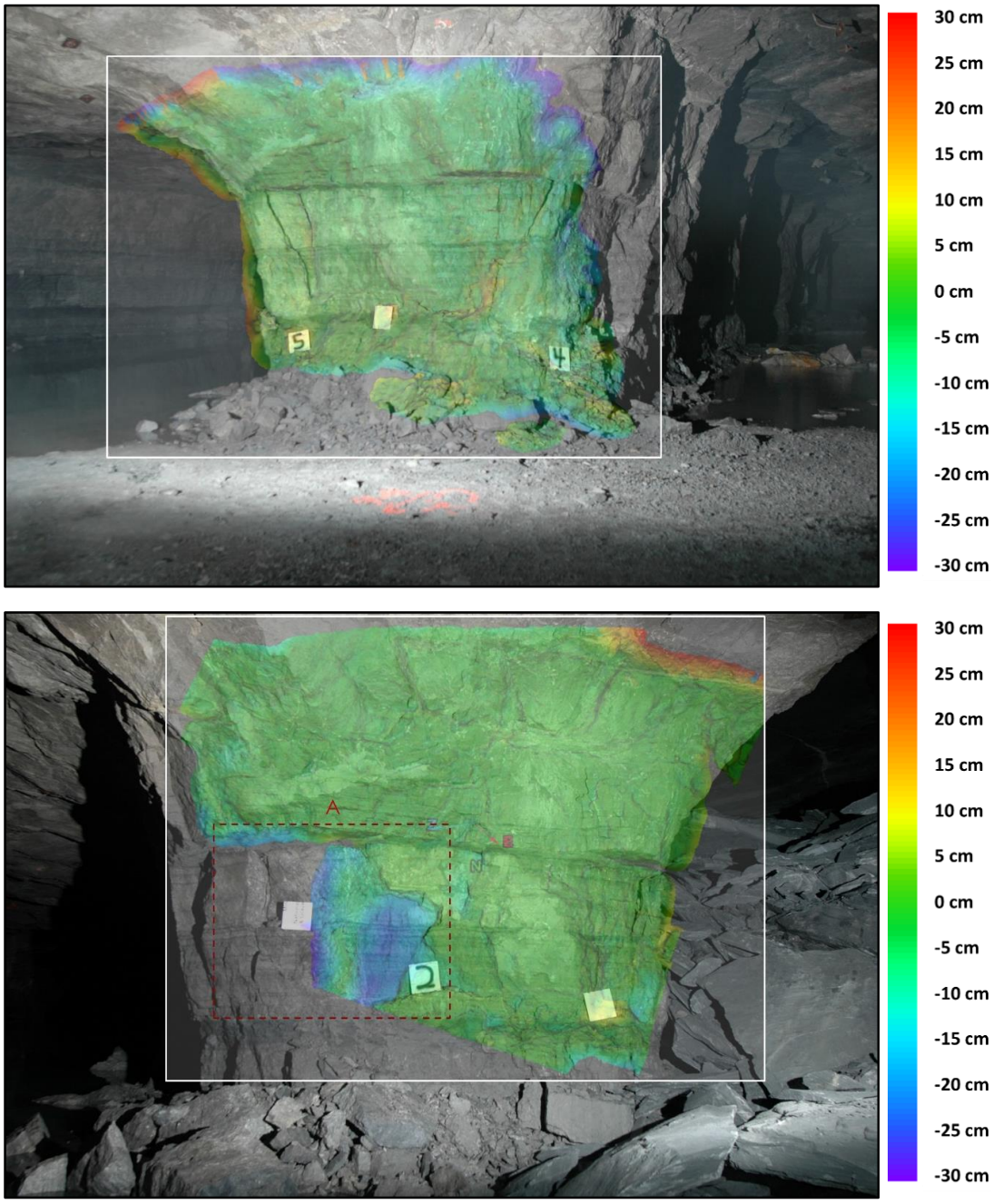

Figure 5.4: Change at Pillar 2 from Sep. 16th to Sep 26th (top) and Sep. 26th to Oct. 28th (bottom)

The other visible side of Pillar 2, shown in Figure 5.4, exhibited little to no deformation between September 16th and September 26th, with the exception of the references placed on the rib, however a large change in the rib was detected sometime between September 26th and October 28th. The area highlighted in Box A showed 0.36 m^3 of change between the time periods. The

change was likely larger than this, but the reconstructed area of Pillar 2 for the second time period was smaller than the first due to insufficient overlap between pictures.

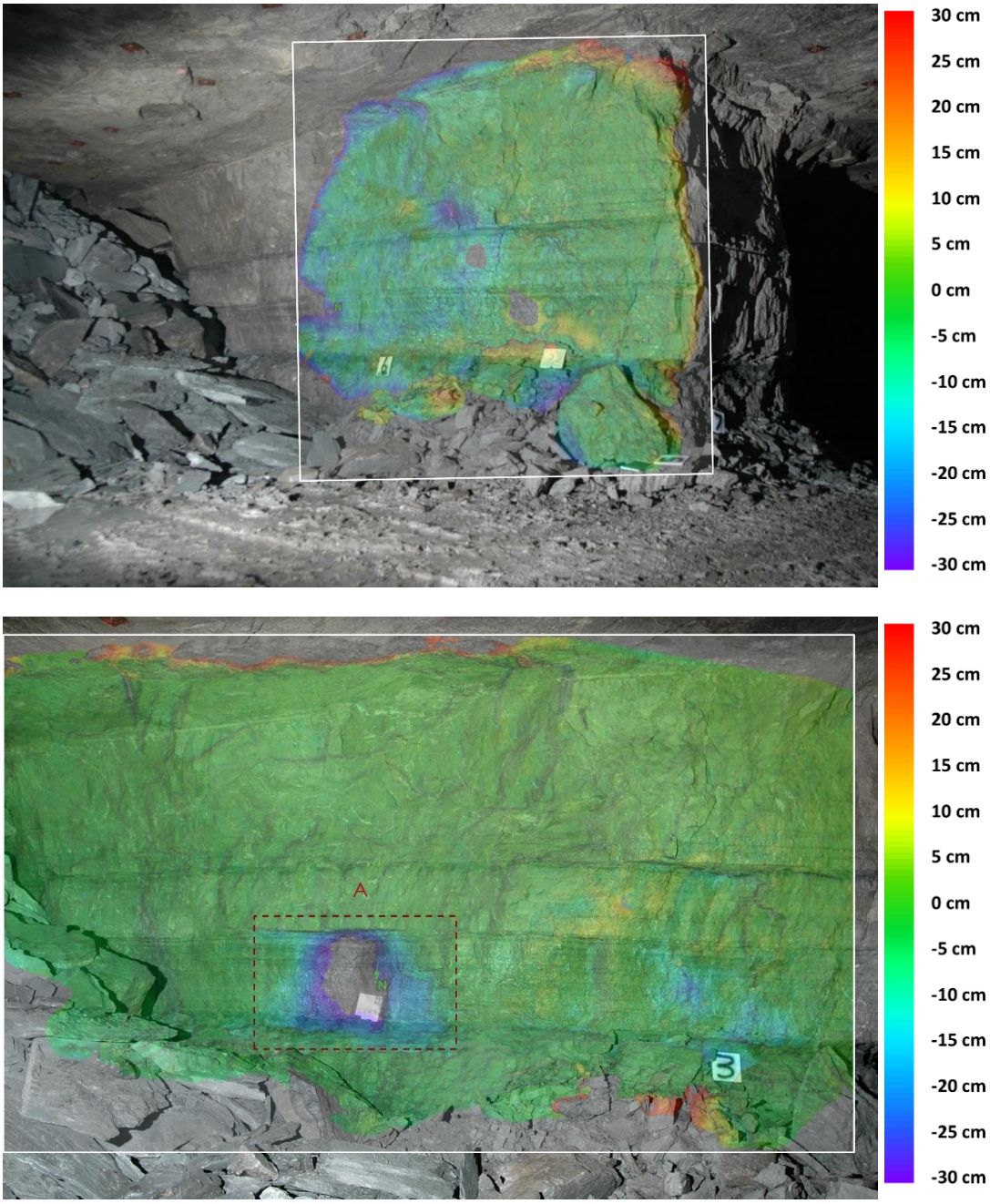

Figure 5.5: Change at Pillar 3 from Aug. 26th to Sep. 26th (top) and Sep. 26th to Oct. 28th (bottom)

Three sides of Pillar 3 were photographed. The first side, Figure 5.5, shows widespread removal of material along the left side in the August 26th to September 26th time frame, however,

there were only two photographs in the first set (Aug. 26th), and both were blurry. The widespread change cannot be verified in the pictures due to the image quality, with the exception of the dark blue area near the center where a change does appear to have occurred. A clear change is visible in the September 26th to October 28th time frame, with the area enclosed by Box A showing a volume change of 0.52 m^3 and an average displacement of 16.5 cm.

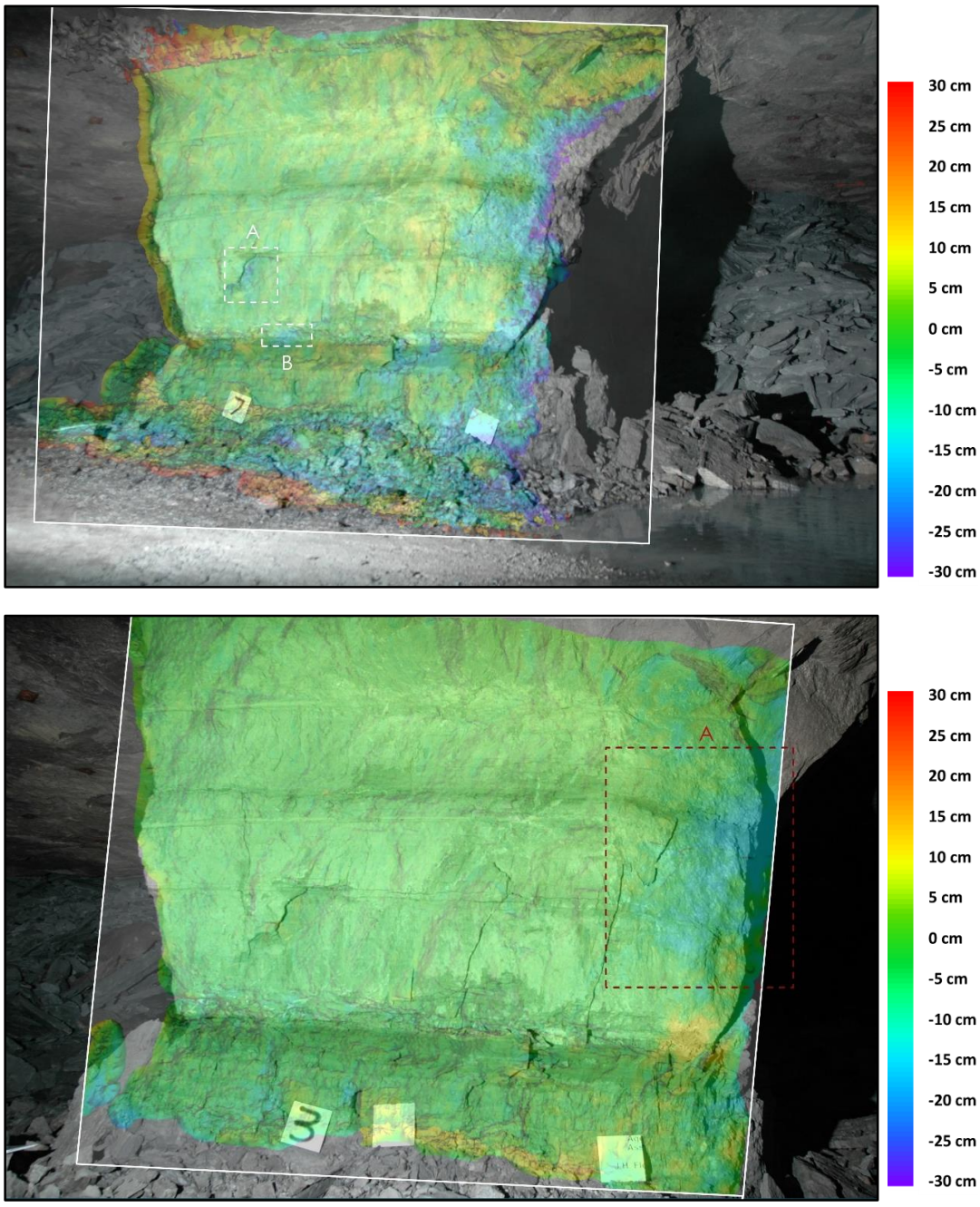

Figure 5.6: Change at Pillar 3 from Aug. 26th to Sep. 26th (top) and Sep. 26th to Oct 28th (bottom)

Both periods at Pillar 3 in Figure 5.6 show a small amount of movement on the right side of the pillar, with a crack clearly visible by September 26th, which separates the moving region of the rib from the stationary region. The areas inside Box A and Box B also show small, but distinct displacement. The change shown in Box A for the September 26th to October 28th time period shows 0.29 m^3 of change, however, this occurs in an area with pronounced shadows that may be affecting the results. The remaining pillar face is free of shadows and shows no significant change.

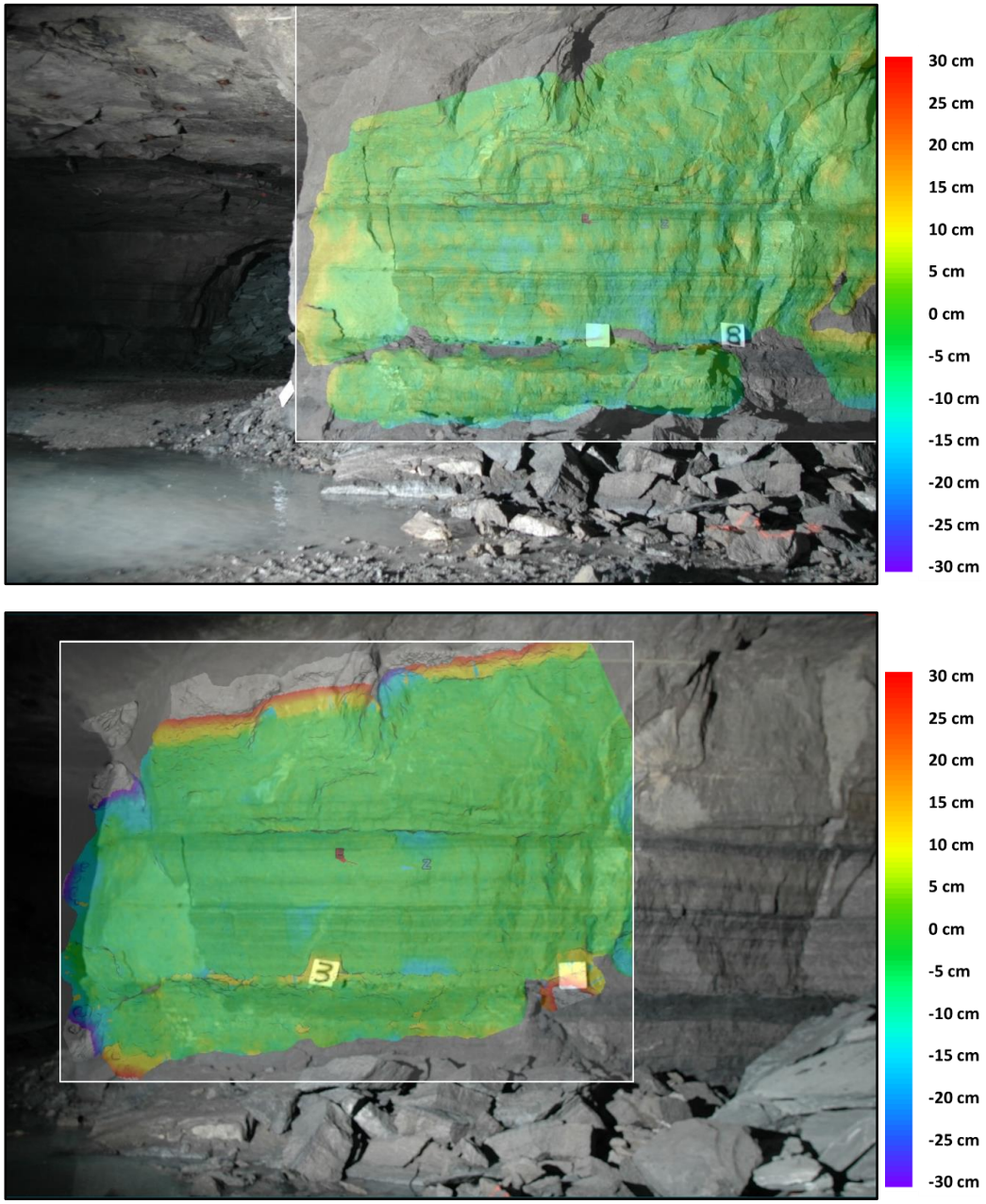

Figure 5.7: Change at Pillar 3 from Sep. 16th to Sep. 26th (top) and Sep. 26th to Oct. 28th (bottom)

Figure 5.7 shows the last side of Pillar 3, which includes numerous pockets of change between September 16th and September 26th. This is most likely due to shadows, which were significantly pronounced in one of the two photos from September 16th. The September 26th to October 28th time period does not include the shadowed photographs and shows far fewer, but verifiable, pockets of change, although no large rib movements.

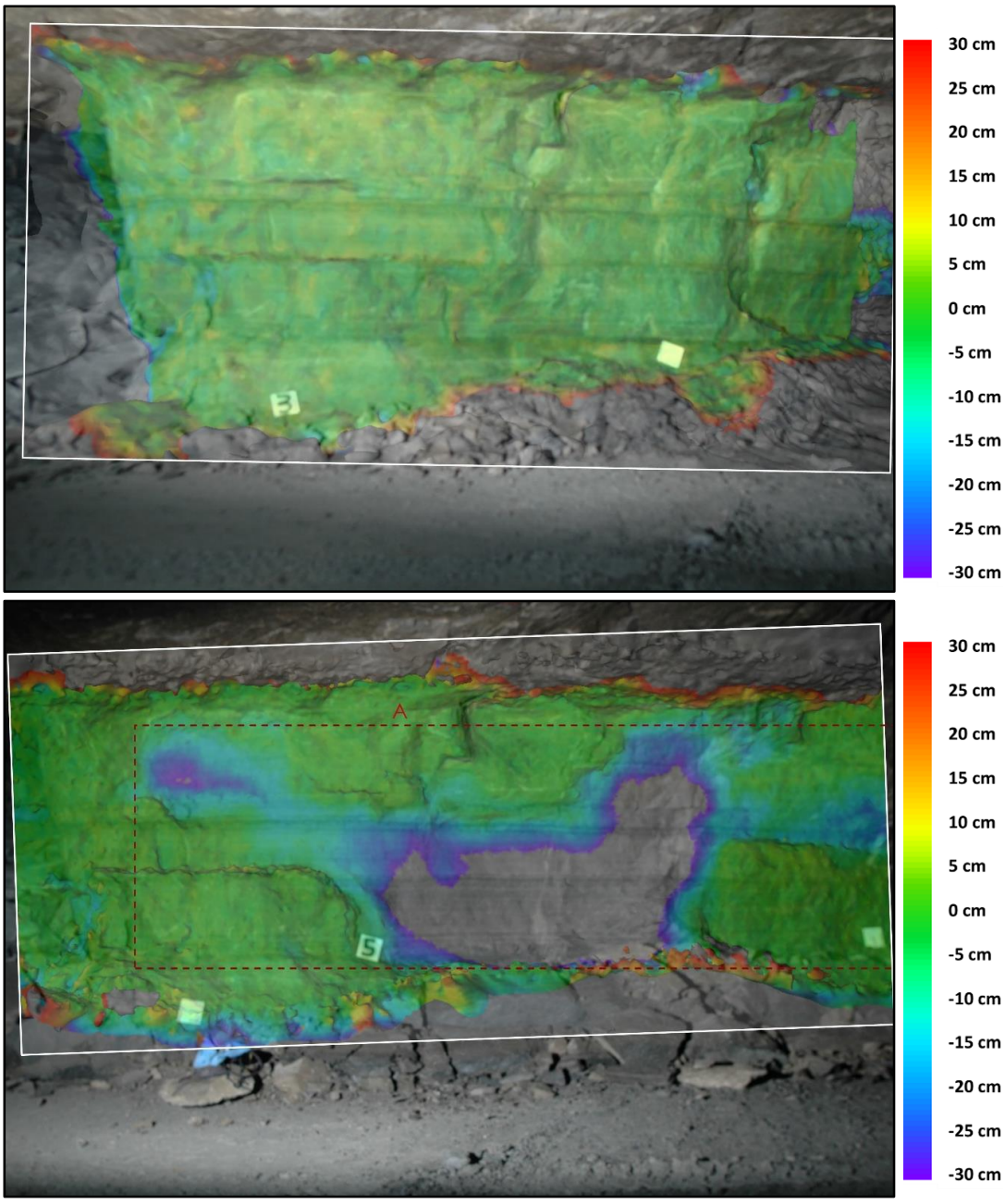

Figure 5.8: Change at Pillar 5 from Sep. 16th to Sep 26th (top) and Sep. 26th to Oct. 28th (bottom)

The first time period, from September 16th to September 26th, in Figure 5.8, shows no significant movement, with the small color variations likely due to the poor quality of the photographs used. The second time period, from September 26th to October 26th, a large displacement of rib material was detected. In the area enclosed by Box A, 4.03 m^3 was displaced. The larger displacement, which exceeds the color scale, showed an approximate average displacement of 34.5 cm. The other sides of this pillar were inaccessible when the next visit occurred on October 28th.

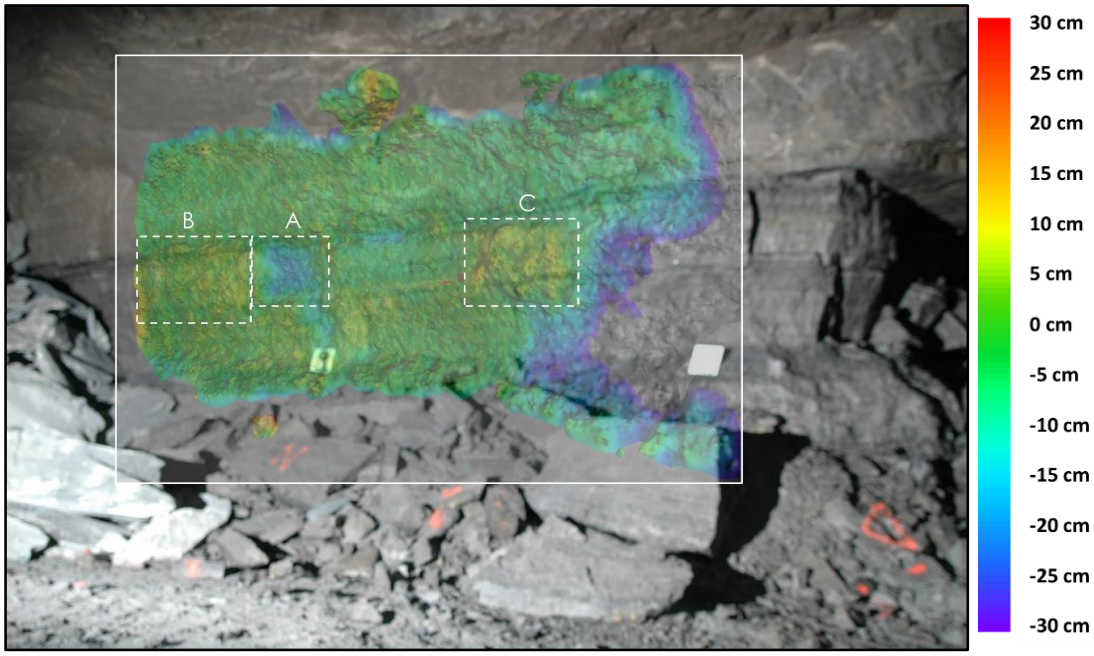

Figure 5.9: Change at Pillar 6 from Aug. 26th to Sep. 16th

It is difficult to verify the change present in Figure 5.9, due to the blurriness of the photographs. Change does appear to have occurred in the area enclosed by Box A, however Box B and Box C are inconclusive. A photograph of this area was taken on September 26th, and it showed significant damage across the rib face, possibly a result of the movement shown taking place between August 26th and September 16th. In addition to the pillars shown, observations at the remaining photographed pillars are summarized in Table 5.3.

Table 5.3: Summary of conditions at each pillar

Pillar	Condition	Notes
1	An example of a poorly aligned point cloud	Blurriness negatively impacted the reconstruction of the Aug 26th to Sep. 16th time period.
2	A large part of the corner of the rib was displaced, and there was significant displacement in the weak shale band	Overlapping between photographs was not high enough to capture fully the displacement.
3	An isolated 0.52 m^3 displacement occurred	Blurriness negatively influenced the reconstruction of the Aug 26th to Sep. 16th time period.
4	Good	No detectable change occurred during the monitoring period.
5	A large 4.03 m^3 displacement occurred	Two sides of the pillar were inaccessible following the displacement between Sep. 16th and Oct. 28th.
6	Small areas of localized rib spalling and rib expansion are detected	Photographs from Oct. 28th show significant damage in the areas that were expanding, but the photographs were blurred.
7	Significant rib spalling occurred between Aug. 26th and Sep. 16th, but none after that time period	The Aug. 26th and Sep. 16th photographs were blurry, but less pronounced than at Pillars 1 and 3. Fog may have played a role in reducing the quality of these photographs.

The pillar behaviors observed can be classified into four categories: spalling, expansion, weak band failure, and no movement. Nearly all the pillars exhibited spalling, which is shown on Pillars 2, 3, 5, 6, and 7. This spalling ranges from 0.29 m^3 to 0.52 m^3 of material being displaced from the rib. The spalling behavior shown on Pillar 2 and 3 occurred at the corner of the pillar and was poorly quantified as a result. Due to the light positioning, another set of photos would need to be taken solely of the pillar corner in order to reconstruct it properly. Photographs were not taken of the corner, but instead each side of the pillar was reconstructed, leaving the corner deformation quantitatively unknown. Pillars 3, 5, 6, and 7 all showed some degree of spalling away from the corners, although the 4.03 m^3 displaced on Pillar 5 was the largest by far. This spalling did not appear preferentially located at certain parts of the rib.

Expansion, or an observed movement of the rib towards the camera, was shown on several pillars, but this could also be indicative of a poorly aligned or reconstructed point cloud. Considering the photographic quality at each site, Pillar 6 is the only likely candidate for showing

actual expansion of the rib. A photograph taken on the visit following the observed expansion shows significant damage in one of the expanding areas. That photograph showed no change in the area that had already shed material. With the uncertainty associated with the photographs, this is not conclusive, but is potentially predictive of areas that would experience failure.

A weak shale band near the base of the pillar showed distinct spalling on one side of Pillar 2. Large displacements were confined to this band. The short sides of the pillar did not show the same displacement in this band. No other pillars showed widespread failure of this shale band.

Many of the pillars also show no movement at all, or the majority of their surface area is left unchanged between observation periods. An unchanging rib face makes quantification of rib displacement inapplicable, but it does demonstrate the reliability of that surface's orientation. Properly oriented triangulation surfaces will show zero movement if none occurred, and any reported change in geometry must be a result of material movement or disruptive photographic elements, such as moving reference targets. Additional pillars exhibiting this behavior are contained in Appendix B.

5.5 Conclusions

An Ohio limestone mine experienced large roof falls due to structural instabilities caused by weak strata bands. The structural problems were evident in the pillar geometry as varying amounts of material spalled, or were scaled, from the pillars. The change in pillar geometry over time was monitored at seven different pillars using photogrammetry. The photographs were taken at four separate dates: August 26th, September 16th, September 26th, and October 28th 2014. Not all pillars were photographed at each date, nor were all photographs of the same quality, although efforts were taken to keep camera settings consistent throughout an entire visit.

Four different pillar behaviors were observed during this monitoring period: weak band failure, spalling or scaling, expansion, and no movement. All of the pillars photographed showed signs of significant damage prior to the photographs being taken, and the results presented here only accounts for pillar behavior during the monitoring period. The weak band failure was observed in one pillar, with a weak shale band approximately 20 cm to 30 cm in width losing material between September 16th and September 26th. Any subsequent structural issues the band failure may have caused were not observed between those two dates.

Spalling was observed on four pillars, with three being relatively small amounts of material, 0.29 m^3 - 0.52 m^3, displaced between monitoring periods. Another pillar showed significantly more material, 4.03 m^3, displaced between monitoring periods.

One pillar face showed a small amount of spalling while simultaneously showing other areas of expansion. The expansion was generally less than 15 cm, but the quality of the photographs was not high enough to locate clear tension cracking as a result. The picture following the expansion between August 26th and September 16th, on September 26th showed significant damage in the areas that had been expanding. This damage would be expected if the pillar was inelastically expanding.

Some pillars experienced either no movement or very little movement across the monitoring period. Just as it is important to be able to detect material movement, it is also important to be able to detect the absence of movement, and not suggest that structural instabilities exist where they do not. Several triangulated surfaces do show false movements between periods, but these generally show anomalies across the entire surface, and are a result of a poor photogrammetric reconstruction.

The time-lapse photogrammetric monitoring performed at this site resulted in seven pillars being successfully reconstructed. The precision of measurements varied with photograph quality, but expected rib changes were modeled and capable of being quantified. Additionally, the photographs were taken remotely by a researcher not associated with photogrammetry, who was at the mine for different purposes. This highlights one of the greatest strengths of photogrammetry as a rock mass monitoring tool: the ease with which the data collection steps can be communicated and performed. Photogrammetry has been shown to be uniquely suited for measurement of large mine areas, and can offer a fast and cost-effective supplementary perspective on the mine behavior of which traditional point measurement techniques may be incapable.

Chapter 6 Time-Lapse Photogrammetric Monitoring of an Artificially Loaded Standing Roof Support

B. A. Slaker, Graduate Research Associate

E. C. Westman, Associate Professor

Geomechanics Observation and Imaging, Mining and Minerals Engineering

Virginia Polytechnic Institute and State University, Blacksburg, VA, 24061

6.1 Abstract

Photogrammetry has found many uses is industrial applications, including the mining industry, but its usefulness as a tool in monitoring standing roof supports in underground coal mines has not yet been established. Collection of meaningful underground deformation data is crucial to understanding rock mass behavior, but the ability to do so can be unreliable, expensive, and time-intensive. This study involves testing using photogrammetry at the Mine Roof Simulator (MRS) in at the National Institute for Occupational Safety and Health (NIOSH) Research Laboratory in Pittsburgh, Pennsylvania during the loading of a standing support. At stages during the standing support's loading, an ATEX certified explosion-proof digital camera is used to collect an object panorama and determine the object deformation between convergence stages. Comparing the photogrammetric results to the MRS stroke measurements, the point cloud support heights differ from the actual support heights by between 0.2% and 0.6%, depending on the convergence stage. The strain experienced by the support as calculated through photogrammetry and measured on the MRS differs by 0.2% and 0.3% after the first and second displacement stages. While the results may not achieve the same level of accuracy or precision as other industrial photogrammetric applications, the level of precision does not preclude its use as a monitoring tool.

6.2 Introduction

Underground mines commonly experience ground deformations as a result of changing states of stress in the rock mass surrounding excavation. Monitoring rock deformations is critical to understanding the mechanical behavior of a rock mass and designing support systems to prevent unwanted deformations or stress concentrations.

Longwall mines in the United States rely heavily on standing secondary support systems to prevent the closure and maintain stability of gate roads. A design methodology for secondary support systems was developed by NIOSH that incorporates ground reaction data into the selection of the different, available standing support systems, called the Support Technology Optimization Program (STOP). Without this, a mine is typically required to create a trial section where the new support system is monitored for its response to abutment loading [35]. To collect the necessary ground reaction data, in order to properly design a support system for a mine, the displacement of the individual supports must be monitored.

One way of assessing the support design requirements is by examining the ground response curve, shown in Figure 6.1. This curve represents how support systems interact with rock mass expansion and failure when an opening is created. Predicting the shape of the ground response curve is difficult, due to the heterogeneity and anisotropic nature of the rocks that surround underground coal mining operations. The only known points along the curve are those that have been measured along the support reaction line. The design curves for standing supports have been experimentally determined from laboratory testing, and by measuring the displacement of the support, the pressure being exerted by it can be estimated.

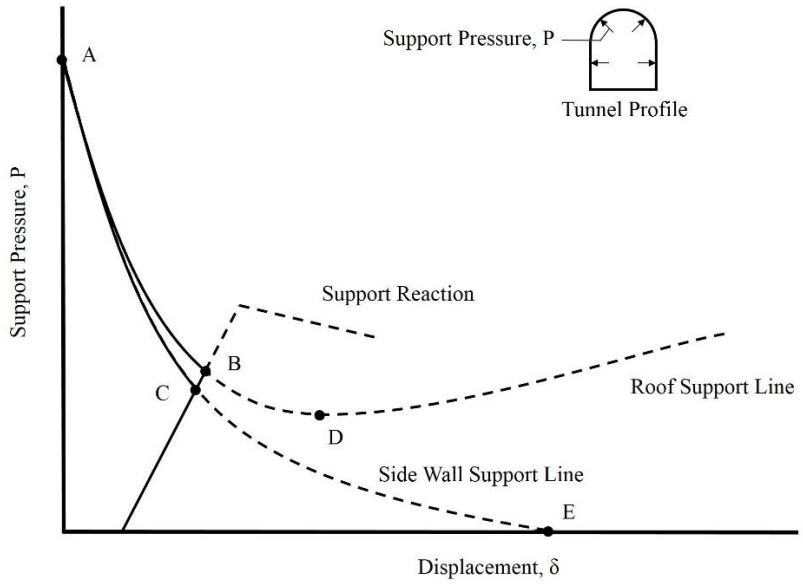

Figure 6.1: Ground response curves and a support reaction (after [16])

Measuring the displacement of a standing support is typically performed using point measurement devices, such as contact extensometers. Their measurement precision may be high, but their accuracy is dependent on how they are installed on the support and how the support deforms. An alternative measurement technique, being proposed in this paper, is photogrammetry. Photogrammetry is a form of image measurement that derives the geometric properties of an object or scene from one or more photographs. The primary purpose of this process is to recreate a three-dimensional object in a digital format [9].

The purpose of this experiment is not to create a perfect scenario in which a standing support can be modeled with the highest degree of precision. The purpose of this experiment is to evaluate photogrammetry as a monitoring or measurement tool for deformation in an underground coal mine. The regulatory, environmental, and operational limitations of underground coal mines limit camera selection and picture-taking practices. Therefore, it is the goal of this experiment to closely replicate what is operationally feasible and obtain the most accurate and precise results possible within those confines. Inducing a load on a standing support, and using photogrammetry to monitor that change, will constitute a first step in quantifying the reliability of photogrammetry as a monitoring tool for standing roof supports.

6.3 Methods

The experiment will involve artificially inducing a convergence on a standing roof support and capturing the deformation with photographs at different intervals. The photogrammetric results can then be compared to the measured convergence to determine their accuracy. There are three major components to this process: the camera, the support and hydraulic press, and the software used to process the photographs.

The camera selected for this experiment is a CorDEX ToughPIX II digital camera [106], shown in Figure 6.2, was designed for use in hazardous environments. It is ATEX and IECEx certified for petrochemical and mining environments, with an armored LCD screen and flash. The camera does not have Mine Safety and Health Administration (MSHA) approval, however, it has camera specifications that could likely be maintained or surpassed while meeting MSHA design standards, if a manufacturer decided to seek such approval.

Figure 6.2: CorDEX ToughPIX II [106]

Pertinent design specifications for the camera include a 16-megapixel capture resolution, 3x optical zoom, 16-gigabyte image storage, removable and rechargeable battery, and a weight of 0.9 kg. The camera does not offer much flexibility in changing shutter speeds or focal length, but such concessions must be made when the camera models available are severely limited by the regulations concerning explosive atmospheres.

The photogrammetry subject is a cylindrical steel support filled with an aerated concrete, and is a commonly used yielding support in United States longwall mines. These supports are

especially common where timber is scarcer, such as in Western longwall mines [41]. Due to the high deformability of the support, large deformations can be monitored, ensuring that the change in total length of the support will not fall below the sensitivity of the monitoring capabilities. The support photographed in this study has a 22.9 cm diameter and stands 274.9 cm tall.

The support will be loaded by the Mine Roof Simulator (MRS), located at the NIOSH Pittsburgh Research Laboratory. The MRS, shown in Figure 6.3, was manufactured by MTS Systems Corp, and originally used for testing longwall shields. The MRS is a servo-controlled hydraulic press that applies loads of 13.3 MN from each of its four actuators. It has a maximum opening height of 4.9 m, a maximum convergence of 0.610 m, and platens measuring 6.1 m x 6.1 m. The experimental configuration, with the support inside of the MRS is shown in Figure 6.4 [107].

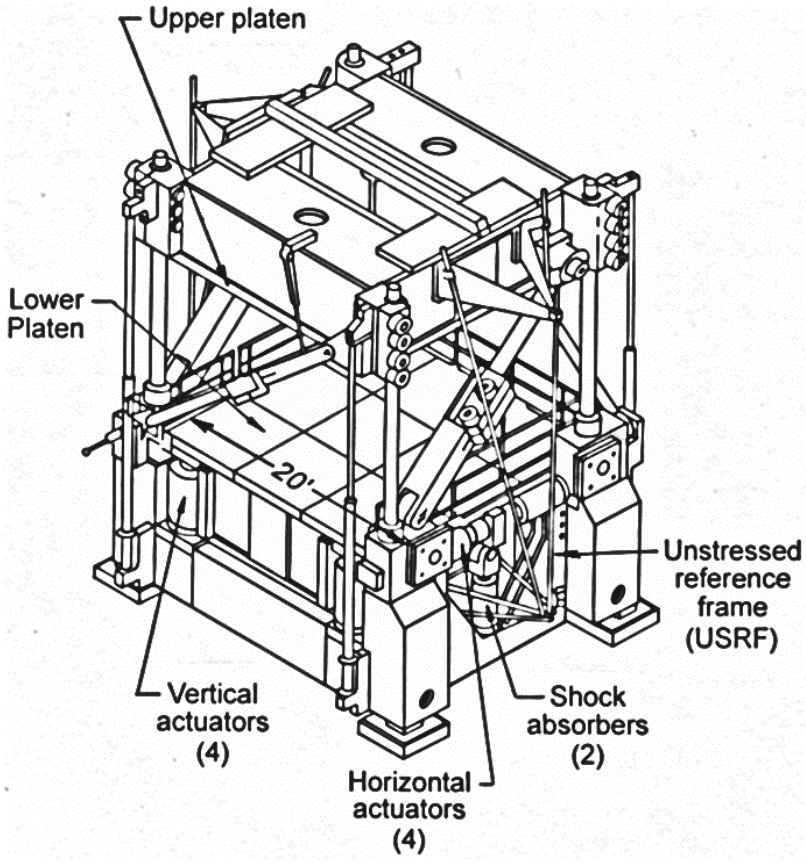

Figure 6.3: Mine Roof Simulator [107]

Figure 6.4: Standing support inside the MRS

For this experiment, pictures were taken of the support at three different convergence levels. The first level is before convergence has started, and the MRS has merely been lowered to establish a contact with the support. The second level is after 5.1 cm of convergence has occurred. The third level is after an additional 25.4 cm. of convergence has occurred, or 30.5 cm from the original height. After the convergence at each stage has occurred, loading was paused and a series of pictures were taken. A layout of the estimated camera positions is shown in Figure 6.5. Each picture had a resolution of 4608 x 3456, a focal length of 5 mm, and was captured at a distance of 1 to 2 meters from the support. These distances were chosen because they allowed as much of the support to be photographed as possible while remaining at a geometrically reasonable distance from the support considering the dimensions of a coal mine entry. Each camera position shown in the x-y views consists of either two or five photos, as illustrated in the z-x view.

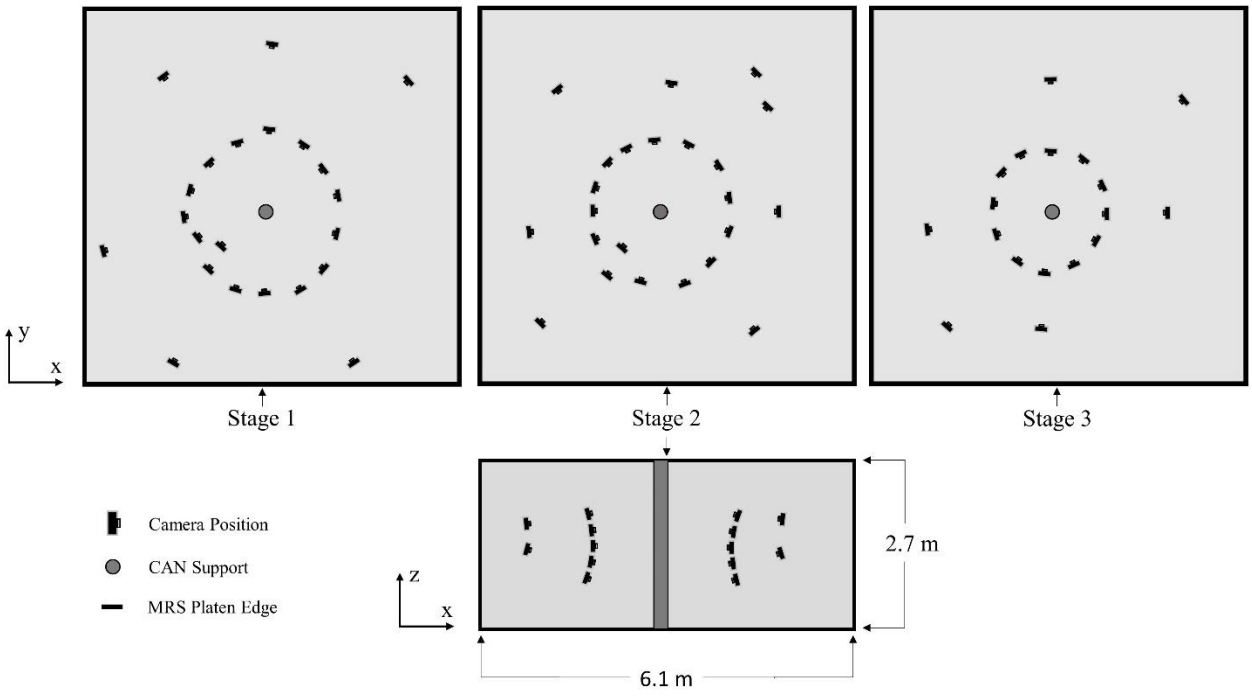

Figure 6.5: Camera positions for Stage 1, 2, and 3

Both Agisoft's PhotoScan [108] software and Maptek's iSite [94] software were used to process the images and point clouds. PhotoScan was used to generate point clouds and triangulated surfaces of the standing support at the different convergence stages, and scale them appropriately. Scaling and orienting of the scene was performed by applying the software's ground control points to known bolt spacing on the MRS of 50.8 cm. A summary of the number of points, triangles, and scaling error associated with each convergence stage is shown in Table 6.1.

Table 6.1: Point cloud information by convergence stage

Stage	Photos	Number of Points on Support (approximate)	Number of Triangles on Support (approximate)
1	78	703,000	120,000
2	81	558,000	75,000
3	82	617,000	92,000

After the point clouds and surfaces were generated, the objects were imported into iSite. In the software, the triangulated meshes were compared to each other to find the average distance

between them, as well as the approximate height of the support as determined by the scaled point cloud.

6.4 Results

As the MRS converged, the support began to crumple near the top platen. The state of the support after no convergence (Stage 1), 5.1 cm convergence (Stage 2), and 30.5 cm convergence (Stage 3) are shown in Figure 6.6. All visually recognizable deformation of the support is occurring at the top of the support.

Figure 6.6: Stage 1 (left), Stage 2 (middle), and Stage 3 (right)

The calculated convergence is the difference between the top platen of the MRS and the bottom platen of the MRS. To assist in the visualization of this convergence, the distance between the top platen and an artificially constructed plane at a z position of 274.9 cm (the measured height of the support) is shown in Figure 6.7. A triangulation was generated for each stage. To orient each vertical axis of the triangulation surface with the z-axis, planes of best fit were determined for the calculated geometry of the top platen. The normal vector for this plane was then rotated to align itself with the z-axis for all three stages. The three stages were translated by hand to the same approximate location. The hand translation should not affect height calculations, as they are independent of x, y, and z position.

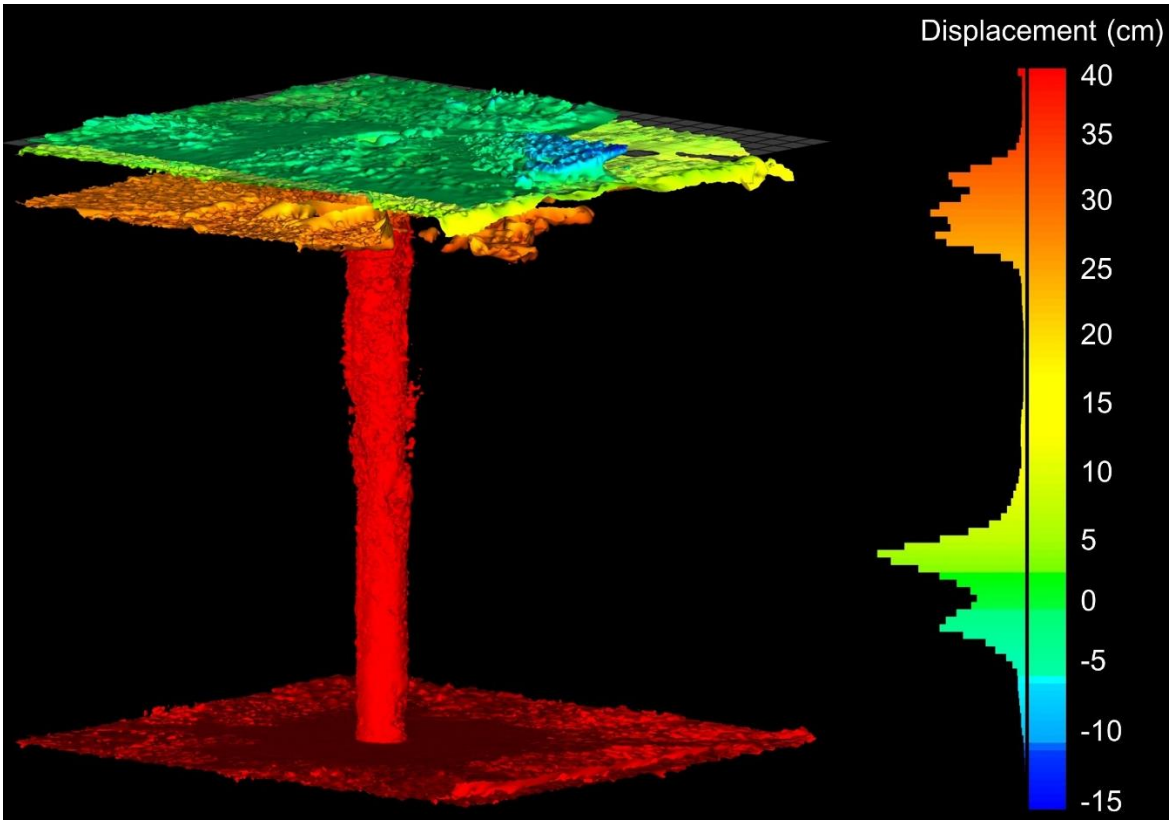

Figure 6.7: Convergence for each stage, measured as the difference between the calculated top platen positions and a construction plane at 274.9 cm

The photogrammetric results did not yield platen surfaces that were as uniform as those found on the MRS. Standard deviations for the calculated elevations of each platen ranging from 0.27 to 1.32 cm are shown for each stage in Table 6.2.

Table 6.2: Standard deviation of platen elevations

Stage	Platen	Standard Deviation (cm)
1	Top	0.49
1	Bottom	0.41
2	Top	1.32
2	Bottom	0.56
3	Top	0.89
3	Bottom	0.27

The top and bottom platen surfaces of the MRS are assumed to have no vertical deviation. The triangulation surfaces that resulted from the photogrammetry do not form smooth top and

bottom platen surfaces without vertical deviation. The height of the support could be measured by finding the perpendicular distance between the two platens at any given point, or by subtracting the z-coordinates of two areas that appear to best represent the flat surface of the platen. It may be necessary to arbitrarily choose locations to measure in a field study, but this research benefits from a convenient plane-to-plane distance that can be used as the height of the support.

The exact height of a standing support in an underground coal mine would be unknown after any convergence, but would be known to the precision of manufacturer specifications before installation. When these supports are installed underground, they are commonly prestressed with timber wedges or inflatable bladders at the support/roof interface [34]. At any subsequent monitoring stage, the deformation would be unknown prior to collecting measurements. One proposed method for determining this height through photogrammetry is to determine the roof-to-floor distance by assigning a z-coordinate position to roof and floor. Isolating the roof and floor triangulations from the rest of the scene allows them to be analyzed independently to determine their z-position. An average of the z-coordinates for each vertex in the triangulation could be an inaccurate representation of position due to skin control issues in the roof or accumulation of material on the floor. The mode may be a better indicator of position, representing the most probable occurrence. To lessen the effect of bin sizes when creating a histogram from a set of continuous distance measurements, the probability density function was smoothed using the kernel density estimation function in MathWorks' MATLAB [109].

In order to determine the height of the support at each loading stage, a construction plane was created at a z-coordinate of 274.9 cm. The z-coordinates corresponding to the points that comprise the reconstructed top and bottom platens were measured as the distance of each point in the platen to that construction plane. This creates an array of distance values from which a mode, or most likely outcome, can be determined through a kernel density estimation. Bandwidths for the kernel density estimation were adjusted to give each platen location a single, clear peak. This was most necessary for the top platen at stage 3, which with a rough bandwidth could be considered trimodal. The maximum values along each of these bimodal curves, shown in Figure 6.8, are considered to be the z-positions of the top and bottom platens.

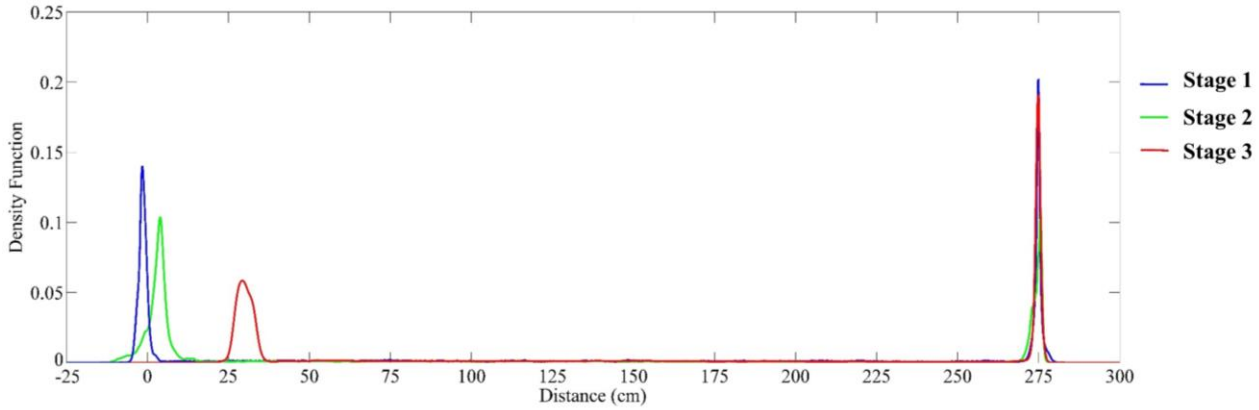

Figure 6.8: Kernel density estimation for the platen positions

Using the peak-to-peak distance, a height for the MRS at each of the three stages can be calculated. The height, change, and strain of each MRS displacement stage is shown in Table 6.3. The measured height is the distance between platens as measured by the MRS. The calculated height is the distance between platens as estimated through photogrammetry in Figure 6.8. The remaining measured and calculated columns are derived from the measured and calculated heights.

Table 6.3: Measured vs calculated convergence

Stage	Measured Height (cm)	Calculated Height (cm)	Measured Change (cm)	Calculated Change (cm)	Measured Strain (%)	Calculated Strain (%)	Strain Error (%)
1	274.88	276.43	N/A	N/A	N/A	N/A	N/A
2	269.80	271.60	-5.08	-4.83	-1.85	-1.74	5.94
3	244.40	245.50	-30.48	-30.93	-11.09	-11.19	0.90

Between stage 1 and 2, a 4.83 cm convergence is calculated, and between stage 1 and 3, a 30.93 cm convergence is calculated. These convergences differ from the measured values for stage 1 to 2 and 2 to 3 by -0.25 cm and 0.45 cm respectively. The magnitude of change between stage 1 and 2 does not differ proportionally from stage 2 to 3, suggesting that there is an error independent of the height of the support, and likely instead dependent on the distance between the

photographs and the subject as well as camera parameters. All of the calculated heights are larger than the measured heights, possibly indicative of consistent scaling error.

It is difficult to distinguish between error caused by scaling and inaccuracy or imprecision in the photogrammetry. The calculated height differs from the measured height by between 0.45% and 0.56%, which could reasonably fall within an expected margin of error when manually selecting points for scaling. Despite this error, the measurements, if reproducible in an underground environment, are of an accuracy that could be useful for measuring roof to floor convergence.

6.5 Conclusion

The ability to quantify the deformation of underground standing supports is important for understanding rock mass behavior. In order to see if photogrammetry can be used as a tool for monitoring underground rock mass movements, a standing support was subjected to different displacements, photographed, and then modeled. The environment for the experiment is markedly different from an underground coal mine. There are no issues with inadequate lighting, and the geometries available for scaling and referencing the scene are favorable. Both lighting and unfavorable geometries would be significant concerns in an underground environment. However, the laboratory setting allows for highly controlled displacement of the standing support, which could not be performed underground, and is an important step in applying photogrammetry to the monitoring of standing supports underground.

After modeling the standing support at different displacement levels, the results of photogrammetry showed a calculated convergence of 4.93 cm compared to a measured convergence of 5.08 cm after the first MRS movement, and a calculated convergence of 30.93 cm compared to a measured convergence of 30.48 cm after the second MRS movement. The difference between the calculated and measured convergence is not likely dependent on the size of the support, but instead of the quality of the photographs and relative size of a pixel to the support.

The accuracy of measurements required in an underground environment will be mine-dependent, but the sub-centimeter accuracy calculated from the photogrammetry in this study should be adequate for many applications of deformation monitoring in underground mine

environments. In addition to providing precise measurements at current specifications, photogrammetry is a photographic quality-dependent technology that will only grow more precise with improved camera technology or an increased development of cameras that meet MSHA approval.

Chapter 7 Underground Photogrammetric Monitoring of Standing Supports

7.1 Abstract

An underground longwall coal mine in Central Appalachia was studied for ground movement in response to abutment loading. Photos were taken of a wooden crib and sand-filled steel support at different visits, with a changing state of stress, for a time-lapse photogrammetric analysis of displacement. This photogrammetric analysis was performed in conjunction with extensometer measurements of change during the monitoring period. Both the wooden crib and the steel support were successfully modeled using photogrammetry in different dynamic lighting conditions. During the monitoring period, a roof-to-floor convergence of 0.62 cm was recorded by an extensometer on the modeled crib, with a roof-to-floor convergence of 0.62 cm measured using the three-dimensional models created through photogrammetry. No extensometer was placed on the steel support, but a modeled 0.28 cm of roof-to-floor convergence was detected according to the photogrammetric point cloud. As expected, photogrammetry accuracy was found to be highly dependent on photograph quality, lighting, and overlap, but modeling of standing supports was found to be possible within sub-centimeter precision using a point-and-shoot camera.

7.2 Introduction

Underground coal mining was responsible for producing 343 million tons of coal in 2012 in the United States [1], of which 52% was excavated by longwall [2]. Coal remains an important part of the United States' energy portfolio, as well as the world's and it is important to continue improving coal mine safety. In the United States, falls of ground in underground coal mines have led to 2300 operator and contractor injuries, as well as 35 fatalities between January 2007 (the year of the Crandall Canyon mine disaster) and July 2013 [3]. The injury and fatality rate has been decreasing in recent decades [4], due to better safety practices and increased understanding of underground mining environments.

In longwall mining, large abutment stresses form following the removal of support that accompanies excavation of panels. These abutment stresses can present ground control problems, specifically in the gate roads, if not adequately addressed. These abutment stresses are usually addressed with regularly installed standing supports. The behavior of these supports in laboratory settings are well documented, and by using observed deformations, the ground response curve for the rock mass can be determined. The anisotropy and heterogeneity of the typical stratified rock masses found in underground coal mines leads to conditions that differ widely enough to necessitate site-specific monitoring and customization of standing support arrangements, typically with a trial section to determine proper support [29].

Two standing supports were monitored for this research, the strain-softening conventional timber support and a non-yielding sand-filled steel support. Conventional timber supports, also known as wooden cribs, were until recent decades the only available support for longwall tailgates. Wooden cribs provide support over a large deformation, are easy to install, and are generally low-cost. The steel support used in this study behaves differently than wooden cribs do under load. It is capable of providing high support pressures, but does not allow more than several centimeters of convergence before failure.

The means of measuring support deformation was photogrammetry. Photogrammetry is a method of determining the geometric properties of an object by analyzing photographs. The purpose of modern digital photogrammetry is to create a three-dimensional object in the digital space [5]. This study focuses on an application of close-range digital photogrammetry (CRDP), typically contrasted with aerial photogrammetry. CRDP is a photogrammetric technique where the object is within 100 meters and the cameras either are contained within, or surround, the object [53]. Photogrammetry has wide interdisciplinary use, but is also being applied in an underground mining environment for fracture characterization [57], geotechnical mapping [58][59], and blast rock volume measurement [60].

Underground mine movements are widely measured using equipment limited to the response of a single point, such as extensometers. These systems require an extrapolation of rock mass movement and are subject to local biases and method of installation. These systems usually come with a high degree of precision, but they lack the ability to capture movements beyond the one-dimensional axis on which they are affixed. Photogrammetry offers an ability to capture the three-dimensional movement of an entire scene. The usefulness of photogrammetry as a fast, cost-

effective, and precise supplementary tool for monitoring underground mine displacements will be explored in this research.

7.2.1 Site Description

The underground coal mine visited in this study is located in the Central Appalachian region of the United States and its primary means of ore extraction is through longwall mining. The mining depth ranges from 187 m to 193 m, with an average entry height of approximately 2.4 to 2.7 m in the study area. The roof consists of 0.3 to 1.2 m of shale, overlain by 0 to 2.4 m of sandy shale. The floor strata consists of 0.3 to 2.4 m of shale and fireclay, underlain by 0 to 3 m of sandstone.

When monitoring first began at the site, little development had occurred, and how the standing support system would respond to abutment loading was unknown. The standing support system used to reinforce gate roads consisted of concrete-filled metallic cylinders, wooden cribs, and sand-filled steel supports. The photogrammetry research was performed coinciding with the installation of extensometers on standing supports at various locations throughout the mine. These were installed to monitor the ground response, and improve the standing support plan. Inconsistencies in the extensometer results led to only two locations providing reliable data, which are marked on Figure 7.1.

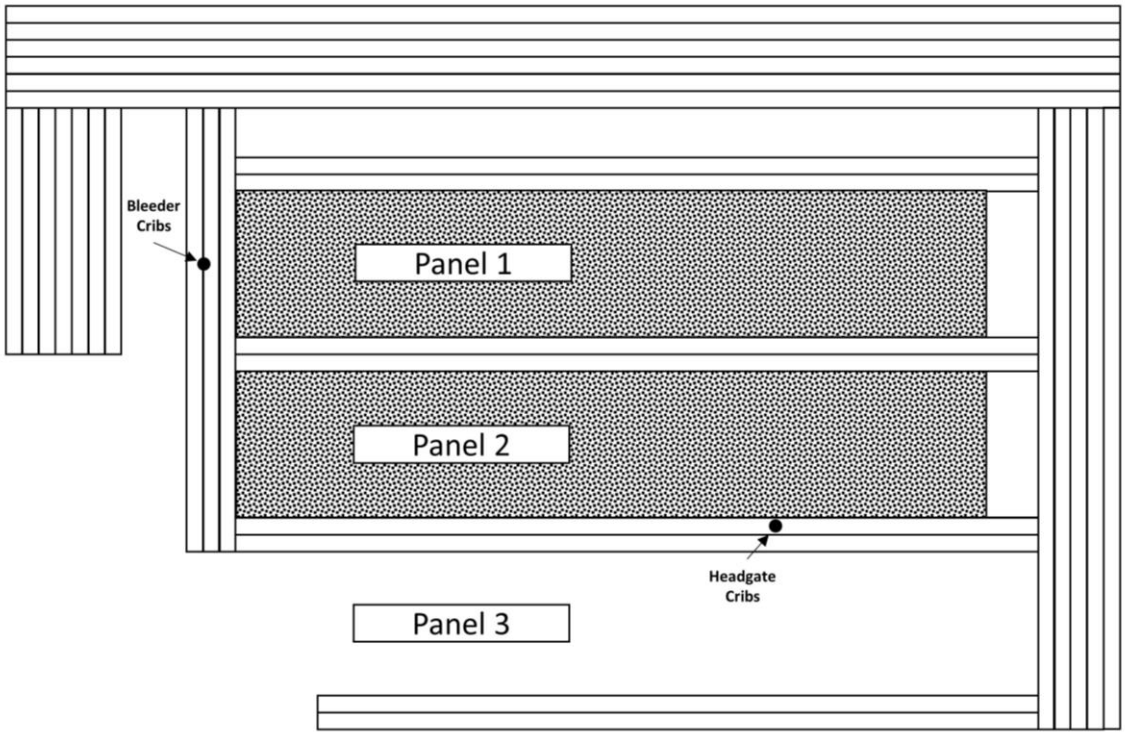

Figure 7.1: Approximate mine layout in the monitoring region. The bleeder cribs are located in the bleeder entries and the headgate cribs are located in what, at the time of monitoring, was the headgate.

It was not common at the mine to install supports far in advance of the longwall face, however, the mine had a crosscut heavily supported with wooden cribs and steel supports, approximately 369 m ahead of the longwall face. This area, labeled as "headgate cribs" in Figure 7.1, was supported as a remedial measure in response to unexpected deformation. The headgate crib area was photographed at different visits to monitor a time-lapse change. The bleeder cribs were not photographed due to safety regulations, however, extensometer data is available for this region, which can help to understand the ground response.

7.3 Methods

Two subjects at the headgate site were chosen, one wooden crib with no apparent deformation and one steel support with significant deformation already present. A photograph of this crosscut is shown in Figure 7.2, the steel support is shown in Figure 7.3, and the wooden crib is shown in Figure 7.4.

Figure 7.2: Photogrammetry study site

Figure 7.3: Steel support photogrammetry subject

Figure 7.4: Wooden crib photogrammetry subject

7.3.1 Camera and Lighting

Two cameras were used in this experiment. The first is a CorDEX ToughPIX II digital camera [106], was designed for use in hazardous environments. It is ATEX and IECEx certified for petrochemical and mining environments, with an armored LCD screen and flash. This camera is not certified with the Mine Safety and Health Administration, but has representative specifications that could be expected in a camera designed for use in a hazardous environment. The camera has a 16 megapixel capture resolution, 3x optical zoom, 16-gigabyte image storage, removable and rechargeable battery, and a weight of 0.9 kg. The zoom was not used for this study. The second camera used was a 12 Megapixel Canon PowerShot. The third set of photos was collected remotely by an employee of the mine who did not have access to the ToughPIX II, and used the most similar point-and-shoot camera available.

Lighting was provided by either the camera flash or a wearable array of cap lamps, shown in Figure 7.5. The array was fabricated specifically for this task and consisted of six Polaris Cordless Cap Lamps [113], set to their brightest setting. The array was worn around the neck to

leave the hands free for photography. The lighting was changing throughout the study, although the changes were minimalized with the cap lamp array. This auxiliary lighting was necessary because the battery life of the ToughPIX II camera could not sustain flash photography throughout the experiment.

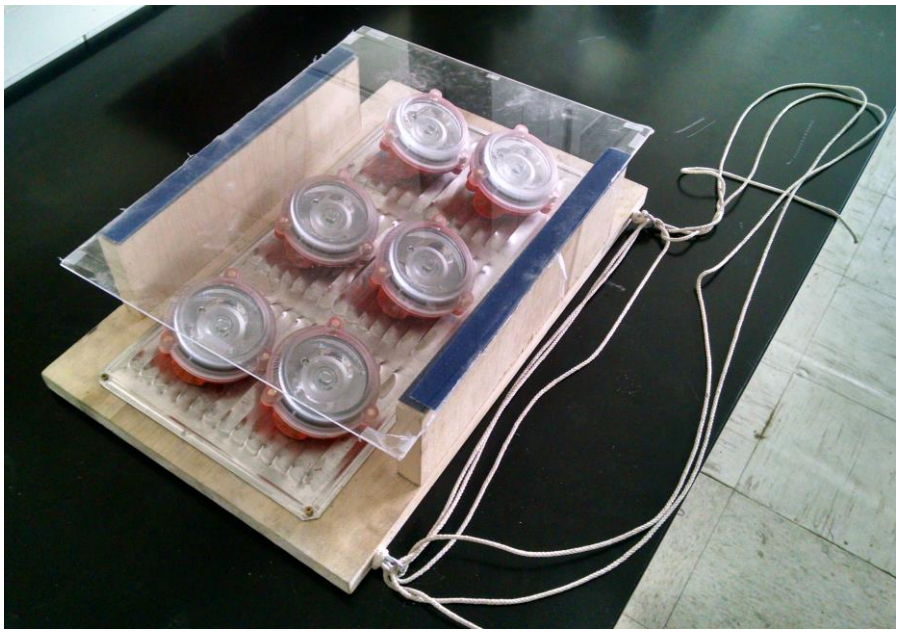

Figure 7.5: Mobile array of cap lamps for use in underground mine illumination

7.3.2 Image Capture and Software Methodology

Time-lapse photographs were taken of both the steel support and the wooden crib. The second set of photographs was taken 25 days after the first, with a third set being taken of just the wooden crib two days after the second set. The light source for the first set of photograph was the cap lamp array. The camera flash was not used for the first set due to battery concerns. The second set of photos included both a cap lamp light source and the camera flash, with each having a set unique to that light source instead of both light sources being used simultaneously. An additional battery was taken to compensate for the increased power requirements from the camera flash. The last set of photos was acquired by an employee of the mine using a 12 megapixel point-and-shoot camera and the onboard flash as a light source. These photograph sets are shown in Table 7.1

along with the number of photos in each set. The camera settings are shown in Table 7.2. Thumbnails of the photographs are available in Appendix A.

Table 7.1: Summary of the time-lapse photograph sets

Date	Subject	Photographs Taken	Photographs Used	Light Source
10/10/2014	Steel Support	74	29	6 Cap Lamps
10/10/2014	Wooden Crib	95	95	6 Cap Lamps
11/5/2014	Steel Support	18	18	6 Cap Lamps
11/5/2014	Wooden Crib	41	20	6 Cap Lamps
11/5/2014	Steel Support	47	47	Camera Flash
11/5/2014	Wooden Crib	41	38	Camera Flash
11/7/2014	Wooden Crib	26	26	Camera Flash

Table 7.2: Photograph EXIF data from each visit

Date	Resolution	F Stop	Exposure	Focal Length	Max Aperture
10/10/2014	4608 x 3456	f/3	1/12 sec	5 mm	3
11/5/2014	4608 x 3456	f/3	1/12 sec	5 mm	3
11/7/2014	4000 x 3000	f/2.8	1/60 sec	5 mm	3

The longwall was advancing at an average of approximately 12.1 m/day between October 10th and November 7th. The longwall position, as it relates to the monitoring area is shown in Figure 7.6. The photographed area was outside of the influence of the front abutment, and should not have been experiencing abnormal stresses beyond the development loading. However, it had already converged significantly, as evidenced by the deformed steel support in Figure 7.3.

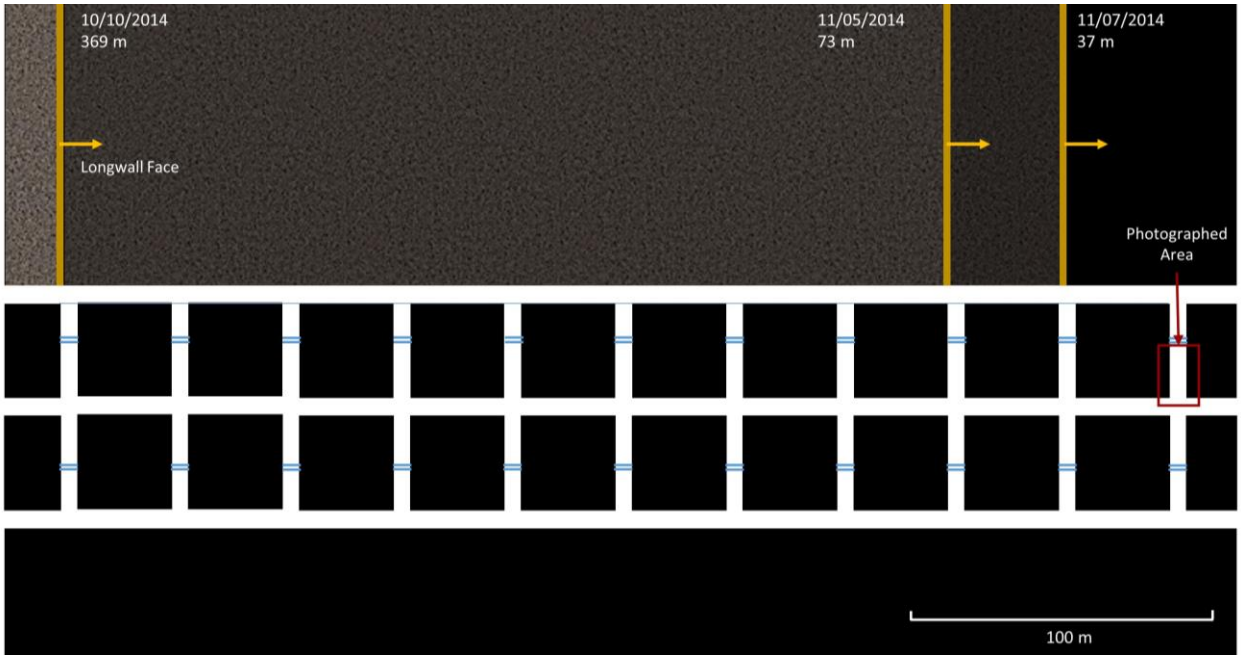

Figure 7.6: Approximate position of the longwall face relative to the photographed crosscut

The photographs were processed through a combination of software packages. The first, Agisoft PhotoScan [108], was used to generate a three-dimensional point cloud from the photographs. The number of photographs used, from Table 7.1, corresponds to the number used in reconstruction in PhotoScan. A sparse point cloud was generated first, followed by a densely constructed point cloud. The dense point cloud, depending on the quality of photographs, often contains many erroneous points, which are removed prior to mesh construction if they are geometrically unreasonable. Triangulated surfaces were then created for each of the standing supports in PhotoScan using the dense point cloud as a base for construction. These objects were then exported into CloudCompare, an open source 3D point cloud and mesh processing software, for scaling and orienting. The midpoint of each 0.12 m x 0.12 m wooden face was used to translate and rotate the point clouds onto the same coordinate system. They were then scaled assuming an average 12.2 cm thickness for the wooden beams. The workflow for processing the photos into manageable three-dimensional surfaces is illustrated in Figure 7.7.

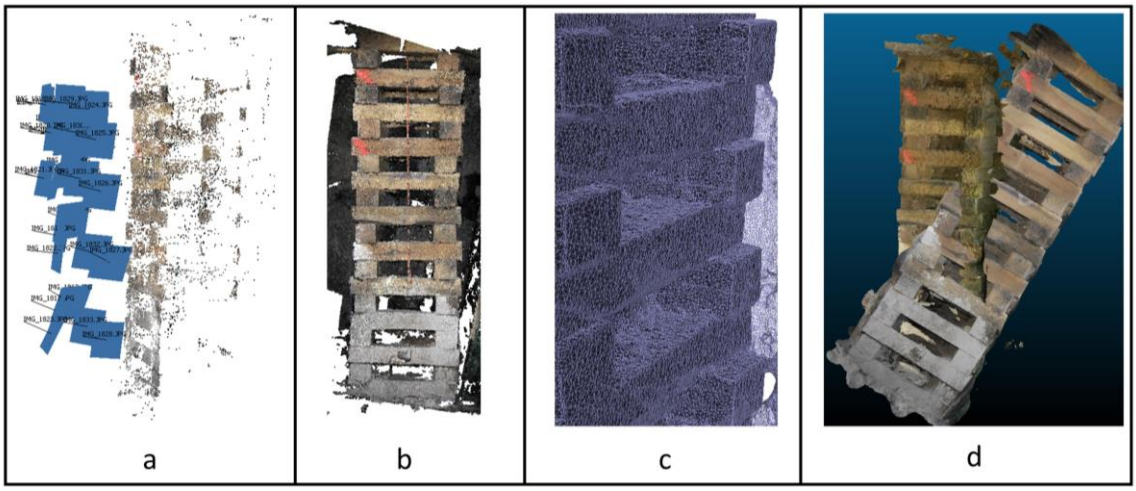

Figure 7.7: Photogrammetry workflow a) constructing a sparse point cloud in PhotoScan, b) generating a dense point cloud in PhotoScan, c) creating a wireframe model in PhotoScan, d) orienting and scaling objects in CloudCompare

Following this, Maptek's iSite software [94] was used to rotate the supports and calculate differences between the meshes. The objects were rotated such that the y-axis follows the vertical axis of the supports. Lastly, Mathworks' MATLAB [109] was used to determine the vertical or horizontal extents of crib structure components and the steel support. The MATLAB code used for determining the geometric extents of wooden beams is available in Appendix C.

The MATLAB Kernel Density Estimation allows for determination of the edges of structures within the scene that contained significant noise. For example, the wooden crib has a number of features that can be used for comparison or scaling, including, but not limited to, the vertical extents of individual wooden beams, the horizontal extents of individual wooden beams, and the roof and floor interface.

7.4 Results

The steel support was reconstructed with ease using the November 5th flash lighting photograph set, but was reconstructed with difficulty using the October 10th and November 5th photograph sets using the cap lamp lighting. The cap lamp lighting caused much of the steel support to be obscured by reflectance, and the lit area excluded much of the surrounding wooden cribs. The excluded surrounding cribs and obscured steel support features are believed to be

responsible for poor point matching in the photographs, especially towards the center of the support. Because of this, the November 5th photograph set using the cap lamp lighting was discarded, and instead the flash-lit photograph set from this time period was compared to the October 10th cap lamp-lit photograph set. Both the wooden crib and steel support reconstructions are shown in Figure 7.8 along with the anchor points that were used for roof-to-floor convergence measurements.

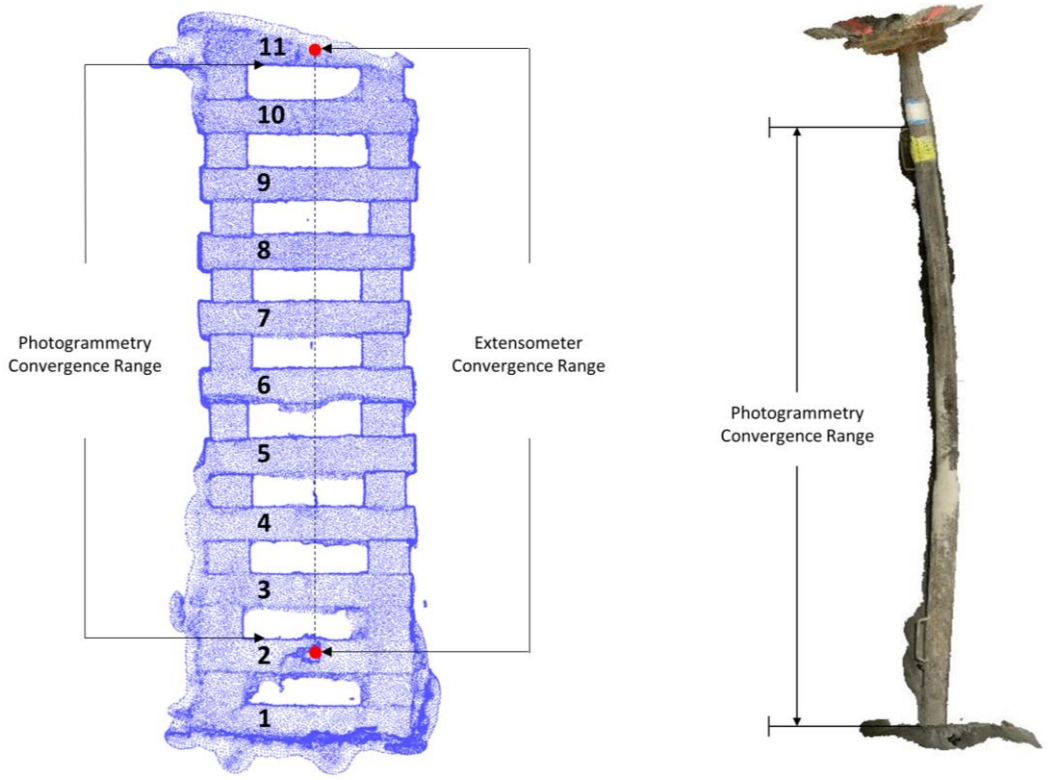

Figure 7.8: Measurement range for the extensometer and photogrammetry

The reconstructed steel support showed a roof-to-floor convergence of 1.10 cm between October 10th and November 5th. The convergence range on October 10th was calculated to be 227.02 cm, and on November 5th was calculated to be 228.11 cm. The points selected for comparison on the steel support were not as well defined as the planes created by the individual beams for the wooden crib, increasing the difficulty with which convergence anchors could be precisely determined on the October 10th reconstruction.

Extensometer data from October 10th to October 31st on the photographed wooden crib shows a significant convergence on October 13th, and small movements afterwards that resulted in

a slight expansion by the end of the 21 day period. Unfortunately, the extensometer readings did not continue through to the second set of pictures. The extensometer was vandalized and stopped producing useful readings until it was repaired on November 5th. The extensometer readings continued to show no significant trend in convergence until November 8th, when the longwall face was 25 m from the test site and one day following the last set of pictures. At this point, a clear convergence is visible throughout the remainder of the data collection period. The extensometer measurements are shown in Figure 7.9.

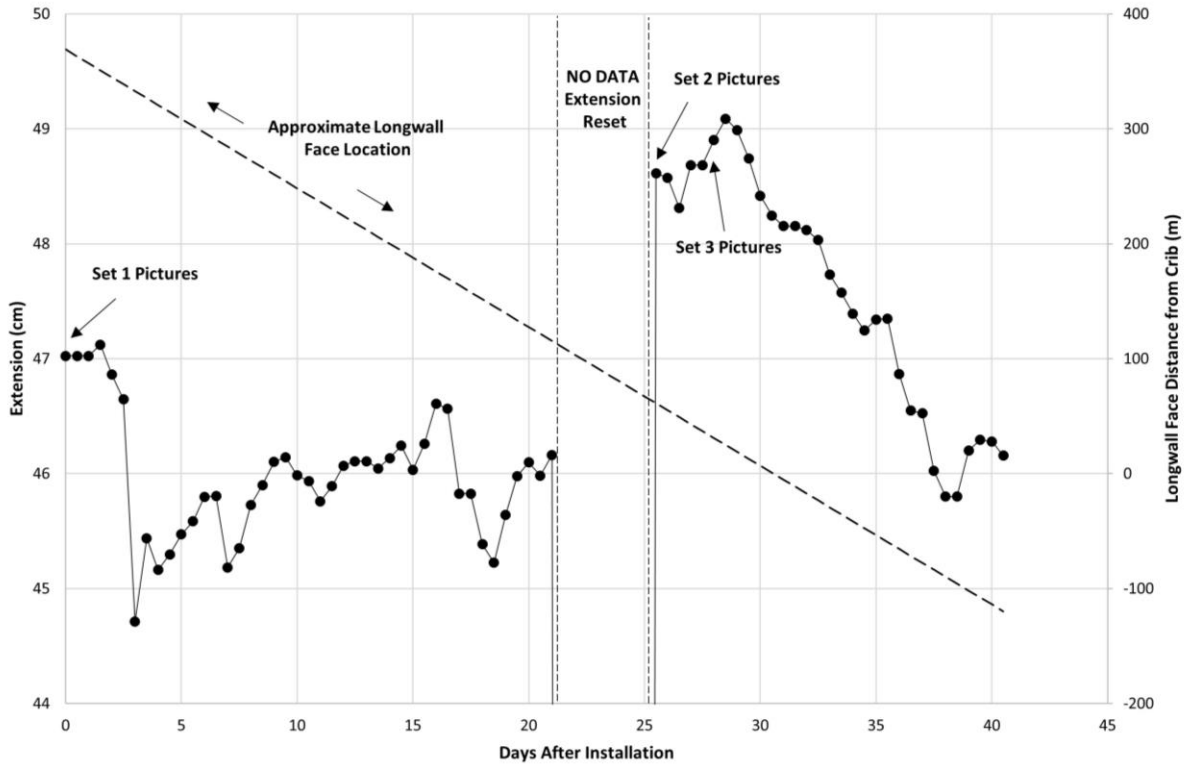

Figure 7.9: Extensometer measurements, at 12-hour intervals, for the convergence of the crib throughout the experiment

The measured extensometer convergence from October 10th to October 31st is 0.86 cm, with a measured expansion of 0.24 cm from November 5th to November 7th. The cumulative convergence recorded by the extensometer is 0.62 cm, although this does not include any convergence that may have occurred during the 5 days where the extensometer was not operational. Each of the photogrammetric reconstructions is shown in Figure 7.10.

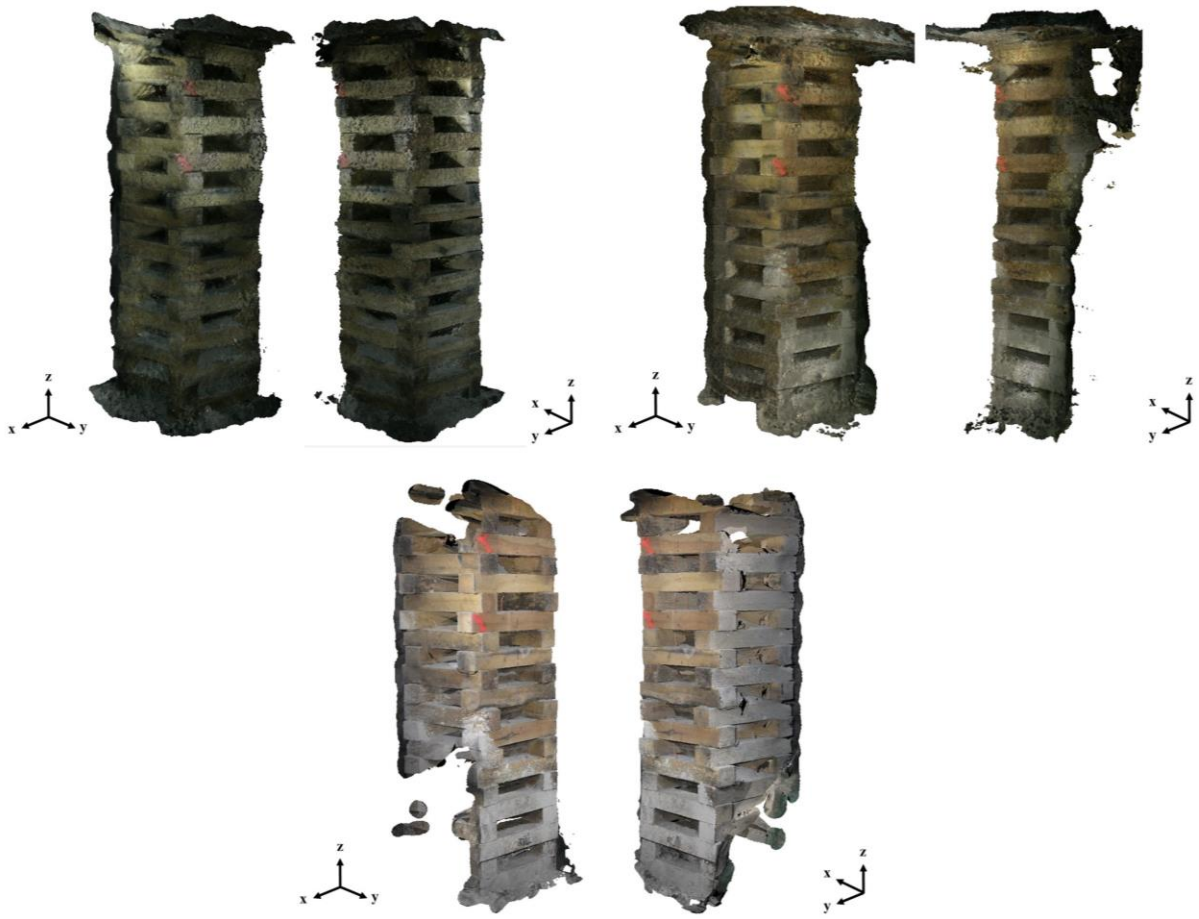

Figure 7.10: Photogrammetric reconstruction of the wooden crib on October 10th (top left), November 5th (top right), and November 7th (bottom)

The two locations where the extensometer was anchored were not known in the first set of photos, and the planar surfaces of the wooden beams made for more convenient photogrammetric measurement points, shown in Figure 7.8. The different anchor points result in a convergence measurement range approximately 12 cm larger for the extensometer data. Neither measurements are true roof-to-floor convergence values, with three wooden beam widths lying outside of the extensometer measurement range.

Using photogrammetry, and measuring between the planes corresponding to the top of the 2nd and bottom of the 11th beam, 1.16 cm of convergence was detected between October 10th and November 5th. An expansion of 0.54 cm was detected in the same physical range between November 5th and November 7th, resulting in a cumulative convergence of 0.62 cm. The absolute differences between the extensometer and photogrammetry measurements for the first-to-second,

second-to-third, and cumulative convergence are 0.30 cm, 0.30 cm, and 0.00 cm respectively. The first-to-second and cumulative convergence values for the extensometer may be in error; however, the second-to-third measurement is consistent. The convergence measured on the reconstructed point clouds are very similar between the steel support and the wooden crib for the October 10th to November 5th time period, differing by only 0.06 cm, although the measurement range for the steel support was 19.5 cm larger.

Three additional extensometers were installed in the photographed crosscut. They should not be used to validate the photogrammetric data, as the local variation in ground response is unknown. However, they can be used to verify that the extensometer installed on the photographed crib is measuring movement consistent with deformation in nearby cribs, and not producing anomalous results, possibly indicative of experimental error. The remaining extensometers are shown in Figure 7.11 at the point where a converging trend first emerges. The trend develops in response to the developing front and side abutment load, as the longwall face approaches and passes. The photographed area shown in Figure 7.6 is the same as the plan view shown in Figure 7.11.

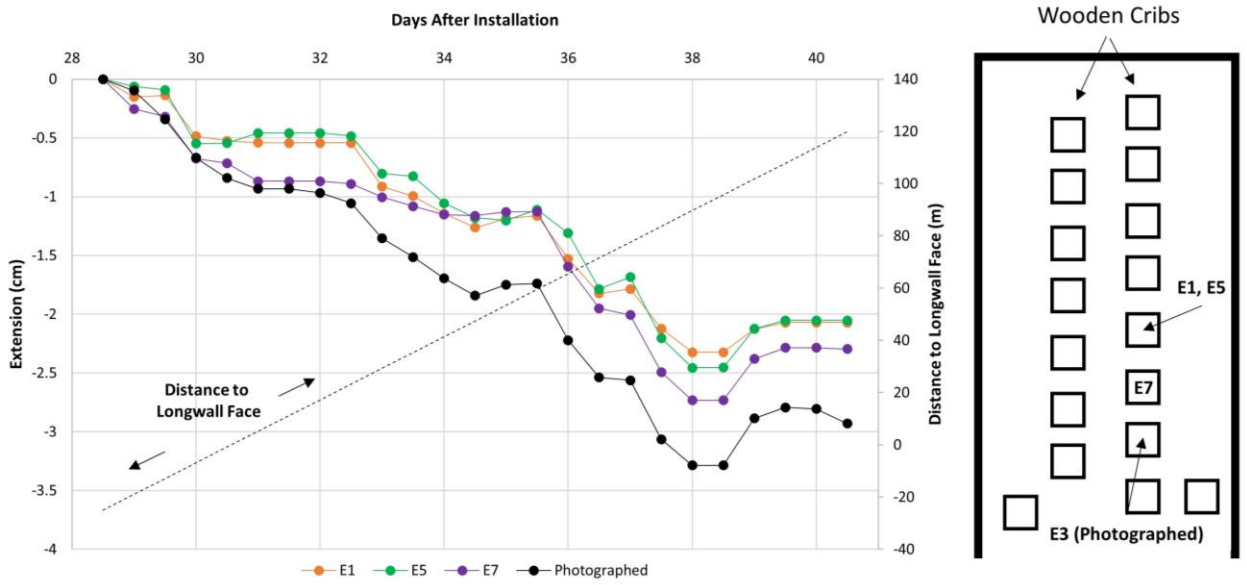

Figure 7.11: Convergence measurements from all four extensometers installed in the monitoring area, starting from the date of a clear abutment stress-induced movement

The extensometers all show a very similar pattern of convergence, with the magnitude convergence becoming more pronounced as the distance from the longwall panel increases. The convergence shown in this crosscut is similar to the convergence experienced on instrumented wooden cribs in the bleeder entries following longwall development.

7.4.1 Other Experiments

In addition to the standing support monitoring, other mine structures were photographed or recorded through video in different ways, to test the versatility of this close range photogrammetry application. Two methods of picture capture were explored: Object Panorama and Straight Line, shown in Figure 7.12. The previous data analysis was performed on photographs collected using the Object Panorama method, however, this may not always be possible due to geometric constraints. The Straight Line method also provides the simplest and quickest method of image capture, often at the cost of an insufficient overlap between photos and a loss of point information on the obscured side of the object.

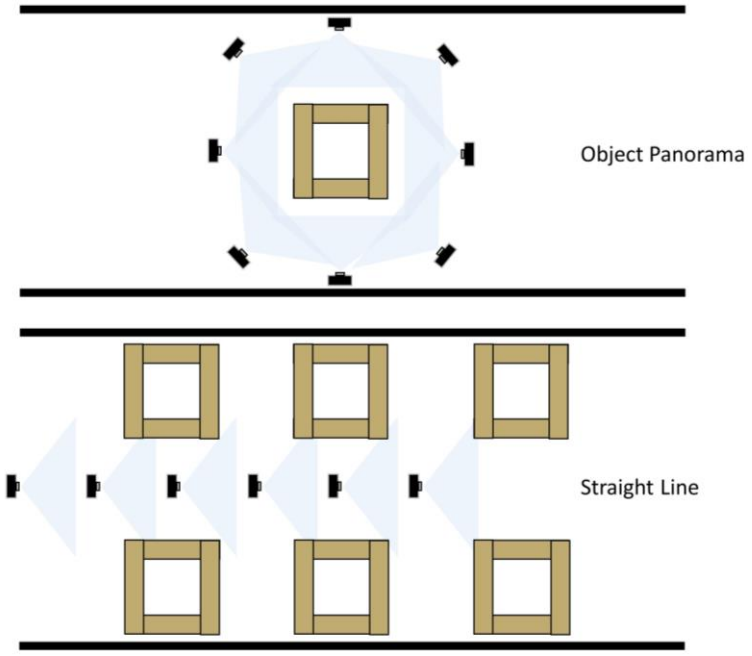

Figure 7.12: The Object Panorama and Straight Line methods of image capture

A series of 32 photos were taken using the Straight Line method in the supported crosscut in intervals of 1 m, taking enough pictures to capture the entire roof to floor geometry of the supports at each interval. The onboard flash was used as the primary source of light, and the camera settings for these photos are the same as the November 5th photos in Table 7.2. The reconstructed point cloud as well as a triangulated surface of the photographed supports are shown in Figure 7.13.

Figure 7.13: A reconstructed standing support triangulation from the camera position (left) and a dense point cloud as viewed perpendicular to the long axis of the crosscut (right).

Anomalous points have been manually removed from the scene, and the remaining points show clearly resolved objects. There are several objects in the scene that could provide a scale, such as the wooden beam widths or steel support labels, however there is no extensometer data for these supports, nor was there a time-lapse data collection. The resolution with which the camera-facing side of the supports were reconstructed suggests that they could be used to measure convergence.

Using video converted into image sequences was explored for its viability in producing quality photogrammetry images. Using video to reconstruct three-dimensional objects is often called videogrammetry, but as image sequences are being extracted from these videos and the same

methods previously discussed are being applied, it will continue to be referred to as photogrammetry in this paper. Two experiments were conducted using videography instead of photography: a Straight Line walkthrough of a crosscut and a steel support Object Panorama.

Two obstacles associated with photogrammetry become significantly more pronounced when working with video image sequences: motion blur and image resolution. There is a tendency, when taking photographs, to keep the camera still. When taking a video, the camera is in near constant motion, the degree to which is controllable by the operator. The motion blur will reduce the quality of the reconstruction, or render it incapable of being reconstructed altogether. The most common high-definition video recording resolutions currently available are 720p or 1080p, which corresponds to an image resolution of 1280 x 720 and 1920 x 1080 respectively. This resolution is significantly lower than the photograph resolution used for the object panorama.

Both experiments using the image sequences extracted from 720p video proved unsuccessful. The lower resolution combined with a high degree of motion blur, caused by the rough walking terrain, resulted in subpar images. Three-dimensional reconstruction was possible to a limited degree, but always resulted in sparse or incomplete point clouds, unfit for scientific measurement.

7.5 Conclusions

Monitoring underground mine movements is critical to understanding the rock mass response. Photogrammetry has been explored as a tool for increasing the availability of mine deformation information, by providing a faster and more comprehensive data collection technique than traditional point measurements. An underground coal longwall mine was used as a test site for monitoring the support response of two standing supports installed ahead of a longwall face. An instrumented wooden crib support as well as a steel support were photographed in a time-lapse manner using different lighting conditions.

The photogrammetric reconstruction of the wooden crib showed a cumulative convergence of 0.62 cm from October 10th to November 7th 2014. An extensometer installed on the crib recorded a cumulative convergence of 0.62 cm over the same time. Vandalism of the extensometer resulted in 5 days with no data being recorded between the first and second visit to the support. Between the second and third visit, the photogrammetric reconstruction showed a 0.54 cm

expansion in this time, while the extensometer recorded a 0.24 cm expansion. Larger convergence values would have been more beneficial for establishing the true precision of the reconstruction. However, considering the roof-to-floor height is approximately 6.2 m at this location, sub-centimeter discrepancies in convergence are relatively small.

Additionally, the steel support nearby the monitored wooden crib was also successfully reconstructed. The difference measured between the October 10th and November 5th visits was 0.28 cm. This change, while not validated by an extensometer on the support, was considered geologically reasonable, as other nearby extensometers all reported sub-centimeter convergence. The steel support was more difficult to reconstruct due to a reduced number of features and the reflectance of the surface. Future photogrammetric studies on similar supports should take care to diffuse the light source and ensure large overlap between photographs if possible.

Lastly, experiments were performed to test the feasibility of using a Straight Line method as opposed to the previously demonstrated Object Panorama method of capturing photographs, and if image sequences extracted from video recordings could substitute photographs. The Straight Line method was demonstrated to be capable of reconstructing an underground scene, despite the complex lighting situation. The image sequences extracted from captured 720p video footage contained too much motion blur and was of too low a resolution to adequately construct the underground scene. Improving the video resolution and reducing movement while recording are both within current technological and operational capabilities, and would likely improve results.

Photogrammetry has been shown to be capable of monitoring support deformation. The magnitude of deformation measured through photogrammetry is very similar to that measured by extensometers, which are widely used in research capacities to measure ground movements. Photogrammetry offers an advantage over extensometers in its ability to capture the entire geometry of the region being monitored, rather than a single point. Photogrammetry as a tool for monitoring is not biased by the method of installation nor does it require additional data acquisition units. Quality photogrammetric results do depend on quality photographs, and monitoring requires repeated visits to the scene. The limitations of photogrammetry do make its use situational, but the ability to measure three-dimensional change underground quickly, cost-effectively, and with accuracy comparable to extensometers makes it a valuable tool for assessing rock mass movements.

Chapter 8 Discussion and Conclusions

8.1 Summary of Work

Photogrammetry and laser scanning were both used to reconstruct the geometry of several mines and structures within them. Two coal mines, two limestone mines, and the Mine Roof Simulator (MRS) at the Pittsburgh Office of Mine Safety and Health Research were used as test locations for these two technologies and their mining application. The goal of each study was to determine a movement in the scene over time. Three of the experiments involved studying wide-area rib changes while two experiments focused on monitoring standing support convergence. The photogrammetry approach to each of these displacement-monitoring studies was performed in a way considered most practical and cost-effective for application in underground mining.

The rib displacement experiments contained two limestone mine sites and one coal mine site. The laser scanned limestone mine experiment involved was performed at two scanning period, which focused on one spalling pillar and another pillar that was scaled between scans. Calculating the difference between the triangulation mesh reconstructions from the laser scanning data, volume changes of 2.6 m^3 on the spalling pillar, and 2.3 m^3 on the scaled pillar were detected. Anomalous change elsewhere was not found, validating the movement that was detected.

The second laser scanning experiment was performed at one of the underground coal mine test sites, and the displacement being modeled was hand-induced by removing material from the rib. A scan was performed before and after displacement was created, and the scene reconstructions were compared for volume change between them. The laser scanner was moved slightly during the experiment to ensure a marginal need to reference objects in the scene for a proper orientation. Volume changes as small as 57 cm^3 and as large as 57549 cm^3 were detected. Footprints and scaled material were also visible in the time-lapse scans, however the roof and the undisturbed portions of the ribs showed no movements.

The last rib spalling experiment used photogrammetry instead of laser scanning, and was performed by another party remotely, with instructions provided for how to best photograph the scene. Several different behaviors were identified, that corroborated previous observations at the site: no change during the monitoring period, a weak shale band spalling, small pockets of change, and one large pillar spall event of 4.0 m^3. All measurements were performed using 30 cm square

references and without the need for mine coordinates, highlighting the versatility of the photogrammetry method in the absence of surveying data.

Beginning the standing support convergence experiments, the MRS was used to test the ability to precisely monitor the movement of a standing support over time. The MRS was photographed at three different convergence levels, each of which was modeled and compared to the other two to determine the magnitude of displacement taking place. The support was photographed in a way that would best simulate the angles possible in an underground environment. The convergence stages were set at 0 cm, 5 cm, and 30 cm, and the MRS measured convergence agreed with the photogrammetry measured convergence to within 0.5 cm of change at both the 5 and 30 cm stage.

The other standing support experiment was performed in an underground coal mine using photogrammetry, with the goal of detecting convergence caused by an advancing longwall face and the resulting abutment pressures. This study was performed over 28 days, punctuated by three visits to capture the deformation on standing supports at each time. This convergence was simultaneously monitored by extensometers installed on one of the photographed standing supports as well as others nearby. Convergence measurements as obtained by an extensometer on a wooden crib matched the convergence measurements of the same wooden crib as obtained from photogrammetry. The cumulative convergence measured using both methods was 0.62 cm and 0.62 cm respectively. A nearby steel support was also photogrammetrically reconstructed, and showed a convergence of 1.16 cm, over a slightly shorter time frame than the wooden crib comparison.

8.2 Discussion of Results

The photogrammetric and laser scanned reconstructions were studied for each test location. The photogrammetry and laser scanning applied to the limestone mines both revealed small and large areas of rib change, a result of either scaling or spalling. The reliability of these change detection studies can be validated by the absence of change in structures that were not expected to change. The laser scanned limestone mine showed no movement in the mine roof and no movement across large areas of the ribs, suggesting that the triangulation meshes were properly oriented. The laser scanned coal mine showed very similar results, with the roof not indicating

any movement, and undisturbed areas of the rib and floor also not moving. The roughness of the coal rib face did not appear to have a large impact on the ability to reconstruct rib features at large angles of incidence, as demonstrated in the field and laboratory.

The photographed limestone mine also showed areas of rib that experienced clear and quantifiable displacement. Isolated spalling in a weak shale band was identified as well as widespread spalling of the limestone, which was verifiable through careful inspection of the photographs. Not every photograph set, however, was clearly resolved, and some likely showed anomalous movements. The anomalous movement was characterized by a widespread "inward" and "outward" movement of the surface, which could be geotechnically interpreted as pillar spalling and expansion. It was not considered geologically reasonable that the rib was spalling and expanding in the manner displayed, nor was there visual evidence of the change in the photographs. The anomalous readings could be traced to poor quality photographs or highly dynamic lighting conditions.

The standing support modeled in a laboratory setting showed absolute convergence values that agreed with the instrumentation measurement. Error between the MRS convergence and the photogrammetric convergence was within 0.5 cm for both measurements. The scene was scaled using known feature lengths on the MRS rather than an outside scale, which may have contributed to scaling errors within the model. The standing supports modeled in a field setting also agreed with the measurement devices, although the exact deformation that occurred could not be determined, and the precision of the photogrammetry remained vague. Both the steel support and the wooden crib were difficult to model with the cap lamp light array. An increase in lighting as well as improved diffusion of the light would likely improve the quality of the photographs.

Speed is a concern when performing any underground measurement because it controls how much data can be collected and if it can be collected without interfering with operations. Laser scanning and photogrammetry should be divided into two parts, data collection and data processing, when discussing the time required to deliver meaningful engineering measurements. The data collection period, neglecting travel through the mine, for these experiments was approximately 10-20 minutes, with a visit being defined as the monitoring of one specific area or object at one instance in time. Data processing takes significantly longer, and varies significantly based on the quantity and quality of data. Laser scanning data already has a meaningful scale and accurate reproduction, removing some of the computation time. The laser scanning data from

these experiments, if processed again, would likely require 20-60 minutes to obtain rib movement information. Photogrammetry, including the time to reconstruct the scene, would require approximately 1-6 hours to process, depending on the number of photographs being used. Much of the time spent processing in photogrammetry is passive and does not require operator input. The time estimates made here are assuming familiarity with the photogrammetry and laser scanning process.

The methods of monitoring mine displacements presented here have largely focused on rib spalling and roof-to-floor convergence as measured on standing supports. The application of photogrammetry and laser scanning is not limited to measuring these two conditions, but rather any visible mine movement is capable of being reconstructed. The spalling and roof-to-floor measurements were performed because they are most easily controlled and predicted, whereas floor heave or a full-entry deformation profile would be difficult to validate and predict in a permissible environment. These results do show quantifiable measurements of rib displacement as well as extensometer-validated marginal roof convergence, which serves as a foundation for exporting these techniques to monitoring more varied ground movements or collecting large quantities of information to establish a thorough ground response.

8.3 Conclusions

Photogrammetry and laser scanning have been shown capable of reconstructing underground mine scenes with a high level of precision. Several mining and laboratory environments have been successfully reconstructed using these remote sensing techniques and monitored for displacement over time. The ability to capture the entire structure as it moves removes the ambiguity associated with local effects at the anchor points, found with traditional point measurement instrumentation. In addition, the data collection method allows for large areas of a mine to be measured quickly and non-intrusively. Monitoring large areas of a mine using point measurement instruments would require many different installations, and depending on the instrument installed, may disrupt operations.

When determining the rock mass response, as is typically reflected on the ground response curve, detailed measurements of the rock displacement behavior in response to changing states of stress is critical. The discontinuous and anisotropic nature of rock makes site-specific

characterization of rock behavior necessary for mine planning, and photogrammetry and laser scanning are two methods of characterizing that behavior in a precise, fast, and reliable manner. The underground coal mine photogrammetry and laboratory standing support photogrammetry showed that measurement accuracy within 0.5 cm could be achieved both quickly and cheaply, which is important when large amounts of data are required for an accurate quantification of rock mass response.

The precision of laser scanning is usually provided by the manufacturer, and in these tests, has not appeared to be significantly affected by the underground mining environment. The precision of photogrammetric measurements are highly variable, changing with distance to the subject and the quality of images used. The underground environment presented numerous obstacles to this method, most notably lighting and a potentially limited selection of cameras available for use. Despite these obstacles, cameras using typical point-and-shoot specifications have been used to generate precise point clouds using the flash, and adequate point clouds using a wearable cap lamp light array.

Rock mass behaviors that were previously difficult to capture, such as rib spalling, are easily captured and quantified using laser scanning and photogrammetry. Three different tests using these technologies showed rib displacements ranging from tens of cubic centimeters to several cubic meters. Just as proper installation of instrumentation is required to model rock mass behavior, so too should care be taken to obtain the highest quality photographs. It is unlikely that photogrammetry or laser scanning will match or exceed the theoretical precision of extensometers in practical use, however, the ability to gather data quickly and cheaply over a large area should provide an alternative to extensometers where sub-millimeter precision is not required.

8.4 Suggestions for Future Work

This work shows the application of photogrammetry and laser scanning to monitoring movements in underground mines. The means of obtaining photos are significantly more varied than what has been presented here, and the movements observed in underground mines extend beyond roof-to-floor convergence. The methods of obtaining images and the applications of the technology are two areas that could see significant improvement in future research.

Other means of image capture include the exploration of videogrammetry, specifically as it relates to helmet or vehicle-mounted cameras. The image sequences that were extracted from the video collected in this paper were marred by a combination of low resolution and motion blur, which may be mitigated by different cameras and video capture techniques. In addition to this, improving the lighting conditions during photography will improve results, but generating large amounts of light in heavily supported areas of underground coal mines may be difficult. Innovations in hand-held or worn lighting systems, may allow for individuals to reconstruct underground objects or structures with more precision.

In addition to the rib spalling and convergence measurements taken, other mine behaviors may be measured using photogrammetry, including numerous modes of pillar failure, roof sag, or floor heave. Modeling these behaviors could have a large impact on mine planning, and the means by which these behaviors could be monitored is not fundamentally different from the way roof-to-floor convergence is monitored.

Lastly, photogrammetry should be compared to traditional, trusted measurement techniques at every opportunity. As with many remote sensing techniques, demonstrating the reliability of a new monitoring method becomes more important as the path from data collection to visual or numerical output becomes more nebulous. Awareness of photogrammetry, and to a lesser degree laser scanning, is low, and repeated testing of this technology is necessary to improve operator comfort and trust in the monitoring method.

References

[1] U. S. EIA, “Historical detailed coal production data (2012),” 2014.

[2] S. Fiscor, “America’s Longwall Operations Demonstrate Stability During an Uncertain Period ,” *Coal Age*, vol. 118, no. 2, p. 25, 2013.

[3] Mine Safety and Health Administration, “Injury Experience in Coal Mining,” 2013.

[4] G. Conway, J. G. Dwyer, S. Signer, and F. Jenkin, “Topical Keynote: 50 years of rock mechanics research (1955-2005): The effect on safety in US underground mines,” in *Golden Rocks 2006, The 41st US Symposium on Rock Mechanics (USRMS)*, 2006.

[5] *SME Mining Engineering Handbook*, no. v. 1. Society for Mining, Metallurgy, and Exploration, 1992.

[6] W. F. Chen and J. Y. R. Liew, *The Civil Engineering Handbook, Second Edition*. CRC Press, 2002.

[7] E. Hoek, *Surface and Underground Project Case Histories: Comprehensive Rock Engineering: Principles, Practice and Projects*. Elsevier Science, 2014.

[8] B. P. Boisen, “Borehole Extensometers,” in *Underground Mining Methods Handbook*, 1982, p. 8.

[9] T. Luhmann, S. Robson, S. Kyle, and I. Harley, *Close range photogrammetry: principles, techniques and applications*. Whittles, 2006.

[10] H. Hamrin, W. Hustrulid, and R. Bullock, “Underground mining methods and applications,” *Underground Mining Methods: Engineering Fundamentals and International Case Studies*, pp. 3–14, 2001.

[11] S. S. Peng and H. S. Chiang, *Longwall mining*. John Wiley and Sons, New York, NY, USA, 1984.

[12] T. P. Mucho, T. M. Barczak, D. R. Dolinar, J. Bower, and J. J. Bryja, “Design methodology for standing secondary roof support in longwall tailgates,” in *Proceedings of the 18th International Conference on Ground Control in Mining, Morgantown, WV*, 1999, pp. 136–148.

[13] G. Tarrant, *New Concepts in Tailgate Strata Behaviour and Implications for Support Design*. University of New South Wales, 2006.

[14] "'Roof control plan-approal criteria." 30 "CFR" 75.222. 2014.

[15] E. Cocke, "The Wilberg Mine Fire."

[16] B. Brady and E. Brown, "Rock mechanics for underground mining," 1993.

[17] E. T. Brown, "The Nature and Fundamentals of Rock Engineering," in *Comprehensive Rock Engineering - Principles, Practice & Projects*, John A. Hudson, Ed. Oxford, UK: Pergamon, 1993, pp. 1–23.

[18] R. Seedsman, "The stress and failure paths followed by coal mine roofs during longwall extraction and implications to tailgate support," in *20th International conference on ground control in mining, Morgantown*, 2001, pp. 42–49.

[19] C. Mark and T. M. Barczak, "Fundamentals of coal mine roof support," *New Technology for Coal Mine Roof Support, Proceedings of the NIOSH Open Industry Briefing, NIOSH IC*, vol. 9453, pp. 23–42, 2000.

[20] C. Mark, "Horizontal stress and its effects on longwall ground control," *TRANSACTIONS-SOCIETY OF MINING ENGINEERS OF AIME*, pp. 1356–1356, 1991.

[21] T. Mucho, C. Mark, and D. Dolinar, "Horizontal stress and longwall headgate ground control," *Mining engineering*, p. 61, 1998.

[22] E. Esterhuizen and T. Barczak, "Development of ground response curves for longwall tailgate support design," in *Golden Rocks 2006, The 41st US Symposium on Rock Mechanics (USRMS)*, 2006.

[23] R. M. Cox, "Tailgate roadway convergence: a key indicator of potential ground control problems," in *International Journal of Rock Mechanics and Mining Sciences and Geomechanics Abstracts*, vol. 32, no. 8, 1995, p. 411A–411A.

[24] J. W. Cassie, P. F. Altounyan, and P. B. Cartwright, "Coal pillar design for longwall gate entries," *Proceedings of the Second International Workshop on Coal Pillar Mechanics and Design*, p. 23, 1999.

[25] S. C. Bandis, "Engineering Properties and Characterization of Rock Discontinuities," in *Comprehensive Rock Engineering - Principles, Practice & Projects*, John A. Hudson, Ed. Oxford, UK: Pergamon, 1993, pp. 1–23.

[26] E. Hoek, "The Hoek-Brown failure criterion-a 1988 update," in *Proc. 15th Canadian Rock Mech. Symp*, 1988, pp. 31–38.

[27] Z. Bieniawski, "In situ strength and deformation characteristics of coal," *Engineering Geology*, vol. 2, no. 5, pp. 325–340, 1968.

[28] M. A. Kwasniewski, “Mechanical Behavior of Anisotropic Rocks,” in *Comprehensive Rock Engineering - Principles, Practice & Projects*, John A. Hudson, Ed. Oxford, UK: Pergamon, 1993, pp. 285–312.

[29] C. Mark, G. Molinda, L. M. Burke, and P. Padgett, “Preventing falls of ground in coal mines with exceptionally low-strength roof: two case studies,” in *the Proceedings of the 23rd International Conference on Ground Control in Mining, Morgantown, WV, Aug*, 2004, pp. 3–5.

[30] N. E. Dowling, K. S. Prasad, and R. Narayanasamy, *Mechanical Behavior of Materials: Engineering Methods for Deformation, Fracture, and Fatigue*. Pearson Education, Limited, 2007.

[31] M. A. Kwasniewski, “Constitutive Behavior and Numerical Modeling,” in *Comprehensive Rock Engineering - Principles, Practice & Projects*, John A. Hudson, Ed. Oxford, UK: Pergamon, 1993, pp. 395–426.

[32] F. Beer, E. R. Jr. Johnston, J. DeWolf, and D. Mazurek, *Mechanics of Materials + ARIS Student Access Card*. McGraw-Hill Companies,Incorporated, 2008.

[33] J. C. Jaeger and N. G. W. Cook, *Fundamentals of Rock Mechanics*, Third. Chapman and Hall Ltd, 1979.

[34] T. M. Barczak, “An Overview of Standing Roof Support Practices and Developments in the United States,” in *Proceedings of the Third South African Rock Engineering Symposium, Johannesburg, Republic of South Africa: South African Institute of Mining and Metallurgy*, 2005, pp. 301–334.

[35] T. M. Barczak, “Optimizing secondary roof support with the NIOSH Support Technology Optimization Program (STOP),” in *Proceedings of 19th International Conference on Ground Control in Mining, Morgantown, WV*, 2000, pp. 74–84.

[36] C. P. Harwood, “Optimizing secondary tailgate support selection,” 1996.

[37] Strata Worldwide, “Link-N-Lock: Interlocking Support Crib.”

[38] T. M. Barczak and D. E. Schwemmer, *Effect of load rate on wood crib behavior*. US Department of the Interior, Bureau of Mines, 1988.

[39] T. M. Barczak, “Mistakes, misconceptions, and key points regarding secondary roof support systems,” in *Proc. of the 20th Conference on Ground Control in Mining. Morgantown, WV*, 2001, pp. 347–356.

[40] T. M. Barczak, “A retrospective assessment of longwall roof support with a focus on challenging accepted roof support concepts and design premises,” in *Proceedings of the 25th international conference on ground control in mining, Morgantown, WV*, 2006, pp. 232–243.

[41] T. Barczak and S. Tadolini, “Pumpable roof supports: an evolution in longwall roof support technology,” 2005.

[42] Burrell Mining Products, “The CAN.”

[43] E. T. Brown, J. W. Bray, B. Ladanyi, and E. Hoek, “Ground response curves for rock tunnels,” *Journal of Geotechnical Engineering*, vol. 109, no. 1, pp. 15–39, 1983.

[44] T. M. Barczak, G. S. Esterhuizen, and D. R. Dolinar, “Evaluation of the impact of standing support on ground behavior in longwall tailgates,” in *Proceedings of the 24th International Conference on Ground Control in Mining*, 2005, pp. 23–32.

[45] T. M. Barczak, G. Esterhuizen, J. Ellenberger, and P. Zhang, “A First Step in Developing Standing Roof Support Design Criteria Based on Ground Reaction Data for Pittsburgh Seam Longwall Tailgate Support,” in *Proceedings of the 27th International Conference on Ground Control in Mining*, 2008, pp. 349–359.

[46] L. Prosser, T. E. Marshall, S. C. Tadolini, A. T. Iannacchione, and C. Banta, “Considerations for Using Roof Monitors in Underground Limestone Mines in the USA,” *Retrieved June*, vol. 11, p. 2007, 2006.

[47] T. M. Barczak, J. Chen, and J. Bower, “Pumpable roof supports: developing design criteria by measurement of the ground reaction curve,” in *Proceedings, 22nd international conference on ground control in mining, Morgantown, WV*, 2003, pp. 283–93.

[48] B. Shen, A. King, and H. Guo, “Displacement, stress and seismicity in roadway roofs during mining-induced failure,” *International Journal of Rock Mechanics and Mining Sciences*, vol. 45, no. 5, pp. 672–688, 2008.

[49] E. Hosca, M. Karmis, and C. Haycocks, “Influence of support capacity and geometry on tailgate support,” in *International Journal of Rock Mechanics and Mining Sciences and Geomechanics Abstracts*, vol. 32, no. 8, 1995, p. 395A–395A.

[50] J. Dunnicliff, *Geotechnical Instrumentation for Monitoring Field Performance*. Wiley, 1993.

[51] G. Barrientos and J. Parker, “Use of the pressure arch in mine design at White Pine: 17F, 7R. Trans. Soc. Min. Engrs. AIME, V256, N1, Mar. 1974, P75-82,” in *International Journal of Rock Mechanics and Mining Sciences & Geomechanics Abstracts*, vol. 11, no. 10, 1974, p. 203.

[52] E. Esterhuizen, C. Mark, and M. Murphy, “The Ground Response Curve, Pillar Loading and Pillar Failure in Coal Mines,” in *29th International Conference on Ground Control in Mining 2010*, 2010.

[53] M. Diederichs and P. Kaiser, “Stability of large excavations in laminated hard rock masses: the voussoir analogue revisited,” *International Journal of Rock Mechanics and Mining Sciences*, vol. 36, no. 1, pp. 97–117, 1999.

[54] M. Jeremic, *Strata mechanics in coal mining*. CRC Press, 1985.

[55] G. Molinda and C. Mark, “Ground failures in coal mines with weak roof,” *Electronic Journal of Geotechnical Engineering*, vol. 15, pp. 547–588, 2010.

[56] G. M. Molinda and C. Mark, *Coal mine roof rating (CMRR): a practical rock mass classification for coal mines*, vol. 9387. US Dept. of Interior, Bureau of Mines, 1994.

[57] Z. Bieniawski, “Engineering Classification of Jointed Rock Masses,” *Civil Engineer in South Africa*, vol. 15, no. 12, 1973.

[58] C. Mark and G. Molinda, “Development and application of the coal mine roof rating (CMRR),” in *Proceedings of the International Workshop on Rock Mass Classification in Underground Mining, Information Circular*, vol. 9498, 2007.

[59] S. Fekete, M. Diederichs, and M. Lato, “Geotechnical and operational applications for 3-dimensional laser scanning in drill and blast tunnels,” *Tunnelling and Underground Space Technology*, vol. 25, no. 5, pp. 614–628, 2010.

[60] D. F. Huber and N. Vandapel, “Automatic three-dimensional underground mine mapping,” *The International Journal of Robotics Research*, vol. 25, no. 1, pp. 7–17, 2006.

[61] D. Ferguson et al., “An autonomous robotic system for mapping abandoned mines,” *Advances in Neural Information Processing Systems*, vol. 3, 2003.

[62] J. Mah, C. Samson, S. D. McKinnon, and D. Thibodeau, “3D laser imaging for surface roughness analysis,” *International Journal of Rock Mechanics and Mining Sciences*, vol. 58, pp. 111–117, 2013.

[63] S. Fekete and M. Diederichs, “Integration of three-dimensional laser scanning with discontinuum modelling for stability analysis of tunnels in blocky rockmasses,” *International Journal of Rock Mechanics and Mining Sciences*, vol. 57, pp. 11–23, 2012.

[64] A. Prokop and H. Panholzer, “Assessing the capability of terrestrial laser scanning for monitoring slow moving landslides,” *Natural Hazards and Earth System Science*, vol. 9, no. 6, pp. 1921–1928, 2009.

[65] A. Abellán, J. Calvet, J. M. Vilaplana, and J. Blanchard, “Detection and spatial prediction of rockfalls by means of terrestrial laser scanner monitoring,” *Geomorphology*, vol. 119, no. 3, pp. 162–171, 2010.

[66] K. B. Atkinson, *Close Range Photogrammetry and Machine Vision*. Whittles Pub., 1996.

[67] B. C. Punmia, A. K. Jain, and A. K. Jain, *Surveying*, no. v. 3. Laxmi Publications (P) Limited, 2005.

[68] “Microsoft Photosynth.” [Online]. Available: https://photosynth.net/. [Accessed: 03–5-2015].

[69] G. Pomaska, “Utilization of photosynth point clouds for 3D object reconstruction,” in *Proceedings of the 22nd CIPA symposium, Kyoto, Japan*, 2009.

[70] “Autodesk 123D Catch.” [Online]. Available: http://www.123dapp.com/catch. [Accessed: 03–5-2015].

[71] C. Santagati and L. Inzerillo, “123D Catch: efficiency, accuracy, constraints and limitations in architectural heritage field,” *International Journal of Heritage in the Digital Era*, vol. 2, no. 2, pp. 263–290, 2013.

[72] T. Styles, Y. Zhang, D. Stead, D. Elmo, D. Roberts, and T. Yanske, “A Photogrammetric Approach to Brittle Fracture Characterization In Mine Pillars,” in *44th US Rock Mechanics Symposium and 5th US-Canada Rock Mechanics Symposium*, 2010.

[73] J. Kim, D. Kim, and K. Won, “Measurement of joint orientations of tunnel working face using a new photogrammetric technique,” in *Alaska Rocks 2005, The 40th US Symposium on Rock Mechanics (USRMS)*, 2005.

[74] P. Somervuori and M. Lamberg “Modern 3D Photogrammetry Method for Rock Mechanics, Geological Mapping, 3D Model and Documentation of Open Pit Faces and Tunnels,” 2010.

[75] D. Heal, M. Hudyma, and Y. Potvin, “Assessing the in-situ performance of ground support systems subjected to dynamic loading,” in *Ground support in mining and underground construction, proceedings of the fifth International Symposium on ground support, Perth, Australia*, 2004, pp. 28–30.

[76] N. Maerz, J. Ibarra, and J. Franklin, “Overbreak and underbreak in underground openings Part 1: measurement using the light sectioning method and digital image processing,” *Geotechnical \& Geological Engineering*, vol. 14, no. 4, pp. 307–323, 1996.

[77] C. S. Fraser, “Industrial Measurement Applications,” in *Close Range Photogrammetry and Machine Vision*, Atkinson, K.B., Ed. Whittles Pub., 1996.

[78] T. Hagan, “A case for terrestrial photogrammetry in deep-mine rock structure studies,” in *International Journal of Rock Mechanics and Mining Sciences & Geomechanics Abstracts*, vol. 17, no. 4, 1980, pp. 191–198.

[79] F. Tonon and J. Kottenstette, “Laser and photogrammetric methods for rock face characterization: A Workshop,” in *Report on a workshop held in Golden, Colorado*, 2006.

[80] S. Rezaei and A. Rahnama, “Application of Close Range Photogrammetry to Monitor Displacements in Mines,” in *SME Annual Meeting*, 2013.

[81] Harris Interactive, “Growth in Ownership of Smartphones and Tablets Appears Largely Android-Driven,” 2013.

[82] J.-A. Beraldin, “Integration of laser scanning and close-range photogrammetry-the last decade and beyond,” in *International Society for Photogrammetry and Remote Sensing*, 2004.

[83] “‘Electric Motor-Driven Mine Equipment and Accessories." 30 "CFR" 18. 2014.

[84] S. Foster and D. Halbstein, *Integrating 3d Modeling, Photogrammetry and Design*. Springer, 2014.

[85] R. Singh, D. Chapman, and K. Atkinson, “Digital photogrammetry based automatic measurement of sandstone roof of a mine,” *Journal of the Indian Society of Remote Sensing*, vol. 25, no. 1, pp. 47–59, 1997.

[86] T. Luhmann, “Close range photogrammetry for industrial applications,” *ISPRS Journal of Photogrammetry and Remote Sensing*, vol. 65, no. 6, pp. 558–569, 2010.

[87] J. Birch, “Using 3DM analyst mine mapping suite for rock face characterization,” in *Laser and Photogrammetric Methods for Rock Face Characterization Workshop*, 2006, pp. 13–32.

[88] R. Christiansson, “The latest development for in-situ rock stress measuring techniques,” in *Proceedings of the International Symposium on In-situ Rock Stress. Trondheim, Norway:[sn]*, 2006, pp. 3–10.

[89] J. Kemeny, K. Turner, and B. Norton, “LIDAR for rock mass characterization: hardware, software, accuracy and best-practices,” *Laser and photogrammetric methods for rock face characterization. ARMA Golden, Colorado*, 2006.

[90] M. Lato, M. S. Diederichs, D. J. Hutchinson, and R. Harrap, “Optimization of LiDAR scanning and processing for automated structural evaluation of discontinuities in rockmasses,” *International Journal of Rock Mechanics and Mining Sciences*, vol. 46, no. 1, pp. 194–199, 2009.

[91] "FARO Laser Scanner Focus 3D Manual," 2011.

[92] K. Thiel and A. Wehr, "Performance Capabilities of Laser-Scanners-An Overview and Measurement Principle Analysis," *International Archives of Photogrammetry, Remote Sensing and Spatial Information Sciences*, vol. 36, no. Part 8, p. W2, 2004.

[93] "FARO Scene Manual," 2011.

[94] "I-Site Studio Software." [Online]. Available: http://www.maptek.com/products/i-site/i-site_studio.html. [Accessed: 03–6-2015].

[95] H. N. Maleki and J. R. McVey, *Detection of roof instability by monitoring the rate of movement*. US Department of the Interior, Bureau of Mines, 1988.

[96] F. Lemy, S. Yong, and T. Schulz, "A case study of monitoring tunnel wall displacement using laser scanning technology," in *The 10th IAEG International Congress, IAEG2006*, 2006.

[97] S. J. Gordon and D. D. Lichti, "Modeling terrestrial laser scanner data for precise structural deformation measurement," *Journal of Surveying Engineering*, vol. 133, no. 2, pp. 72–80, 2007.

[98] M. Tsakiri, D. Lichti, and N. Pfeifer, "Terrestrial laser scanning for deformation monitoring," 2006.

[99] J. Shan and C. K. Toth, *Topographic laser ranging and scanning: principles and processing*. CRC Press, 2008.

[100] A. Davis, "Chapter 2 - The Reflectance of Coal ," in *Analytical Methods for Coal and Coal Products* , Karr, Clarence, Ed. Academic Press, 1978, pp. 27 – 81.

[101] W. Boehler, M. Bordas Vicent, and A. Marbs, "Investigating laser scanner accuracy," *The International Archives of Photogrammetry, Remote Sensing and Spatial Information Sciences*, vol. 34, no. Part 5, pp. 696–701, 2003.

[102] E. R. Bauer and D. R. Dolinar, "Skin failure of roof and rib and support techniques in underground coal mines," *Proceedings of New Technology in Coal Mine Roof Support. NIOSH, Pittsburgh, PA Information Circular*, vol. 9453, 2000.

[103] M. Colwell and C. Mark, "Analysis and Design of Rib Support (ADRS) A Rib Support Design Methodology for Australian Collieries," in *Proceedings of the 24th International Conference on Ground Control in Mining*, 2005, pp. 12–22.

[104] T. Peynot, J. Underwood, and S. Scheding, “Towards reliable perception for unmanned ground vehicles in challenging conditions,” in *Intelligent Robots and Systems, 2009. IROS 2009. IEEE/RSJ International Conference on*, 2009, pp. 1170–1176.

[105] T. Peynot, J. Underwood, and A. Kassir, “Sensor Data Consistency Monitoring for the Prevention of Perceptual Failures in Outdoor Robotics,” in *Proceedings of the 7th IARP Workshop on Technical Challenges for Dependable Robots in Human Environments*, 2010, pp. 145–152.

[106] Cordex Instruments, “ToughPIX 2.” [Online]. Available: http://www.cordexinstruments.com/products/intrinsically-safe-digital-cameras/toughpix-ii/toughpix-2/. [Accessed: Jun-2014].

[107] T. M. Barczak, “NIOSH safety performance testing protocols for standing roof supports and longwall shields,” *the Proceedings: New Technology for Coal Mine Roof Support, Pittsburgh, PA: US Department of Health and Human Services, Public Health Service, Centers for Disease Control and Prevention, National Institute for Occupational Safety and Health, DHHS (NIOSH) Publication*, no. 2000–151, pp. 207–221, 2000.

[108] “Agisoft Photoscan.” [Online]. Available: http://www.agisoft.com/. [Accessed: 03–6-2015].

[109] “Matlab: The Language of Technical Computing.” [Online]. Available: http://www.mathworks.com/products/matlab/. [Accessed: 03–6-2015].

[110] M. Murphy, J. Ellenberger, G. Esterhuizen, and T. Miller, “Roof and Pillar Failure Associated with Weak Floor at a Limestone Mine,” in *2015 SME Annual Meeting & Exhibit*, 2015.

[111] “Nikon D70s.” [Online]. Available: http://www.nikonusa.com/en/Nikon-Products/Product-Archive/dslr-cameras/D70s.html. [Accessed: 03–6-2015].

[112] B. Slaker, E. Westman, B. Fahrman, and M. Luxbacher, “Determination of volumetric changes from laser scanning at an underground limestone mine.,” *Mining Engineering*, vol. 65, no. 11, 2013.

[113] “Northern Light Technologies Cap Lamp Systems: Polaris.” [Online]. Available: http://www.nltinc.com/cap-lamp-systems/polaris/. [Accessed: 03–6-2015].

Appendix A: Thumbnails of Photograph Sets

Stone Mine Trip 1

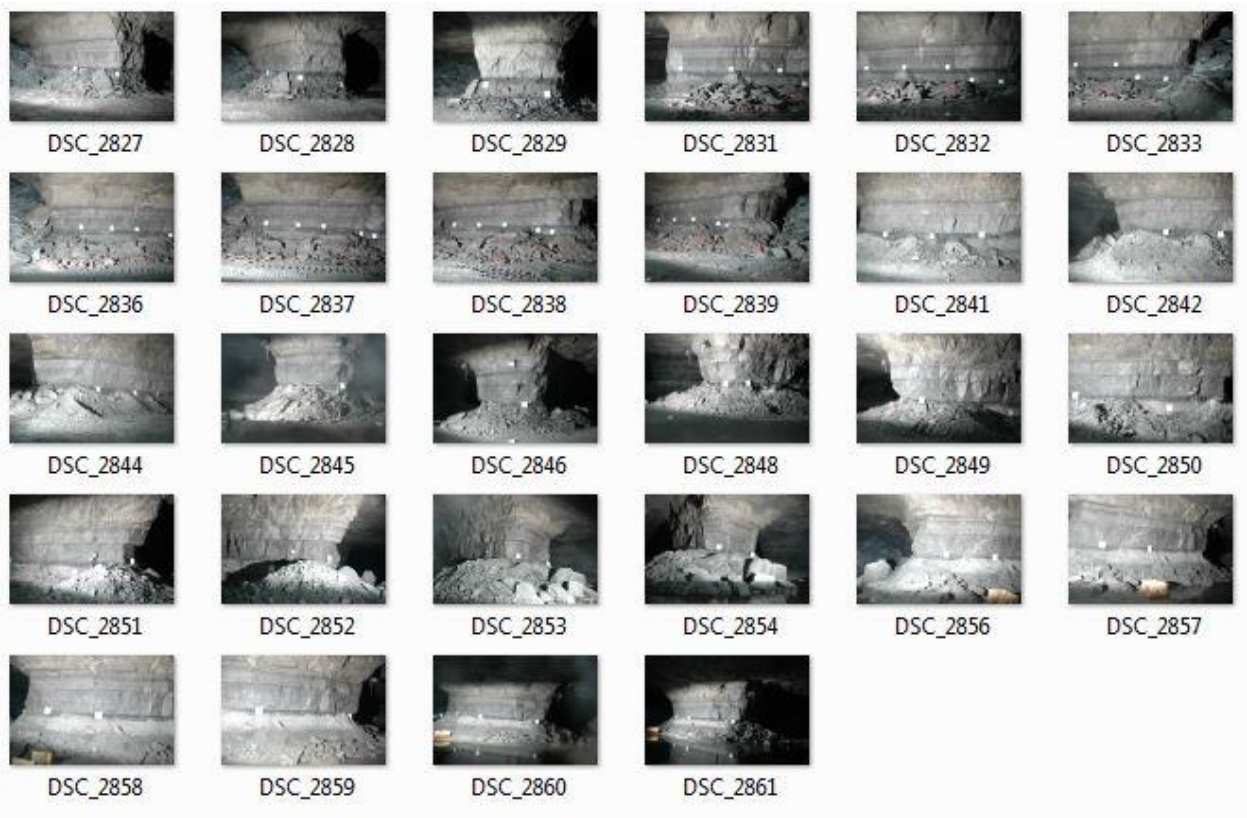

Stone Mine Trip 2

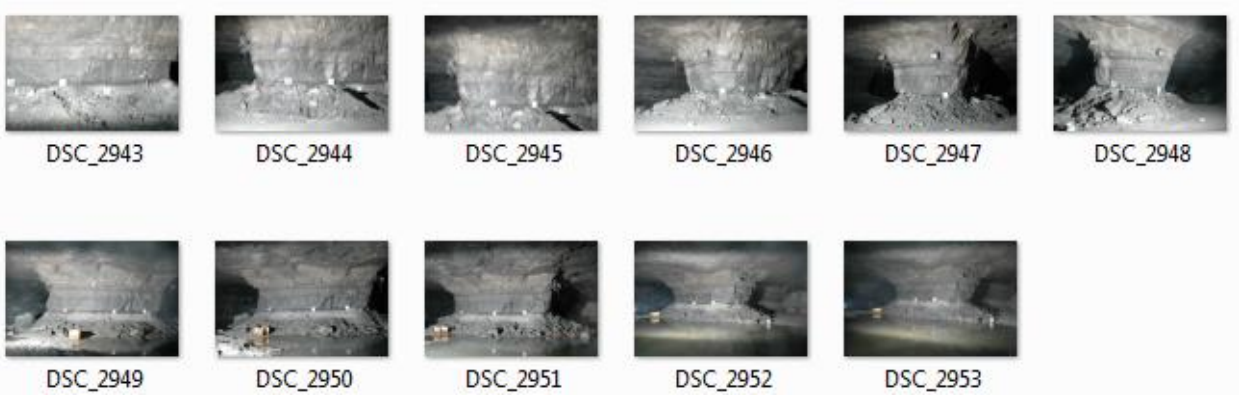
DSC_2943
DSC_2944
DSC_2945
DSC_2946
DSC_2947
DSC_2948
DSC_2949
DSC_2950
DSC_2951
DSC_2952
DSC_2953

Stone Mine Trip 3

Stone Mine Trip 4

Steel Support Trip 1


PTDC0271
PTDC0272
PTDC0273
PTDC0274
PTDC0275
PTDC0276
PTDC0277
PTDC0278
PTDC0279
PTDC0280
PTDC0281
PTDC0282
PTDC0283
PTDC0284
PTDC0285
PTDC0286
PTDC0287
PTDC0288
PTDC0289
PTDC0290

Steel Support Trip 2

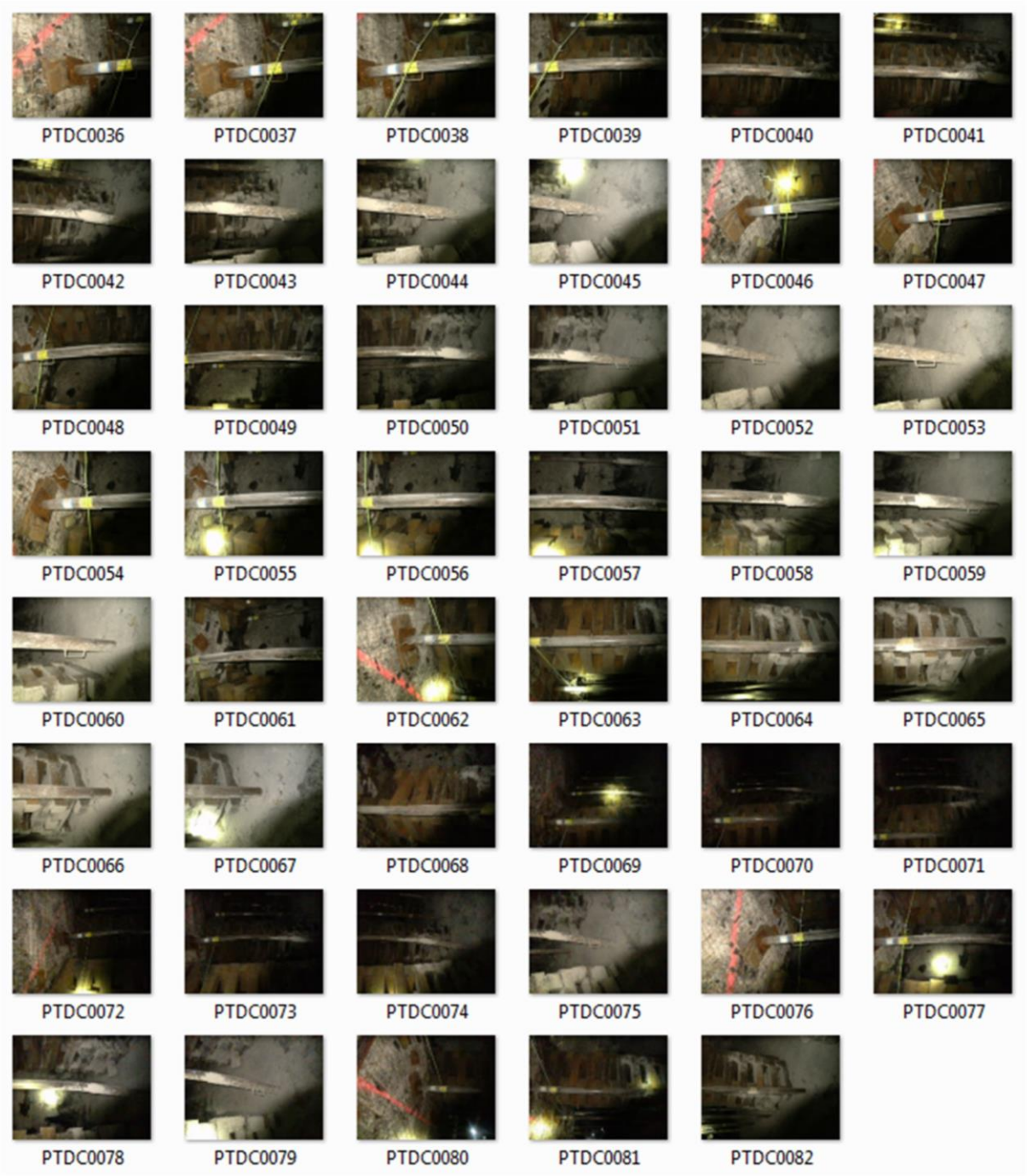

Wooden Crib Trip 1

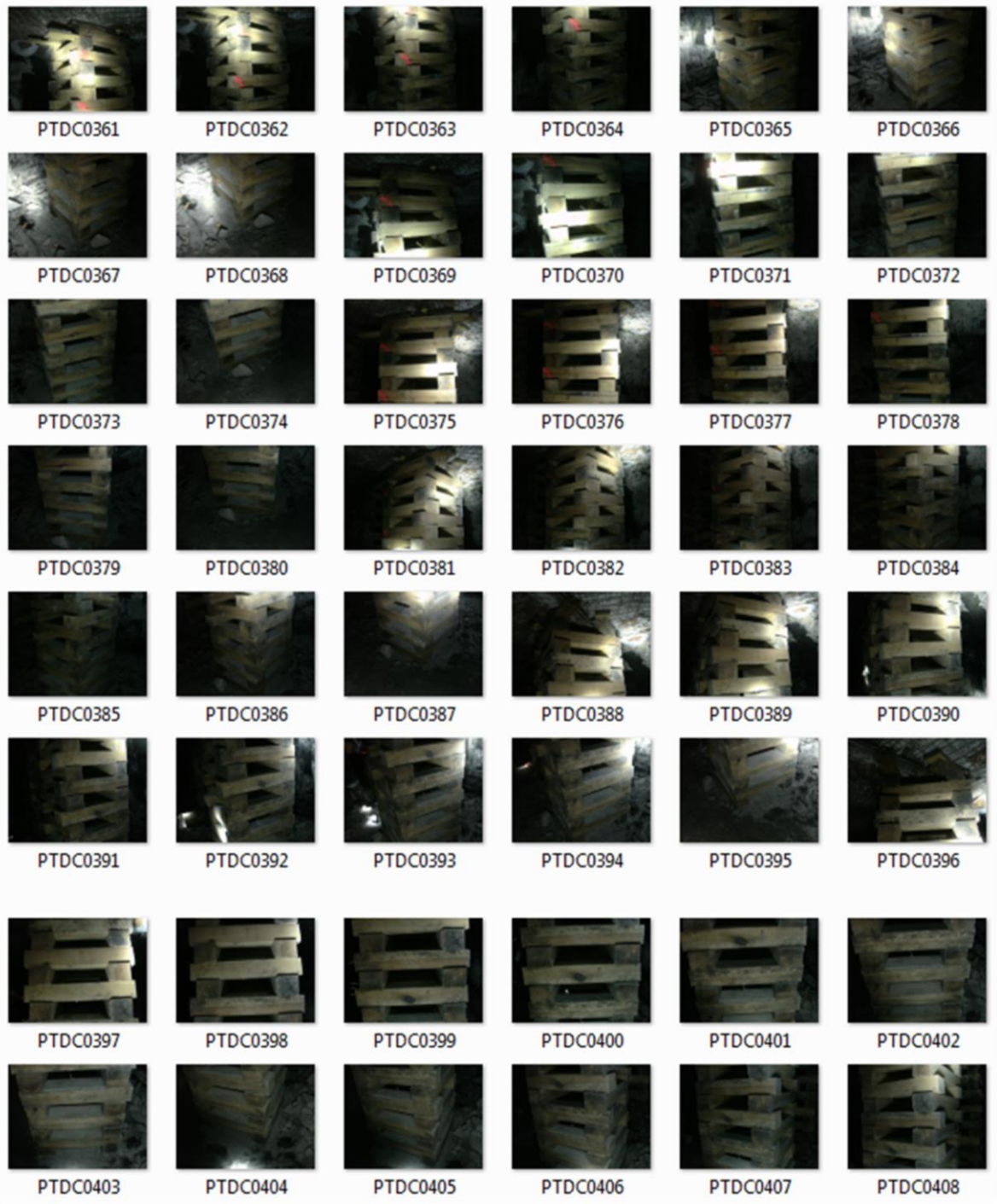

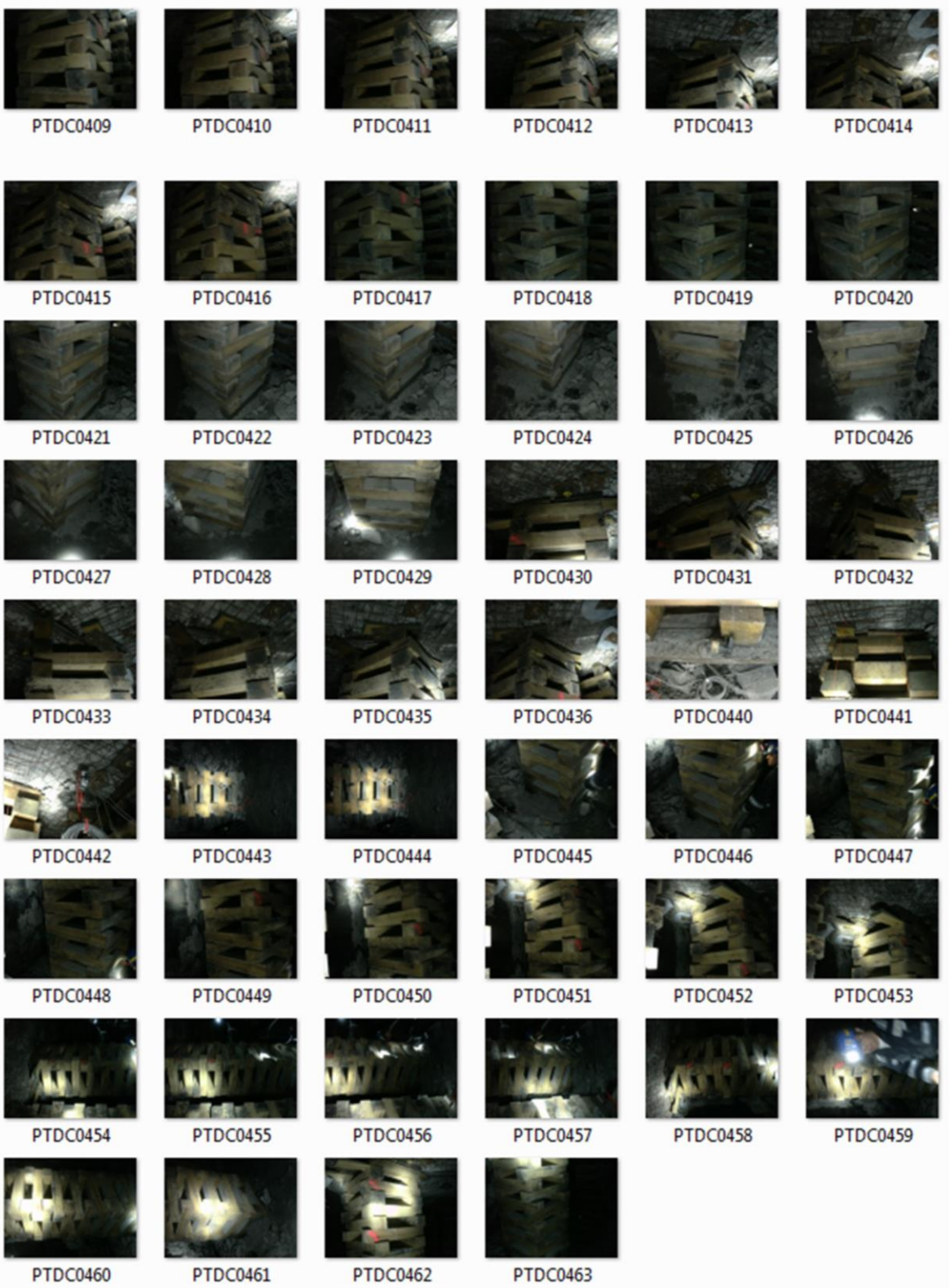
PTDC0409
PTDC0410
PTDC0411
PTDC0412
PTDC0413
PTDC0414
PTDC0415
PTDC0416
PTDC0417
PTDC0418
PTDC0419
PTDC0420
PTDC0421
PTDC0422
PTDC0423
PTDC0424
PTDC0425
PTDC0426
PTDC0427
PTDC0428
PTDC0429
PTDC0430
PTDC0431
PTDC0432
PTDC0433
PTDC0434
PTDC0435
PTDC0436
PTDC0440
PTDC0441
PTDC0442
PTDC0443
PTDC0444
PTDC0445
PTDC0446
PTDC0447
PTDC0448
PTDC0449
PTDC0450
PTDC0451
PTDC0452
PTDC0453
PTDC0454
PTDC0455
PTDC0456
PTDC0457
PTDC0458
PTDC0459
PTDC0460
PTDC0461
PTDC0462
PTDC0463

Wooden Crib Trip 2

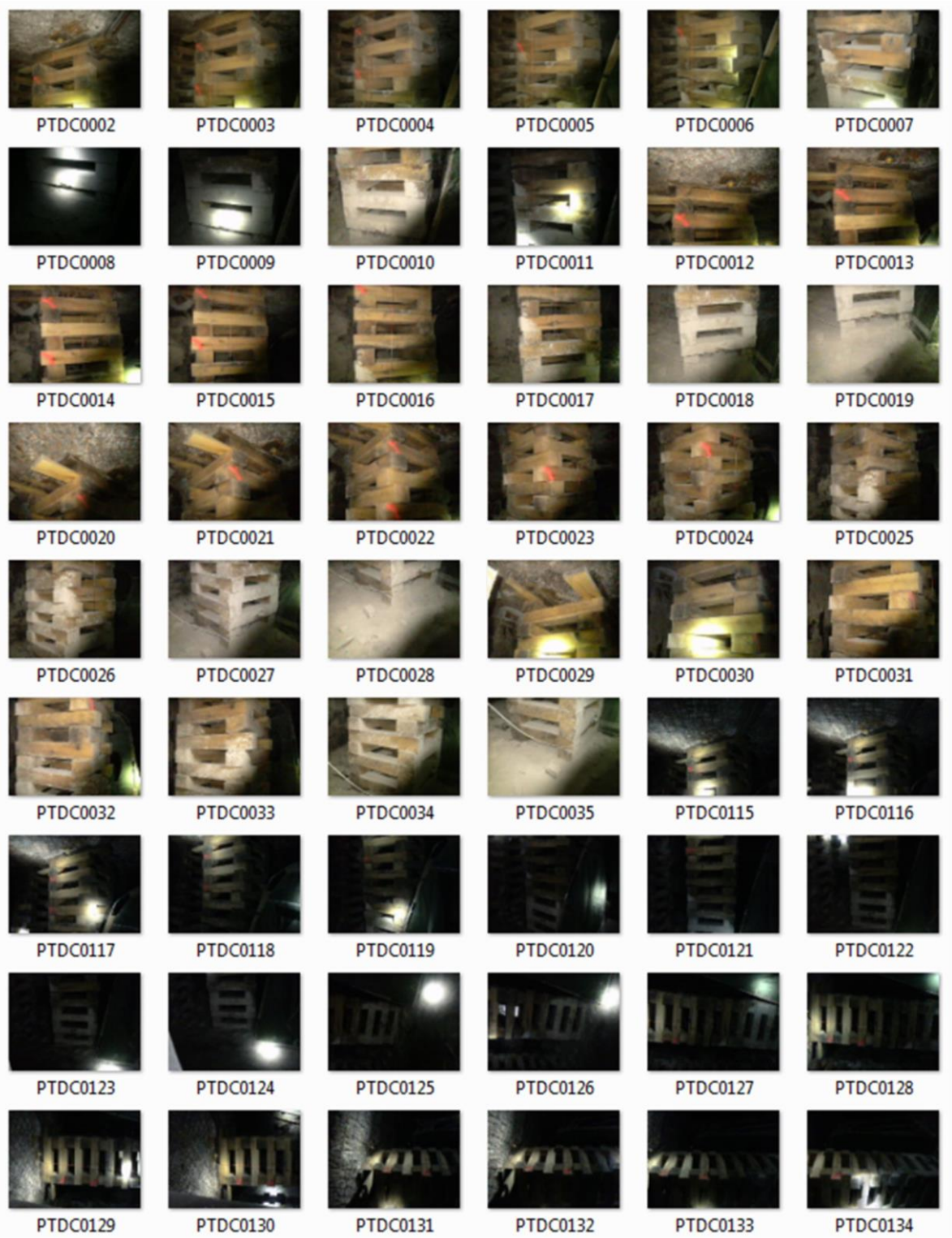

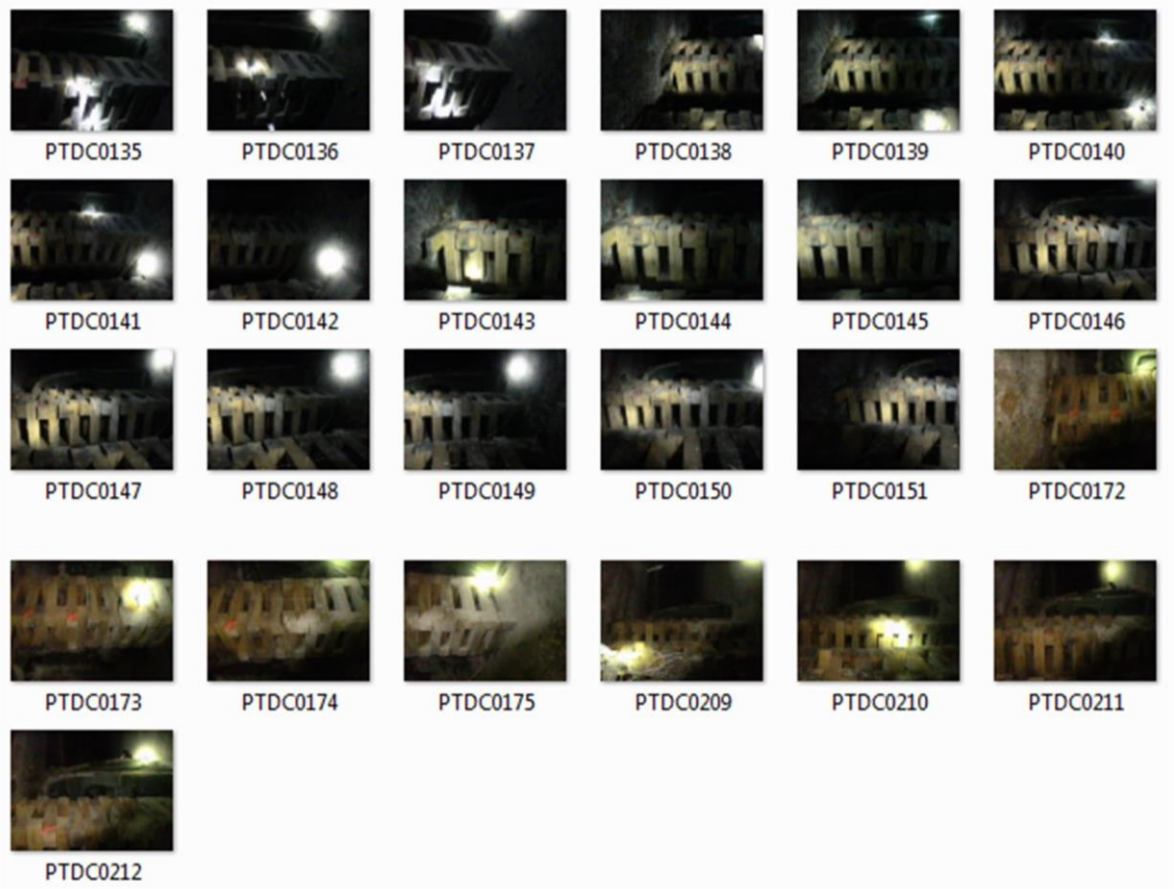
PTDC0135
PTDC0136
PTDC0137
PTDC0138
PTDC0139
PTDC0140
PTDC0141
PTDC0142
PTDC0143
PTDC0144
PTDC0145
PTDC0146
PTDC0147
PTDC0148
PTDC0149
PTDC0150
PTDC0151
PTDC0172
PTDC0173
PTDC0174
PTDC0175
PTDC0209
PTDC0210
PTDC0211
PTDC0212

Wooden Crib Trip 3

Appendix B: Additional Stone Mine Rib Monitoring

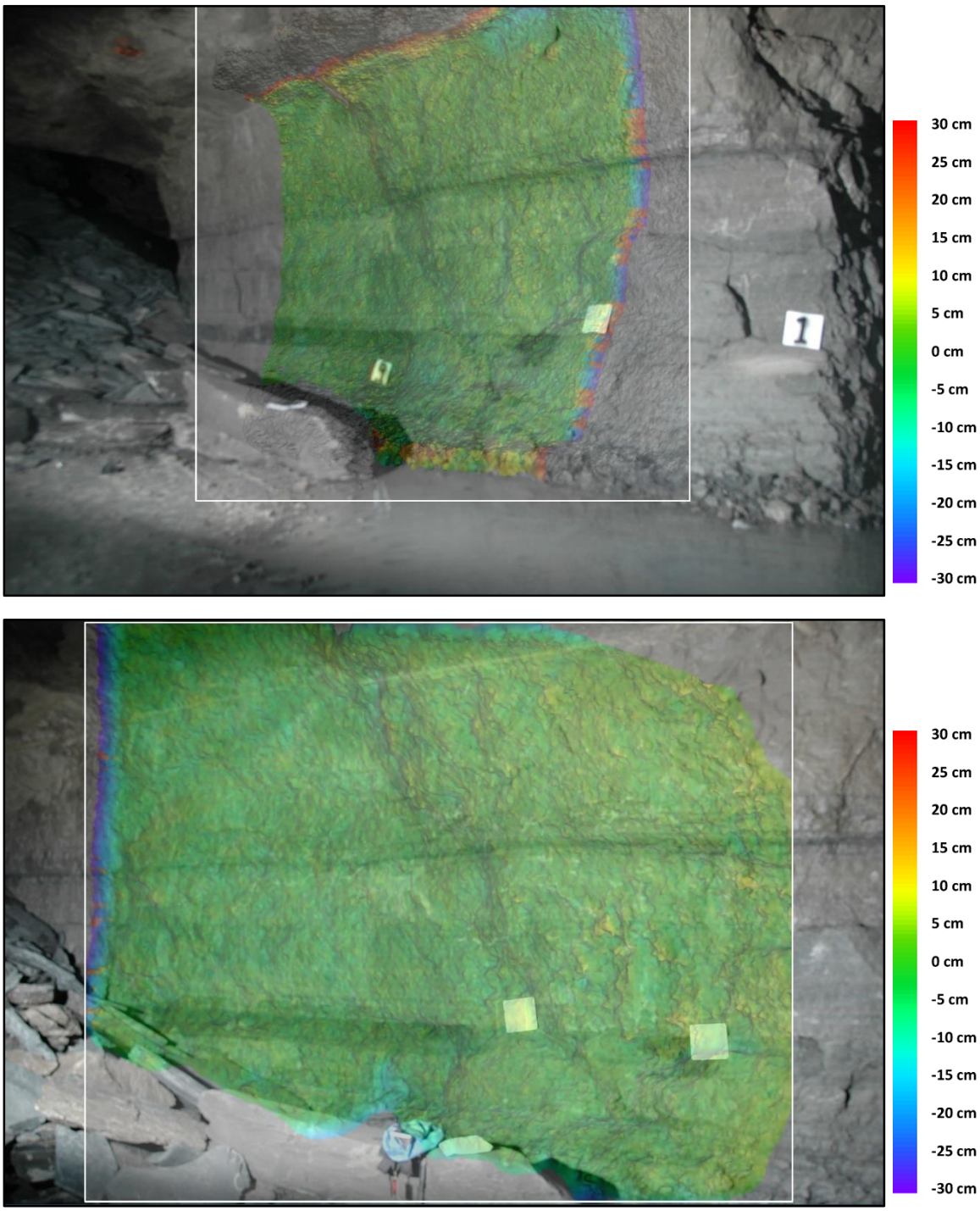

Figure B.1: Change at Pillar 4 from Sep. 16th to Sep 26th (top) and Sep. 26th and Oct. 28th (bottom)

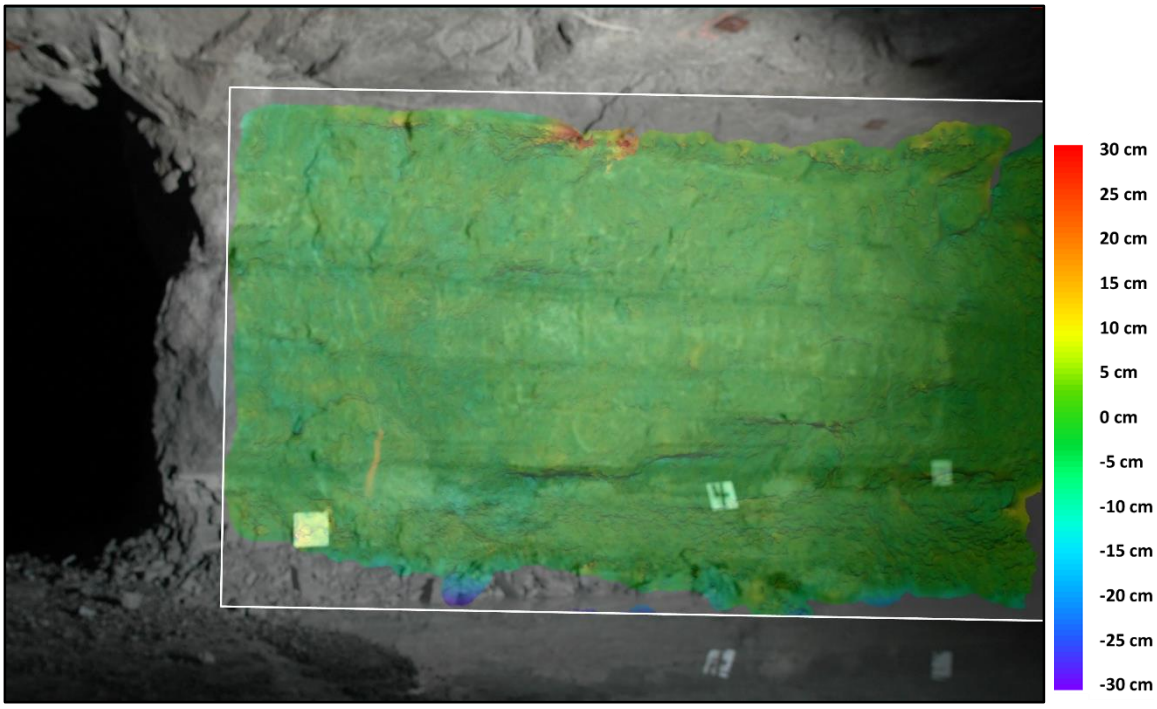

Figure B.2: Change at Pillar 4 from Sep. 26th to Oct. 28th

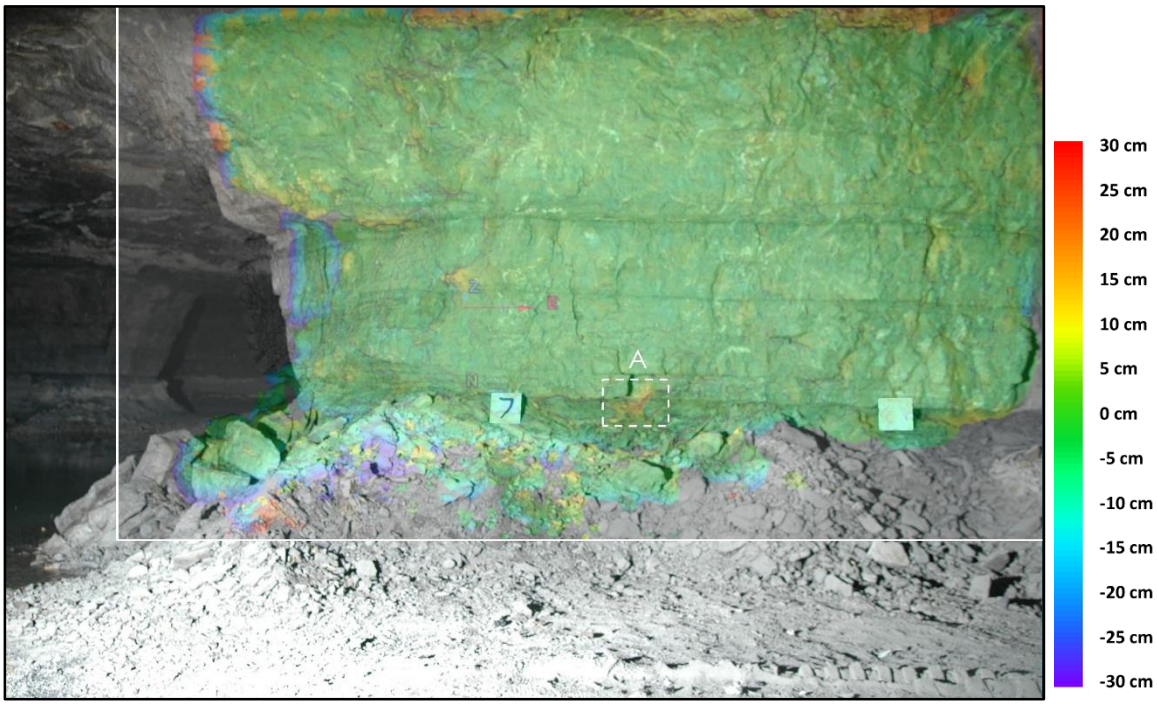

Figure B.3: Change at Pillar 5 from Aug. 26th to Sep. 26th

Appendix C: MATLAB Code for Kernel Density Estimations

```
%% DETERMINING VERTICAL EXTENTS OF SUPPORT
%Point clouds should be already oriented with y as the vertical axis
%copy and paste point cloud data into TimePeriod1
TimePeriod1 =[];

%converting from feet to meters
%TimePeriod1 = TimePeriod1*0.3804;

y_TimePeriod1 = TimePeriod1(:,2);

Range_TimePeriod1 = [min(y_TimePeriod1):0.001:max(y_TimePeriod1)];

%change bandwidth until there is a single clear peak at the extremes
band_val = 0.01;

[x1b,f1b,bw11] = ksdensity(y_TimePeriod1,Range_TimePeriod1,'width',band_val);

plot(f1b,x1b)


%% DETERMING HORIZONTAL EXTENT OF WOODEN BEAMS
%Point clouds should be already oriented with x following the long axis of
the wooden beam
BeamPoints =[];

%Fill in the vertical extents of the beam you wish to measure
min_Beam = 0.770;
max_Beam = 0.894;

z=1;
for i = 1:numel(TimePeriod1(:,1));
if y_TimePeriod1(i,1) > min_Beam;
    if y_TimePeriod1(i,1) < max_Beam;
        BeamPoints(z,:) = TimePeriod1(i,:);
        z=z+1;
    end
end
end

%change bandwidth until there is a single clear peak at the extremes
band_val = 0.014;

Range_BeamPoints = [min(BeamPoints):0.001:max(BeamPoints)];

[x2b,f2b,bw22] =
ksdensity(BeamPoints(:,1),Range_BeamPoints,'width',band_val);
plot(f2b,x2b);
```

Appendix D: Photogrammetry Best Practices

There were many practices employed and difficulties encountered through this application of photogrammetry that are not technically presented previously in this document. However, an outline of suggested practices is presented here for applying photogrammetry to an underground mining environment practically and using low-cost equipment and software. It is also the belief of the author that there are three distinct areas of photogrammetry that can be improved by increased allocation of resources: quality, speed, and reliability. Quality of results is most affected by camera and lighting hardware. Speed of processing results is most affected by software, through both computationally sophisticated methods and user-friendliness. Reliability of results is most affected by personnel experience. These can all be improved independently of one another should a particular application be lacking in one or more areas.

Hardware and Software Selection

Photogrammetry hardware will need to be considered as two major components: camera and lighting. The cameras used in this research included an explosion-proof point-and-shoot camera, a standard point-and-shoot camera, and a DSLR camera. The DSLR provided the best results, per photograph, of the cameras used, with the explosion-proof camera providing the worst results, which was expected as they contained the best and worst camera specifications respectively. Budget and regulations permitting, DSLR cameras should be used whenever possible, however, a point-and-shoot camera may be sufficient. Point-and-shoot cameras have the advantage of being more prevalent, and lower cost, resulting in a lower-risk investment.

Lighting will need to be tailored to site-specific needs. Temporary lighting of an underground space can be classified into three categories: stationary, operator-mobile, and on-board flash. Stationary lighting refers to auxiliary work lights or equipment lighting (i.e. trucks or mining equipment). This light source will be stationary until the camera operator moves to an area that is no longer being sufficiently lit. The stationary method of lighting may be prefereable for large, cavernous environments, and the lack of change in lighting conditions will improve the reconstruction of the actively-lit face.

Operator-mobile lighting is auxiliary lighting that either is held, worn, or moves with the camera as the camera moves. As the operator moves, so too will the light, causing a different lighting scenario for each photo. This method of lighting is less favorable, since it alters the visual features in each photograph, however, it is easier to implement. A method of using cap lamps as auxiliary lighting was presented in this research, although it leaves much room for improvement. Cap lamps are easily accessible at most underground mining operations and any means of allowing a person to use multiple at once may provide enough lighting to use photogrammetry. The cap lamps will need to be arranged in a manner that does not focus them all on one spot, and a means of diffusing the light will need to be employed.

The last method of lighting is on-board flash lighting. Most camera flashes provide enough lighting to illuminate the narrow confines of an underground coal mine, but will not be sufficient for cavernous environments. An on-board flash is the simplest and cheapest method of underground illumination, and will likely suffice in most situations if the battery capable of sustaining repeated flash photography.

Photography

The method of taking photographs should be methodical instead of haphazard, not necessarily due to computational restrictions, but rather ensuring proper overlap in the scene is being achieved. Ideally, photographing an object should be performed in an object-panoramic manner, where the object is circled with photographs being taken at incremental arc lengths. If a scene is being photographed, such as an entry or room, the scene should still be photographed in a similar manner, where the camera changes position between photos. There is an inclination to take photos standing in a central point and rotating about that point without moving camera positions, which will likely result in a poor photogrammetric reconstruction.

There is no rule for overlap required in the photos, and it will depend on the quality of photos being used in the reconstruction, but at least 75% overlap in photos has yielded the best results in these studies. This means that 75% of the subject visible in one photograph is also visible in the next photograph, accounting for any decreased visibility of an object due to viewing angle change. Be mindful, that the first and last photos, in an incrementally progressing set, will need to extend past the area of interest if a full object-panorama was not captured, as they will both

contain areas that were not found in any other photo. Care should be exercised when taking the photos because a single blurry or insufficiently lit photo can cause a gap in overlap that causes the scene to lose connectivity. Until the camera operator is comfortable with judging the lighting and level of motion blur in a photograph, as it is taken, taking redundant pictures that increase the degree of overlap is advisable.

In a low light environment, if possible, the camera should be set to maximize the light reaching the sensor. The method of doing this was not optimized in this research, as the camera did not allow for a significant degree of customization. An adjustment of the camera's ISO was possible, and a high ISO setting was chosen to accommodate the low-light environment. This produced a very grainy image, and if possible, adjusting the camera shutter speed or aperture size may be preferable. These will both affect the depth of field and motion blur of the photographs, and will likely need to be developed on an application-specific and operator-specific basis.

Photogrammetry often has the ability to use points in the background of the scene for reconstruction purposes, if they are present in multiple photographs. This results in a stark contrast between performing photogrammetry in well-lit environments and poorly-lit environments. In the case of a supported underground coal entry, the background objects may not be visible, resulting in fewer points available for matching. This is especially pronounced with thin supports when photographed near their middle, which can be exacerbated if the surface is reflective and the light source is not diffused. When photographing the top and bottom of thin supports, the roof and floor appear in the photographs and contain numerous visual features, but these are often nonexistent when photographing the middle of the support.

The onboard camera flash was sufficient as a light source for the majority of underground coal mining photogrammetry performed. Photogrammetry in large, cavernous, dark environments will require an additional light source or the camera will have to be positioned very close to the area of interest. Due to this different light requirement, it is more likely that in a cavernous mining environment, a supplemental, stationary light source will be used, instead of a dynamic light source in an underground coal mine. The stationary light source will improve the photogrammetric reconstruction, and the overlap or redundant photos can be minimized.

If using lighting to supplement the onboard camera flash, ensure that it is diffuse enough to not cause the focused light to obscure large portions of the scene. Cap lamps tend to create highly focused beams of light which obscure the region they are focused on and insufficiently light

the surrounding regions. Cap lamps should either be turned off during photography or focused away from the scene as to not negatively affect the photos. If cap lamps are to be used as a light source, some means by which to diffuse them must be devised, and it is likely that several will be required to produce enough for photography.

When using a stationary light source, the effect of shadows on features in the photos become more pronounced. This is especially pronounced when rounding corners using quasi-dynamic lighting, such as stationary auxiliary lighting that is moved when the subject becomes too far from the light source. In these situations, few photographs will be necessary to capture a side of an object, however, a larger number of photographs will be required when photographing the corner of the object. A large number of photographs ensures that similar features do exist in the photos and the photo set is not split into several smaller and distinct photo sets.

Data Processing

Photogrammetric reconstruction can be performed through a variety of different software packages. This discussion will only concern basic processes that are common to many of the low-cost options available and point cloud manipulation. All of these practices and issues will not necessarily apply to specific software options available.

Not every photo taken needs to be included in the photogrammetric reconstruction process. Often, poor photos will only harm the reconstruction by either causing the camera to be improperly located, resulting in incorrect points being added to the scene, or causing the process to fail altogether. Identifying which photographs are harmful can usually be done beforehand, although removing bad photographs after they were processed, and then reconstructing the scene again is often possible. There is no universal value that quantifies motion blur, graininess, poor lighting, overexposure, etc. It will likely require trial and error to determine what a particular software package requires for image quality.

Photogrammetry can be computationally intensive, depending on the number and resolution of photographs used in reconstruction. If the overlap in photos was high and the image quality was high, then redundant photographs may be removed to expedite the reconstruction process. Additionally, pieces of a scene can be reconstructed individually and later stitched together, in either the photogrammetry software or point cloud manipulation software. This can

help to isolate a problem if the reconstruction is being performed multiple times due to poorly located camera locations or a failed reconstruction.

After a successful reconstruction, the units associated with the coordinate system as well as the camera orientations are likely to be incorrect, and will require a coordinate system transformation. The transformation is usually performed by locating three or more points common to a reference coordinate system. If the reconstructions are not being used for surveying purposes, and can function on an arbitrary coordinate system, the most accurate point cloud should be used as the reference. There are typically numerous features in a scene that can be used for referencing without the need for external targets, although many software packages will automate the process if reference targets are used. The software will attempt to translate, rotate, and scale a scene to match selected points with the reference system, while minimizing tension, or distance error, between points.

Including as many points as possible in the coordinate system transformation will reduce the impact of one poorly located point. Other than artificially included reference targets, the best visual features for referencing tend to be stark coloration differences on flat surfaces. Small, complicated geometries in a scene are often the most difficult to reconstruct, and choosing a reference point on them is both difficult to ensure the correct point was selected and it is more likely to have been poorly located. In an underground coal mine, discolorations on a roof bolt plate, impurities in wood, or scratches on a metal support often make the best features.